NUMERICAL STUDY OF THE IMPACT OF BAFFLE ON FLOW AND HEAT TRANSFER INSIDE A SKEWED ENCLOSURE
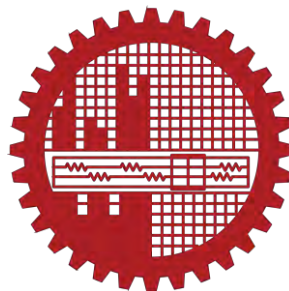
By

Md. Shamim Hasan

Student No. 0419092506

Registration No. 0419092506, Session: April- 2019
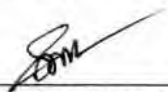
MASTER OF SCIENCE

IN

MATHEMATICS

Department of Mathematics

Bangladesh University of Engineering and Technology (BUET),

Dhaka-1000

April 2022

The thesis entitled

NUMERICAL STUDY OF THE IMPACT OF BAFFLE ON FLOW AND HEAT TRANSFER INSIDE A SKEWED ENCLOSURE

Submitted by

Md. Shamim Hasan

Student ID: 0419092506F, Registration No. 0419092506, Session: April-2019 has been

accepted as satisfactory in partial fulfillment for the degree of Master of Science in

Mathematics on April 17, 2022.

BOARD OF EXAMINERS

1.

   Dr. Md. Manirul Alam Sarker   Chairman
   Professor   (Supervisor)
   Department of Mathematics
   BUET, Dhaka-1000

2.

   Dr. Khandker Farid Uddin Ahmed
   Professor & Head   Member
   Department of Mathematics   (Ex-Officio)
   BUET, Dhaka-1000

3.

   Dr. Md. Mustafizur Rahman   Member
   Professor
   Department of Mathematics
   BUET, Dhaka-1000

4.

   Dr. Salma Parvin   Member
   Professor
   Department of Mathematics
   BUET, Dhaka-1000

5.

   Dr. Md. Tajul Islam   Member
   Professor
   Department of Mathematics
   Begum Rokeya University, Rangpur

CANDIDATE'S DECLARATION

I hereby announce that the work which is being presented in this thesis entitled "**NUMERICAL STUDY OF THE IMPACT OF BAFFLE ON FLOW AND HEAT TRANSFER INSIDE A SKEWED ENCLOSURE**" submitted in partial fulfillment of the requirements for the degree of Master of Science in Mathematics, Bangladesh University of Engineering and Technology, Dhaka-1000 is my own work with proper citation and acknowledgement.

All thoughts expressed in the dissertation are those of the author and in no way or by no means represent those of Bangladesh University of Engineering and Technology (BUET), Dhaka. Furthermore, this dissertation has not been submitted to any other university for examination either at home or abroad.

Md. Shamim Hasan
Date: April 17, 2022.

ACKNOWLEDGEMENT

Md. Shamim Hasan

Date: April 17, 2022.

ABSTRACT

The effectiveness of natural convection heat transfer in a skewed enclosure is investigated in this study with respect to variations of baffle lengths and the skew angles. The non-dimensional governing equations are solved using finite element techniques based on Galerkin weighted residuals. The effect of the baffle length and skew angles ($15^0 \leq \alpha \leq 165^0$) on fluid flow and heat transfer for various Rayleigh numbers ($10^3 \leq Ra \leq 10^6$) are explored in this study. The analyses are carried out for different values of Rayleigh number (Ra), baffle lengths (L) for fixed baffle thickness and baffle position while Prandtl number is maintained constant at 1.41. In addition, various features such as streamlines, isotherms, velocity profiles, temperature profiles, local Nusselt number, baffle effectiveness, skew-angle effectiveness, and heat transfer rate in terms of the average Nusselt number (Nu_{avg}) and average fluid temperature was shown for the relevant parameters. Several comparisons have been made between the results of this study and previously published studies to assess the reliability and consistency of the data. Streamlines, isotherms, local and average Nusselt numbers, mean fluid temperature, baffle effectiveness and angle effectiveness were used to illustrate the results of simulations.

 The findings of the study showed that heat transfer rate improves with the increase of Rayleigh number. Furthermore, the results showed that the heat transmission rate rises when the skew angle is progressively raised to 90^0. But after that, when the angles are further raised up to 165^0, the heat transmission rate reduces. The findings of this study are highly consistent with those of previous research.

TABLE OF CONTENTS

NOMENCLATURE

A_{ef}	Skew effectiveness
b	Baffle position
B	Dimensionless baffle position, b/S
C_p	Specific heat, J/kg k
d	Baffle thickness
D	Dimensionless baffle thickness, d/S
E_f	Baffle effectiveness
g	Gravitational acceleration, m/s
h	Heat transfer coefficient
k	Thermal conductivity, W/m. K
l	Baffle length
L	Dimensionless baffle length, l/S
Nu_{avg}	Average Nusselt number
Nu_L	Local Nusselt number
Pr	Prandtl number, ν / α
Q_{baffle}	Average fluid temperature with baffle
$Q_{withoutbaffle}$	Average fluid temperature without baffle
$Q_{\alpha=90^0}$	Average fluid temperature for skew angle of 90^0
$Q_{\alpha<90^0<\alpha}$	Average fluid temperature for skew angle without 90^0
Ra	Rayleigh number
Gr	Grashof number
S	Cavity height and width
u	Velocity in x direction
U	Dimensionless velocity in X direction
v	Velocity in y direction
V	Dimensionless velocity in Y direction
x	Horizontal coordinate
X	Dimensionless Horizontal coordinate
Y	Dimensionless vertical coordinate
y	Vertical coordinate

Greek symbols

α	Thermal diffusivity
β	Thermal expansion coefficient
ρ	Density
λ	Amplitude
μ	Dynamic viscosity
ν	Kinematic viscosity
θ	Dimensionless temperature

Subscripts

h	Hot wall

c	Cold wall
avg	average

LIST OF FIGURES

LIST OF TABLES

CHAPTER 1

INTRODUCTION

1.1 INTRODUCTION

Heat transfer is a science that attempts to anticipate the flow of energy between two material objects due to a temperature difference between them. According to the laws of thermodynamics, this transmission is characterized as heat. Because of this, the science of heat transfer aspires not only to explain how heat energy may be transmitted but also to anticipate the rates at which thermal energy is transferred under certain circumstances. In the prehistoric era, when humans utilized sun radiation as a heat source for cooking, heat transfer phenomena were well-known to them. In the early days of human civilization, the development of fire marked the beginning of heat transmission in its basic form. Since it is closely tied to the expansion of human society since then, its understanding and application have been steadily rising with each passing day. The heat transfer phenomenon received its first practical attention with the creation of the steam engine by James Watt in 1765 A. D. Its use was expanded to a wide range of engineering sectors and became well known. It has been possible to determine heat transfer of greater complexity over the past three decades, especially with the development of modern systems, mathematical analysis, and simulation methods of heat transfer. This has enabled a new approach to thermal management design to be established. More details could be found in Hagen [1].

Temperature and heat transport are essential topics for engineers to understand since they occur virtually universally in many research and engineering fields. For example, aircraft performance relies on the care with which the architecture and engines can be cooled, even though thermal transfer modeling is much more necessary for the right size of transportation fuel in nuclear reactor cores to avoid nuclear plant burning. The design of chemical industries is often based on convective heat transfer and equivalent mass transfer procedures, which are then implemented. All heat transfer processes are defined as transferring and reconfiguring energy from one form to another. As a result, they are regulated by the

first and second laws of thermodynamics, which are the fundamental laws of physics. When it comes to fluid mechanics, heat transport is often mentioned. Heat transport analyses need an understanding of heat transfer characteristics since heat flow occurs only when there is an increase or decrease in temperature in a system. One may compute the heat flux from the physical regulations that apply to the thermal gradient and the heat flow, which is defined as the quantity of heat transfer per unit surface area in a given period.

All physical occurrences are subject to natural laws, as discovered through extensive research into the cosmos. In describing the structure or scheme of basic and worldwide necessity inside this methodology or mechanism, the word "natural" might be employed. The processes for heat transport are one such system. Heat transfer is an interdisciplinary field of research meteorology that deals with heat transport. In this process, it calculates the rate at which data is transported throughout the application domain when exposed to specified temperature variations and the temperature profile of the framework. On the other hand, conventional thermodynamics is concerned with the requirement to raise the temperature that is transmitted throughout the process. Heat transfer mechanisms have become a fundamental aspect of human surroundings in our daily lives.

1.1.1 Modes of Heat Transfer

Heat is more than just energy that could be transmitted from one system to another due to temperature variations. A thermodynamic analysis is concerned with the heat transfer rates that occur when a system transitions from one equilibrium state to another. The physics of heat exchange is concerned with establishing the speeds at which energy transfers occur. The transmission of energy as heat occurs only from the more excellent temperature medium to the lower thermal medium, and heat transfer ceases when the temperatures of the two mediums are equal. Heat is transferred via three main techniques or mechanisms: conduction, convection, and radiation. All heat transfer modes need a temperature gradient, and all methods are from a high-temperature medium to a lower-temperature medium. In actuality, the combined influence of these three heat transport mechanisms regulates the temperature profile in a platform [1].

Thermal Conduction

Thermal conduction is the transmission of internal energy by microscopic collisions of particles and the movement of electrons inside a body. It is the most common kind of energy transfer. When colliding particles, which include molecules, atoms, and electrons, transmit disordered tiny kinetic and potential energy, referred to as internal energy, to the other colliding particles. Conduction occurs in all three phases of matter: solid, liquid, and plasma. Heat transfers naturally from a hotter to a colder body when a body is heated. For example, when heat is transferred from the hotplate of an electric stove to the bottom of a saucepan that comes into contact with it, this is known as conduction. Heat loss occurs over time when there is no opposing external driving energy source present, either inside a body or between bodies, and temperature disparities diminish as thermal equilibrium is approached, with temperature becoming more uniform [2].

Convection

Convection, also known as convective heat transfer, is the transfer of heat from one region to another due to the movement of a fluid. Even though it is often regarded as a unique technique of heat transfer, convective heat transfer seems to be the result of the combined processes of conduction (heat diffusion) and advection (heat transfer by bulk fluid flow). When it comes to heat transmission in liquids and gases, convection is generally the most prevalent mode of heat transfer. It is important to note that this definition of convection is only appropriate in the settings of heat transport and thermodynamics. It should not be confused with the dynamic fluid phenomena of convection, which is often referred to as Natural Convection in thermodynamic settings to differentiate between the two.

The basic relationship for heat transfer by convection is:

$$\dot{Q} = hA(T - T_f)^b$$

where $\dot{Q}$ is the heat transferred per unit time, A is the surface area of the object, h is the heat transfer coefficient, T is the surface temperature of the object, T_f is the fluid temperature, and b is a scaling exponent in the equation. There are two kinds of convective heat transfer that may be distinguished:

Free or natural convection occurs when fluid motion is produced by buoyant forces resulting from differences in density induced by fluctuations in thermal temperature in the fluid. For example, when fluid comes into the interface with a heated surface without an internal source, its molecules divide and disperse, causing the fluid to become less dense. As a result, the liquid is displaced, while the colder fluid becomes more viscous, and the fluid sinks. As a result, the hotter volume of fluid transfers heats to the cooler volume of the same fluid. The upward movement of air caused by a fire, or a hot item is a well-known example, as is the circulation of water in a pot that is heated from below.

Forced convection occurs when a fluid is forced to flow over the surface of a solid by an internal source such as fans, churning, or pumps, resulting in an artificially generated convection current. This mechanism is found in a wide range of daily appliances, including central heating, air conditioning, steam turbines, and many more. Engineers developing or studying heat exchangers, pipe flow, and flow over a plate at a different temperature than the stream are often confronted with forced convection.

When natural convection and forced convection processes work together to transport heat, this is called combined forced and natural convection, or mixed convection. Pressure-buoyancy interactions are sometimes characterized as circumstances in which both pressure and buoyant forces are at work. It is primarily governed by the flow, temperature, shape, and direction of the air that each kind of convection contributes to heat transmission. When it comes to determining the Grashof number of a fluid, the nature of the fluid is also essential since the number grows as the temperature of the fluid increases, but it is maximum at a certain point in a gas. In extremely high-power-output devices, when forced convection is insufficient to remove all the heat generated, it is common to see a combination of forced and natural convection. Combining natural convection with induced convection at this moment will often provide the desired outcomes. Nuclear reactor technology, as well as various parts of electronic cooling, are examples of these procedures.
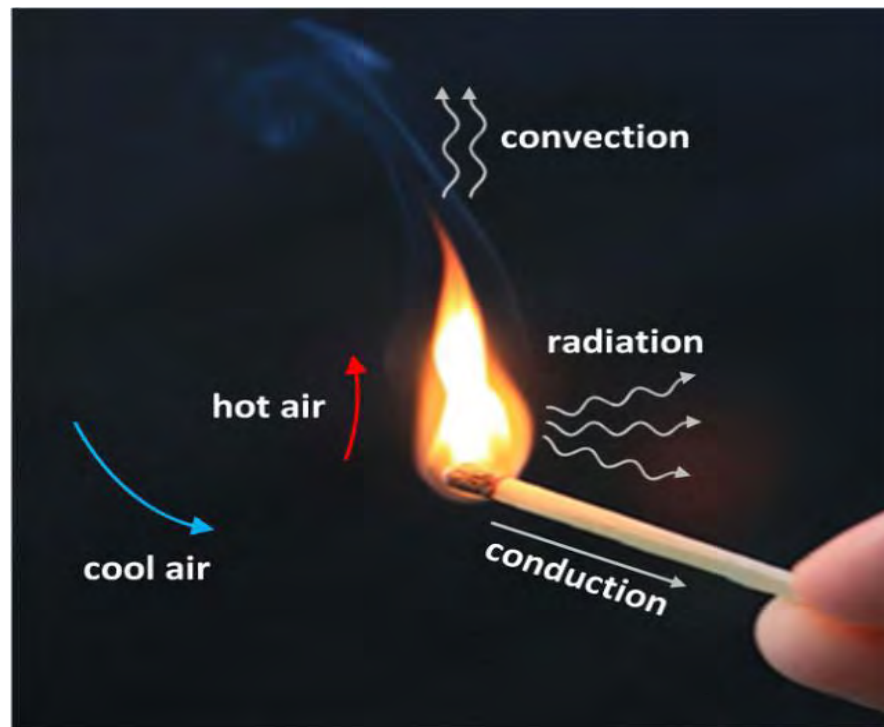
Figure 1.1: The heat transfer mechanism is shown.

Radiation

Radiation is the name given to the heat transfer method in which no medium is needed. It refers to the transfer of heat in waves rather than individual molecules since it does not need molecules to go through. The objects don't need to be in close touch with one another for heat to be transferred. In most cases, when you feel the heat without really touching a thing, you are experiencing Radiation. Furthermore, color, surface orientation, and other surface properties are some of the factors that significantly impact Radiation. As a result of this process, energy is transported by electromagnetic waves, referred to as radiative energy. In general, hot things radiate thermal energy towards their surroundings, which is colder. Radiant energy can move across a vacuum from its source to its colder surrounds, according to Hagen [1] (1999). The most remarkable example of radiation is the solar energy that we receive from the sun, even though it is thousands of miles distant from us. Figure 1.1 depicts an illustration of several modes of heat transfer in movement.

1.1.2 Flow within an enclosure

One of the essential circumstances seen repeatedly in practice is circulation within the enclosures composed of two walls at different temperatures from one another. In all cases, mainly where this circumstance exists, heat transfer happens due to the temperature gradients throughout the fluid layer. One horizontal solid surface is at a higher temperature than the other flat, stable surface. Assuming that the top plate is the hot surface, the lower scale will have a heavier fluid than the upper plate. As a result of buoyancy, the liquid will not reach the bottom plate for the simple reason that the heat transport method is limited to simply transmission in this scenario. However, assume the fluid is contained between two horizontal surfaces, with the top surface being at a lower temperature than the lower surface. Benard cells, which are natural convection currents that flow across cells, will also be present in that scenario. Fluids whose density drops with rising temperature are put in an unstable state due to this phenomenon. Benard referred to this state of instability as a "top-heavy" condition. As a result, the fluid is entirely immobile and only transfers heat across the layer by the conduction process in such a situation. Rayleigh realized that this unstable condition would have to break down at a precise value of the Rayleigh number, at which convective motion would have to be produced. When the air layer is surrounded on both sides by solid walls, Jeffreys concluded that the limiting value of Ra is 1708, according to his calculations. More information might be found in Patankar [3].

1.1.3 Applications of the Enclosure

As a result of the wide range of applications for which free convection is utilized, it is regarded as one of the most significant achievements in thermal activity. Our work often encounters fluid flow and heat transfer in cavities of various orientations. Some of these classical issues have analytical and massive numerical solutions, while others do not. Researchers in this field have developed solar energy collectors, nuclear reactor temperature control systems, room ventilation systems, fire-prevention systems, electrical cooling equipment, and geothermal equipment, among many other applications. It is anticipated that the investigation will be beneficial in a wide range of applications, including air conditioning in rooms, biological

transportation, injection modeling, double-paned windows, building energy conservation, material processing, grain storage, and high-performance building insulation; dynamics of lakes, reservoirs, and cooling ponds; and cryogenics. A substantial amount of research has been done on the various designs of the cavity, with the results being published in scientific journals. For example, many different kinds of geometric structures, simulation algorithms, and fluid frameworks have been researched in recent years. When it comes to heat transfer study, the skewed enclosure with a single horizontal baffle represents a significant advancement and an area of fast expansion in today's modern trend of heat transfer investigation. It is a fast-emerging discipline of fluid flow to study the flow of fluid mechanics and heat transfer via a hollow cavity. Natural convection heat transfer in a skewed cavity with sinusoidal boundary conditions may occur when a magnetic field is present. This is a significant branch of thermo-fluid mechanics that has developed.

1.2 RELEVANT DEFINITIONS

The following are the numerous definitions related to thesis:

1.2.1 Skewed Cavity

A skewed cavity, also known as an inclined enclosure, is a flat supporting surface that has been sloped at an angle, through one end of the cavity being higher than the other end. Skewed cavities are physical structures that use angle differences to get a mechanical advantage. The typical shape of the skewed enclosures is shown in Fig 1.2.
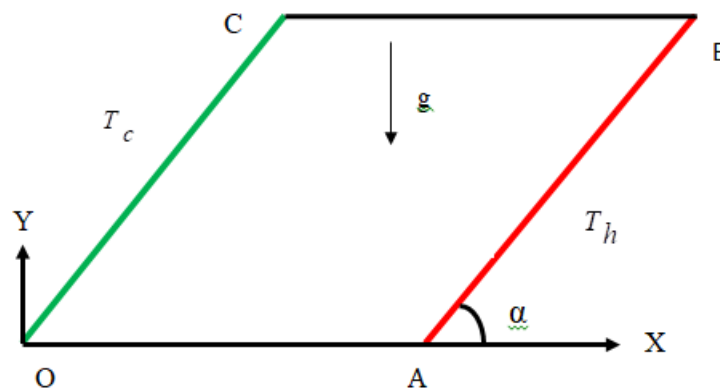
Figure 1.2: Skewed cavity

1.2.2 Stream Function

The stream function is defined for incompressible flows in two dimensions, and in three dimensions with axisymmetric. The derivatives of the scalar stream function may represent the flow velocity components of the flow. It is possible to visualize streamlines, which depict the trajectories of objects in a steady flow, with the help of the stream function. Joseph Louis Lagrange invented the two-dimensional Lagrange stream function in 1781, and it has been in use ever since. In asymmetrical three-dimensional flow, the Stokes stream function is used. It was named after George Gabriel Stokes, who discovered it. The volumetric flow rate (or volumetric flux) through a line connecting two places can be calculated using the stream function difference between any two points in the case of fluid dynamics. The concept of adding a stream function is only productive if the continuity equation can be simplified to two periods. When a function $\psi(x,y)$ satisfy the continuity equation $\frac{\partial u}{\partial x} + \frac{\partial u}{\partial y} = 0$, it is referred to be a stream function. For two-dimensional flows, the relationships between the stream function $\psi(x,y)$ and the velocity components are $u = \frac{\partial \psi}{\partial y}$ and $v = -\frac{\partial \psi}{\partial x}$. Using the above definition of the stream function, the positive sign of $\psi(x,y)$ denotes anti-clockwise circulation and the clockwise circulation is represented by the negative sign of $\psi(x,y)$. More information might be found in Batchelor, G. K. [4].

1.2.3 Thermal Diffusivity

Thermal diffusivity is the rate at which heat is transferred from one side of a material to the other side of the substance. It may be computed by dividing the thermal conductivity by the density and the specific heat capacity at constant pressure. Thermal diffusivity is a measure of how quickly heat diffuses across a substance and is defined as

$$\alpha = \frac{k}{\rho c_p}$$

A material with a superior thermal conductivity or a lower heat capacity will have an effective thermal diffusivity. The higher thermal diffusivity indicates that heat

propagation into the medium is more instantaneous. In contrast, a low thermal diffusivity number implies that the material absorbs most of the heat, and only a small quantity of heat is carried further [4].

1.2.4 Thermal Conductivity

The thermal conductivity is measured in terms of the quantity and speed of heat that can transfer through it. Materials with a high thermal conductivity transmit heat more quickly than those with a low one. Materials with high thermal conductivity are utilized as heat sinks, whereas materials with low thermal conductivity are employed as thermal insulation. Materials' heat conductivity is transferred away from the junction. It is well known that material properties' electrical and thermal conductivity are closely linked; in other words, materials with high electrical conductivity also have high thermal conductivity. The proportionality constant k is referred to as the material's thermal conductivity. More details are available in Çengel and Yunus [2].

$$k = \frac{\text{Heat flow(Q)} \times \text{Thickness of thematerial (L)}}{\text{Surface area of material(A)} \times \text{Temperature gradient } (\Delta T)}$$

$$k = \frac{Q \times L}{(A \times \Delta T)}$$

1.2.5 Newtonian Fluid and Non-Newtonian Fluid

Newtonian fluids are defined as fluids in which the constant of proportionality, i.e., the coefficient of viscosity (μ), does not vary with the deformation rate. In other ways, fluids that obey Newton's viscosity rule are referred to as Newtonian fluids. Newtonian fluids are named after Sir Isaac Newton (1642 - 1726), who defined the flow behavior of fluids using a simple linear relationship between shear stress [mPa] and strain rate [1/s]. Newtonian fluids include substances such as water, air, and mercury, to name a few examples.

A non-Newtonian fluid is a fluid whose viscosity varies according to its amount of stress or force. Cornstarch dissolved in water is the most prevalent daily example of a non-Newtonian fluid. Temperature and pressure are the only variables used to

characterize Newtonian fluids' behavior like water. On the other hand, the physical behavior of a non-Newtonian fluid depends on the forces acting on it from second to second. In other words, non-Newtonian fluids are fluids that neither obey Newton's rule of viscosity nor behave like water. Non-Newtonian fluids include blood, liquid plastic, and polymer solutions. More details are available in Batchelor and G. K. [4].
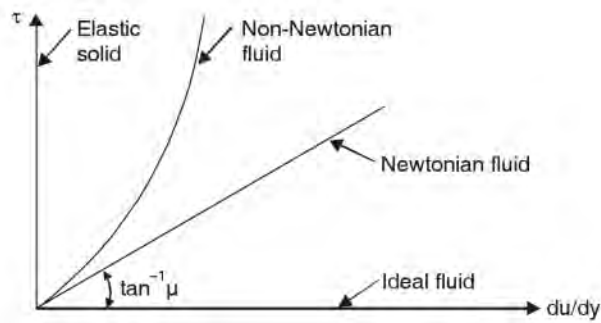
Figure 1.3: Classification of fluid

1.2.6 Compressibility

Compressibility is a property of fluid that measures the change in density and consequently, the change in the volume of a fluid during motion under the action of external forces [5]. The compressibility is expressed in terms of Mach number (M) which is defined by

$$M = \frac{\text{speed of fluid}}{\text{speed of sound}} = \frac{u}{\alpha_0}$$

1.2.7 Compressible Flow and Incompressible Flow

Compressible flow is that type of flow in which the density of the fluid changes from point to point in other words the density (ρ) is not constant for the fluid [54]. Thus, mathematically, for the compressible flow

$$\rho \neq \text{constant}$$

Incompressible flow is that type of flow in which the density of the density (ρ) is constant for the fluid flow. Liquids are generally incompressible gases are compressible [5]. Mathematically, for the compressible flow

$$\rho = \text{constant}$$
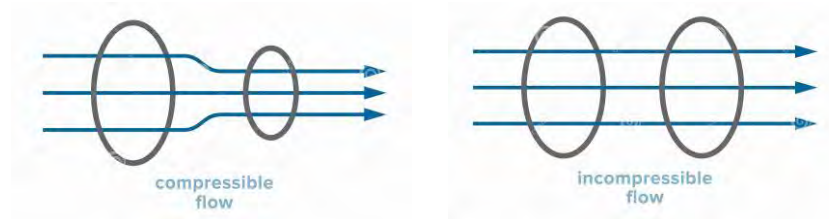
Figure 1.4: Compressibility

1.2.8 Viscosity

The viscosity of a fluid that changes a lot with temperature measures how hard it is to change shape. When two fluid layers move next to each other, friction forces build up between them. The slower layer tries to slow down the faster layer. In this case, the fluid property viscosity is used to measure how much internal resistance there is to flow. All fluid flows have some viscous effects, so no   has no consistency. The viscosity of liquids goes down as the temperature rises, but the viscosity of gases goes up as the temperature rises. More details are available in Çengel and Yunus [2].

1.2.9 Viscous Flow

The viscous properties of the fluid dominate the flow patterns of such flows, which are referred to as viscous flows. This occurs when the velocity gradients in a fluid are rather substantial. The flow near to the pipe walls may be considered as viscous flows [1].

1.2.10 Newton's Law of Viscosity

If the shearing stress, τ , enlargements by increasing the force P, the rate of shearing strain also increases in direct proportion to that,

$$\tau \propto \frac{du}{dy} \ i.e., \ \tau = \mu \frac{du}{dy}$$

where μ is the dynamic viscosity of the fluid. This principle is known as Newton's law of viscosity. More details are available in Çengel and Yunus [2].

1.2.11 Effectiveness

Baffle Effectiveness:

Baffle effectiveness (E_f) is the parameter that quantifies the heat transfer enhancement inside the cavity with a baffle compared to the case with no baffle [17] and is defined as follows

$$E_f = \frac{Q_{baffle}}{Q_{withoutbaffle}}$$

The effectiveness of baffle $E_f =1$ indicates that the addition of baffles to the surface does not affect heat transfer. The heat conducted to the baffle through the base area equals the heat transferred from the same area to the surrounding medium.

The effectiveness of baffle $E_f < 1$ indicates that the baffle acts as insulation, slowing down the heat transfer from the surface. This situation can occur when baffles made of low thermal conductivity materials are used. Effectiveness of baffle $E_f > 1$ indicates that the baffle enhances heat transfer from the surface, as they should. However, the use of baffles cannot be justified unless E_f is sufficiently larger than 1. Baffle surfaces are designed to maximize the effectiveness of a specified cost or minimize cost for the desired effectiveness. More details are available in Hagen [1].

Angle Effectiveness:

Angle effectiveness (A_{ef}) is the characteristic that measures the heat removal coefficient within the cavity when an angle is used, as discussed in previous sections when there is except angle .

$$A_{ef} = \frac{Q_{\alpha<90^0<\alpha}}{Q_{\alpha=90^0}}$$

1.3 DIMENSIONLESS PARAMETERS

Fluid behavior is greatly influenced by a collection of dimensionally insignificant values known as the "dimensionless parameters" of fluid mechanics. Mechanical

engineers often use dimensionless numbers. Here, the variables are either divided into groups that perfectly cancel one another or pure integers with no units. For example, using a dimensionless number as a ratio of two other numbers is possible, and the dimensions of the numerator and denominator will cancel. The dimensionless parameters may gauge certain features of the flow's significance. This investigation will explore several dimensionless parameters relevant to it in this section.

1.3.1 Prandtl Number (Pr)

The relative consistency of the velocity and thermal boundary layers is suitably characterized by the dimensionless parameter Prandtl number, which is defined as

$$Pr = \frac{v}{\alpha} = \frac{\text{Momentum diffusivity}}{\text{Thermal diffusivity}} = \frac{\mu / \rho}{k / (C_p \rho)} = \frac{c_p \mu}{k}$$

where v is the kinematic viscosity (momentum diffusivity), $v = \frac{\mu}{\rho}$, α is the thermal diffusivity and $\alpha = \frac{k}{(\rho c_p)}$, μ is the dynamic viscosity, k is the thermal conductivity, c_p is the specific heat and ρ is the density. It is named after Ludwing Prandtl, who introduced the concept of boundary layer in 1904 and made significant contributions to boundary layer theory. The Prandtl number of fluids ranges from less than 0.01 for liquid metals to more than 100,000 for heavy oils. When the Prandtl number is small, as in $Pr \ll 1$, thermal diffusivity is the dominant factor. In contrast, when $Pr \gg 1$, the momentum diffusivity becomes the dominant factor in the conduct [1].

1.3.2 Rayleigh Number (*Ra*)

The Rayleigh number of a fluid is a dimensionless number connected with heat transport inside the fluid. When the Rayleigh number is less than the significant level for that fluid, heat transfer is mainly in conductance; when the Rayleigh number is more than the significant level, heat transfer is primarily in convection. The Rayleigh number, named after Lord Rayleigh, is described as a Grashof number

function, representing the relationship between buoyancy and viscosity inside fluid and the Prandtl number.

$$Ra_x = Gr_x \Pr = \frac{g\beta}{\nu\alpha}\left(T_s - T_\infty\right)x^3$$

This value is used to describe free convection near a vertical wall.

where Pr = Prandtl number, g = gravity, x = characteristic length (in this case, length of cavity), T_s = Temperature of surface, T_∞ = Quiescent temperature, ν = kinematic viscosity, α = thermal diffusivity, and β = thermal expansion coefficient. More details are available in Çengel and Yunus [2].

1.3.3 Grashof Number (*Ga*)

The Grashof number (*Gr*) is a dimensionless number in fluid dynamics and heat transfer which approximates the ratio of the buoyancy to viscous force acting on a fluid. It frequently arises in the study of situations involving natural convection and is analogous to the Reynolds number, and define as

$$Gr = \frac{g\beta L^3(T_w - T_\infty)}{\nu^2}$$

where g denotes gravity acceleration, β is the volumetric thermal expansion coefficient, T_w denotes wall temperature, T_∞ denotes ambient temperature, L denotes characteristic length, and ν denotes kinematic viscosity. The Grashof number Gr follows the same procedure as the Reynolds number Re does in forced convection in free convection. Therefore, the Grashof number is essential for identifying whether the fluid flow in free convection is laminar or turbulent. The critical value of the Grashof number is about 10^9 for vertical plates. Thus, when Grashof numbers exceed 10^9, the flow regime on a vertical scale becomes turbulent. More details are available in Çengel and Yunus [2].

1.4 LITERATURE REVIEW

Many researchers have extensively explored natural convection within the cavity for different orientations, various types of nano-fluids for both steady and unsteady

numerical cases. The addition of a baffle to the cavity's wall substantially impacts both flow patterns and heat transfer. Davis [7] investigated the natural convection of air in a square cavity and presented a benchmark numerical solution. Tasnim *et al.* [8] analyzed heat transmission inside a squared enclosure by including a baffle on such a heated surface using numerical methods. Moreover, they found that the maximum increase in thermal transmission occurs when the baffle is stretched to its maximum length. Ambarita *et al.* [9] detected laminar free Convection heat transport in an air-filled rectangular cavity having a couple of insulated baffles connected to its horizontal sidewalls. It has been shown that, when compared to the same cavity without baffles and the addition of two baffles having non-dimensional lengths greater than 0.5 changes the flow and temperature fields. Jani *et al.* [10] investigated MHD free convective heat inside a square cavity heated from bottom sides and cooled from another sides. Also, they observed that the intensity of the magnetic field and the Rayleigh number significantly impacted the heat transfer processes, temperature distribution, and flow characteristics inside the cavity. The impact of a thick horizontal partial partition connected to one of the active walls of a differentially heated square enclosure was studied by Nag *et al.* [11]. Barakos *et al.* [12] studied laminar and turbulent models with wall functions for flows revisiting natural convection flow in a square cavity. They reported that for thin boundary layers, dense, non-uniform grids catch most flow and heat transport characteristics exceptionally effective. Due to significant temperature differences, Mayeli and Sheard [13] explored free convection and entropy generation in skew and square cavities: A Gay-Lussac type vorticity stream-function method. Free convective heat transfer in a square porous cavity with sinusoidal temperature distributions on vertical walls covered with nanofluid was analyzed by Sheremet and Pop [14] utilizing Buongiorno's mathematical model. Ren *et al.* [15] investigated Laminar natural convection in a square cavity with 3D random roughness components while considering the fluid's compressibility. Amini *et al.* [16] used numerical simulations to investigate the free convective fluid movement also heat transport within a symmetrically cooled square cavity, including a fin connected through its hot lower wall. They found that the flow and heat transmission within the cavity was very efficient. Elatar *et al.* [17] studied Numerically laminar free convection within a square cavity including a singular horizontal fin. They also found that raising the conductivity ratio for every value of Rayleigh numbers may increase the fin's

efficiency. It is also discovered that, in general, the fin's efficiency improves with the lengthening of the fin. Ali *et al.* [18] scrutinized free convection in a porous square cavity with a sinusoidally changing temperature distribution on the lower wall. Asad *et al.* [19] investigated numerically inside a lid-driven square enclosure with a vertical fin of MHD mixed convection heat transfer. Finally, they found that the Richardson number influences the fluid movement area within the enclosure. The Richardson number (Ri) impacted the magnetic field intensity as well as isotherms.

Pop *et al.* [20] examined heat transmission and entropy generation in combined convection of nanoparticles inside an angled skew enclosure may occur simultaneously. A wide variety of skewed angles, volume fractions, the flow area properties, and heat transference components including Richardson numbers are investigated in that study. Thohura *et al.* [21] carried out mathematical simulations of non-Newtonian power-low fluid movement within a lid- driven skewed enclosure. Erturk *et al.* [22] examined Numerical solutions of two-dimensional relatively constant incompressible flow inside a driven skew enclosure. Nayak *et al.* [23] deliberated a numerical analysis of combined convection with entropy production in a differentially heated skewed enclosure for a Cu-water nanofluid. Sharaban *et al.* [24] studied the mixed convective flow of power-law fluids in a lid-driven skew cavity. The natural convective heat was studied by Misirlioglu *et al.* [25] in a skewed undulating framework filled by a porous medium. According to their research, Heat is often transported from the heated wall inside the porous material. However, the heat transference rate is strongly reliant on the surface waviness and Rayleigh number of the porous channel. Chamkha *et al.* [26] explored the fluid-structure interactions in free convection flow in an inclined enclosure with something like a comfortable undulating fin as well as partly heating. Benmenzer and Si-Ameur [27] evaluated natural convective heat induced by heat generation in an angled porous enclosure. Their research discovered that increasing the heat flow causes an increase in the fluid flow intensity. Baytas [28] analyzed the entropy generation during free convection inside an angled pore enclosure. Selamat *et al.* [29] reported free convection in an angled porous enclosure with temperature differences along the sidewalls. For the most part, they found numerical data that support the notion that the most extraordinary natural convective is based on the inclination angle, with the maximal Nusselt number occurring at various wave

numbers for various incline degrees. Sivasankaran *et al.* [30] examined free convection in a sloping pore triangle cavity with different heat transfer characteristics. For low Rayleigh numbers, heat transmission is influenced by conductance throughout the fluid particles, and subsequently, convective heat is impacted by rising Darcy-Rayleigh numbers.

Free convection in a porous rectangular cavity having sinusoidal temperature distributions on both sidewalls was studied by Wu *et al.* [31], Using a thermal non-equilibrium model. Wang *et al.* [32] studied the impacts of temperature-dependent characteristics on free convection for power-law nanoparticles in rectangular cavity having periodic temperature profile. Bendehina *et al.* [33] examined the consequences of sinusoidal transmission of heat on laminar free convection in a wavy shape rectangular cavity. Varol *et al*. [34] researched a Numerical solution of free convective heat transfer for a porous rectangular enclosure, including a sinusoidally changing temperature gradient on the lower surface. It has also been observed that the effects of aspect ratio become substantial, particularly at more extensive levels of the magnitude of the sinusoid.

Hassinet *et al.* [35] carried out numerical study on natural convection in a porous cavity that was partly hot and cool by periodic heating at the vertical surfaces. Furthermore, they have discovered that the conduction heat-transfer management is also appropriate for low sinusoidal temperature functions. Saeid [36] investigated natural convective flow in a porous medium with sinusoidal temperature fluctuations at the bottom wall. He discovered that, for a certain Rayleigh number, the mean Nusselt number rises when the non-dimensional distance of the heating element is increased. Increasing the size of the hot part, however, results in a reduction in the heat transmission per unit area of the heat source. Using numerical simulations, Zahmatkesh [37] analyzed the heat transmission mechanism and entropy production features within a four equal-sided porous medium with sinusoidal heat fluctuations on the symmetric and anti-symmetric sidewalls. In addition, it was discovered that, even though anti-symmetric temperature boundary conditions result in more excellent thermal conductivity, they are associated with a significantly increased rate of entropy production. Numerical study of free convection in a pore cavity having periodic heated boundary conditions was also

explored by Wu *et al.* [38]. Also observed that the values of the average Nusselt number continuously rise as its porosity grows, and this is true for all periodicity parameters. Chattopadhyay *et al.* [39] studied mixed convection flow patterns in a dual lid-driven oscillatory heated pore enclosure. That was the top priority of their research to investigate the Darcy impact and even the influence of magnitude and phase variations under sinusoidal boundary conditions, which they accomplished. Cheong *et al.* [40] applied various heat sources in a porous shell, including the flow of free convection and internal heat, to explore convection patterns inside a sinusoidal cavity. They saw that the higher magnitude and more significant fluctuations improve heat transmission, and a wavy cavity transfers heat faster than a square cavity. Asad *et al.* [41] numerically studied the heat transfer properties of natural convective flow within an enclosed medium with perpendicular undulating walls. Their experiments indicated that the material's perspective ratio, including surface waviness, significantly influences the heat-releasing properties. Free convection inside an undulating cavity containing three-dimensional heat sources was explored by Oztop *et al.* [42] in their study. According to the findings of their investigation, variations throughout the interior to exterior Rayleigh number ratios and the magnitude of the undulating wall affected both the flow field and heat transport properties. Whenever the magnitude of the undulating wall became prominent, it was anticipated that more excellent heat transferal rates would occur. According to Singh *et al.* [43], Mathematical analysis of free convection inside an wavy enclosure and to use a meshfree strategy: the effect of corner heating. In addition, it has been found that the heat transmission rate for undulating surfaces is more significant than that for flat surfaces. Asad *et al.* [44] investigated the impact of fin size and position on free convection flow in an irregular cavity with a straight fin. They concluded that the size and placement of the Fins had a significant impact on the movement also heat transmission properties inside the undulating cavity. Alsabery *et al.* [45] discussed the impact of non-homogeneous nano-fluid modeling on transient combined convection in a dual lid-driven irregular cavity containing a solid circular cylinder.

According to Hussein *et al.* [46], the Influence of baffles width on free convection in a cavity containing various nanoparticles was investigated. Finally, they discovered that raising the Rayleigh number, the baffle lengths, the material volume

fraction, and the aspect ratio all helped increase the intensity of the fluid flowing and the convection in the system. Taylor *et al.* [47] explored A mathematical model of the Navier–Stokes equation that used the finite element method. Free convection of a two-dimensional enclosure having a periodic top heated wall was inquired by Sarris *et al.* [48]. They took noted the impact of conductance decreases when the Rayleigh number is much enough. Sankar *et al.* [49] studied the impacts of the thin baffle's size and position on free convection in a vertical circular cavity. Asad *et al.* [50] investigated the free convection flow numerically in a hexagonal cavity, including a perpendicular fin. In this study, the effects of fin length variation on the Rayleigh number are discussed in detail. Djaomazava *et al.* [51] conducted numerical instructions of natural convection in an upward channel with sinusoidal process on one of its partitions. In that study, the researchers looked at the impacts of controlling variables such as Rayleigh number, slope angle, baffle measures, solid quantity fraction, and perspective ratio on the system's heat transport properties and movement patterning. Bilgen and Yedder [52] investigated natural convection inside an enclosure with heating and cooling that using sinusoidal temperature profiles on one side. Free convection in a porous horizontal cylindrical annular with sinusoidal boundary conditions was examined by Khudhayer *et al.* [53]. Asad *et al.* [54] studied the effect of an enclosed space rectangle heat source on convective heat transfer via a triangular cavity. Frederick *et al.* [55] analyzed a three-dimensional free convection in a finned cubical cavity. Islam *et al.* [56] investigated the MHD natural convection heat transport and fluid flow of a nanofluid in a skewed cavity numerically.

According to the above literature review, natural convection inside the enclosure was investigated under various boundary conditions, both with and without a baffle. In contrast, only a small number of studies has been done on the effect of skew angles for different Rayleigh numbers on a differentially heated wall inside a skewed cavity. For the aim of this investigation, a skewed cavity with a horizontal baffle connected to the thermal wall, while the other wall is at sinusoidal temperature. To determine the impact of skew angle on heat removal capability within a skewed cavity with sinusoidal temperature distribution, numerical research will be carried out at different Rayleigh number. Additionally, the efficiency and effectiveness of skew angles and baffle lengths will be studied.

1.5 MOTIVATION

From the literature survey, it could be claimed that natural convection inside the enclosure was investigated under various boundary conditions, both with and without a baffle. In contrast, only a small number of studies has been done on the effect of skew angles for different Rayleigh numbers on a differentially heated wall inside a skewed cavity. Furthermore, skew angle efficiency and effectiveness in these circumstances deserve due attention since there has been no systematic study of these features under different design conditions. It is important to use free convection heat transfer when developing efficient heat transfer devices, such as nuclear reactors and solar collectors, as well as electrical equipment. The literature survey indicates that a little attention has been paid to investigate the heat transfer characteristics of the free convection in a skewed cavity having a horizontal baffle using sinusoidal boundary condition. There is ample scope of study to observe the characteristics of fluid flow and heat transfer due to the variation of skew angle as well as baffle size, which forms the basis for the motivation behind the present study.

1.6 OBJECTIVES OF THE PRESENT STUDY

From the review of earlier investigations, it is apparent that very little study has been conducted on the impact of baffle length and skew angle for different Rayleigh numbers on a differentially heated wall within a skewed cavity. This study was carried out numerically, and the related results were shown using streamlines, isotherms, velocity, and temperature profiles, local and average Nusselt numbers and related graphs and charts.

The precise objectives of the current study are to:

    i. Investigate the heat transfer due to horizontal baffle attached to the heated inclined right wall of the skewed cavity with sinusoidal boundary condition at the left wall.

ii. Study the influence of physical parameters such as the Rayleigh number on the flow field within the skewed cavity under sinusoidal boundary condition.

iii. Analyze the effects due to the variation of the skew angles as well as for different length of baffles attached to the right wall of the skewed cavity.

It is expected that the present numerical investigation will contribute to the research for finding more efficient and better energy equipment. The output of this investigation is expected to be helpful for the researchers and experimentalists in the field of solar energy collectors, nuclear reactor temperature control, room ventilation, fire prevention, electrical cooling equipment, biological and geothermal equipment, etc.

1.7 OUTLINE OF THE THESIS

This dissertation is divided into four chapters. In chapter 1, a brief introduction is provided, along with the specific objectives. It also contains an overview of previous work on fluid flow and heat transfer in cavities. It has been categorized in this state-of-the-art review to highlight distinct elements of the preceding research that have been conducted. Following that, a post-mortem of a recent historical event is presented to illustrate the consequences of fluid flow and heat transfer in cavities under various boundary conditions.

The computational technique for the problem of viscous incompressible flow is presented in Chapter 2. The finite element method is used in this work, and it is discussed in detail. With a sinusoidal boundary condition and free convection flow in a skewed cavity, we explored the impacts of the baffle inside the skewed enclosure.

An in-depth parametric investigation of free convection in a sinusoidally skewed cavity with sinusoidal boundary condition is carried out in Chapter 3. The effects of significant characteristics such as Rayleigh number, Prandtl number, and physical parameters such as the skewness of the cavity on the flow and heat field in the enclosure have been investigated for three different values of Rayleigh number.

Finally, in Chapter 4, the dissertation is brought to a close with conclusions and comparisons. Final recommendations for further investigation of the present predicament are presented in this section.

MATHEMATICAL MODELLING AND COMPUTATIONAL TECHNIQUE

2.1 MATHEMATICAL MODELLING

Free convection is a term used to describe the heat transfer that happens as a result of temperature variations that change the density of the fluid and, as a result, the relative buoyancy of the fluid (natural convection). The mathematical model, which comprises a collection of partial differential equations and boundary conditions, serves as the starting point for any numerical approach. Solution methods are often created for specific equations and are not generic. Even if it is impracticable, it is not impossible to develop a general-purpose solution approach, i.e., one that can be used to all flows. On the other hand, as with other general-purpose tools, they are seldom optimal for any one application. The generalized governing equations, based on the conservation laws of mass, momentum, and energy, are employed to calculate the results. Because heat transfer depends on various elements, dimensional analysis is provided to demonstrate the significant non-dimensional components that was impact the dimensionless heat transfer parameter, i.e., the Nusselt number.

2.2 PHYSICAL MODEL

The schematic geometry of two-dimensional convection in a skewed cavity with boundary conditions is shown in Figure 2.1. The inclined left wall is deliberated at a sinusoidal temperature, while the inclined right wall is kept at a constant hot temperature (T_h) and the remaining walls are insulated. The heated right wall is equipped with a baffle. The baffle length, thickness, and location are denoted by l, d, and b, respectively. S indicates the inclined and horizontal wall in the model. For the baffle location, b (x, y) defined by

$$b(x,y) = \left(1 + \frac{\cos\alpha}{2} + \frac{d}{2\tan\alpha}, \frac{\sin\alpha}{2}\right); \text{when } 15^0 \leq \alpha \leq 90^0$$

$$b(x,y) = \left(1 + \frac{\cos\alpha}{2} - \frac{d}{2\tan(\pi-\alpha)}, \frac{\sin\alpha}{2}\right); \text{when } 105^0 \leq \alpha \leq 165^0$$

Furthermore, α denotes the skew angle. Gravitational forces work vertically downward. Additionally, it is referred to as constant, two-dimensional, and incompressible flow.
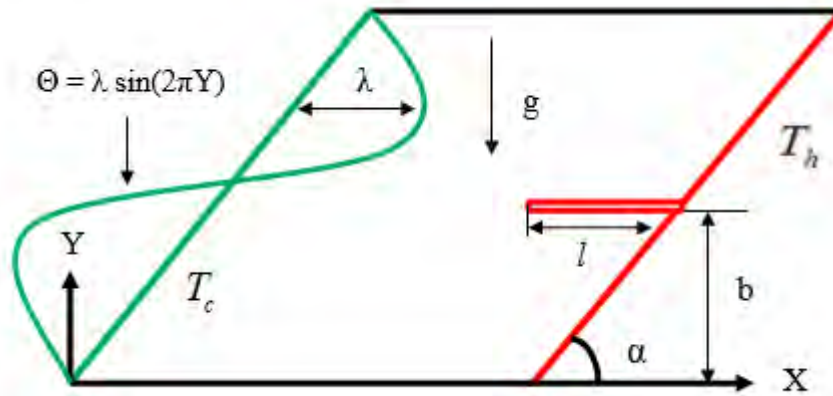
Figure 2.1: Model with boundary conditions.

2.3 COMPUTATIONAL TECHNIQUE

Computational fluid dynamics (CFD) has been rapidly gaining popularity over the past several years for technological and scientific interests. For many problems of industrial interest, experimental techniques are extremely expensive or even impossible due to the complex nature of the flow configuration. Analytical methods are often valuable for studying the fundamental physics involved in a particular flow problem; however, these methods have limited direct applicability in many exciting problems. The dramatic increase in computational power over the past several years has led to a heightened interest in numerical simulations as a cost-effective method of providing additional flow information, not readily available from experiments, for industrial applications, as well as a complementary tool in the investigation of the fundamental physics of turbulent flows, where analytical solutions have so far been unattainable. However, it is not expected (or advocated) that numerical simulations replace theory or experiment, but that they are used in conjunction with these other methods to provide a complete understanding of the physical problem at hand.

Mathematical models of physical phenomena may be ordinary or partial differential equations, subject to analytical and numerical investigations. For example, the partial differential equations of fluid mechanics and heat transfer are solvable for

only a limited number of flows. To obtain an approximate solution numerically, we have to use a discretization method, which approximates the differential equations by a system of algebraic equations, which can then be solved on a computer. The approximations are applied to small domains in space and/or time, so the numerical solution provides results at discrete locations in space and time. Much as the accuracy of experimental data depends on the quality of the tools used, the accuracy of numerical solutions depends on the quality of discretization used. Computation involves forming a set of numbers that constitutes a practical approximation of a real-life system. The outcome of the computation process improves the understanding of the performance of a system. Thereby, engineers need CFD codes to make physically realistic results with good quality accuracy in simulations with finite grids. Contained within the broad field of computational fluid dynamics are activities that cover the range from the automation of well-established engineering design methods to the use of detailed solutions of the Navier-Stokes equations as substitutes for experimental research into the nature of complex flows. CFD has been used for solving a wide range of fluid dynamics problems. It is more frequently used in engineering fields where the geometry is complicated or some vital feature that cannot be dealt with standard methods. More details are available in Patankar [3] and Ferziger & Perić [6].

2.3.1 Discretization Process

After choosing a mathematical model, one must choose an appropriate discretization technique, that is, a method for approximating the differential equations with a system of algebraic equations for the variable at a collection of discrete locations in space and time known as grid points [6].

2.3.2 Numerical Grid

The numerical grid defines the discrete locations at which the variables are to be calculated, which is essentially a discrete representation of the geometric domain on which the problem is to be solved. It divided the solution domain into a finite number of sub-domains (elements, control volumes, etc.). Some of the options available are structural (regular) grid, block-structured grid, unstructured grids, etc.

2.3.3 Finite Approximations

Following the choice of grid type, one has to select the approximations to be used in the discretization process. In a finite difference method, approximations for the derivatives at the grid points have to be chosen. In a finite volume method, one has to select the methods of approximating surface and volume integrals. Finally, in a finite element method, one must choose the functions and weighting functions [5].

2.3.4 Solution Technique

Discretization yields an extensive system of non-linear algebraic equations. The method of a solution depends on the problem. For unsteady flows, methods based on those used for initial value problems for ordinary differential equation (marching in time) is used. At each time step, an elliptic problem has to be solved. Pseudo-time marching or an equivalent iteration scheme usually solves steady flow problems. Since the equations are non-linear, an iteration scheme is used to solve them. These methods use successive linearization of the equations, and iterative techniques almost always solve the resulting linear systems. The choice of solver depends on the grid type and the number of nodes involved in each algebraic equation [5].

2.3.5 Discretization Approaches

The first step to numerically solve a mathematical model of physical phenomena is numerical discretization. Each component of the differential equations is transformed into a "numerical analog," which can be represented in the computer and then processed by a computer program built on some algorithm. Several discretization methods are available for the high-performance numerical computation in CFD [6]. Those include:

- ➢ Finite volume method (FVM)
- ➢ Finite element method (FEM)
- ➢ Finite difference method (FDM)
- ➢ Boundary element method (BEM)
- ➢ Boundary volume method (BVM)

Galerkin finite element method (FEM) has been used in the present numerical computation.

2.3.6 Finite Element Method

The finite element method (FEM) is a powerful computational technique for solving problems that are described by partial differential equations or can be formulated as functional minimization. The basic idea of the finite element method is to view a given domain as an assemblage of simple geometric shapes, called finite elements, for which it is possible to systematically generate the approximation functions needed in the solution of partial differential equations by the variational or weighted residual method. The computational domains with irregular geometries by a collection of finite elements make the method a valuable practical tool for the solution of boundary, initial, and eigenvalue problems arising in various engineering fields. The approximation functions, which satisfy the governing equations and boundary conditions, are often constructed using ideas from interpolation theory. Approximating functions in finite elements are determined in the nodal values of a physical field that is sought. A persistent physical problem is transformed into a discretized limited element problem with unknown nodal values. A system of linear algebraic equations should be solved for a linear problem. Values inside finite elements can be recovered using nodal values. More details are available in Ferziger and Perić [6].

The significant steps involved in finite element analysis of a typical problem are:

1. Discretization of the domain into a set of finite elements (mesh generation).
2. Weighted-integral or weak formulation of the differential equation to be analyzed.
3. Development of the finite element model of the problem using its weighted-integral or weak form.
4. Assembly of finite elements to obtain the global system of algebraic equations.
5. Imposition of boundary conditions.
6. Solution of equations.
7. Post-computation of solution and quantities of interest.

2.3.7 Mesh Generation

Mesh generation is the practice of generating a polygonal or polyhedral mesh that approximates a geometric domain. The term "grid generation" is often used interchangeably. Typical uses are rendering a computer screen or physical simulation such as finite element analysis or computational fluid dynamics. In the finite element method, mesh generation is the technique to subdivide a domain into a set of sub-domains, called finite elements. For example, the Figure 2.2 shows a domain, Γ^c is subdivided into a set of sub-domains, Λ^e with boundary Γ^e [6].
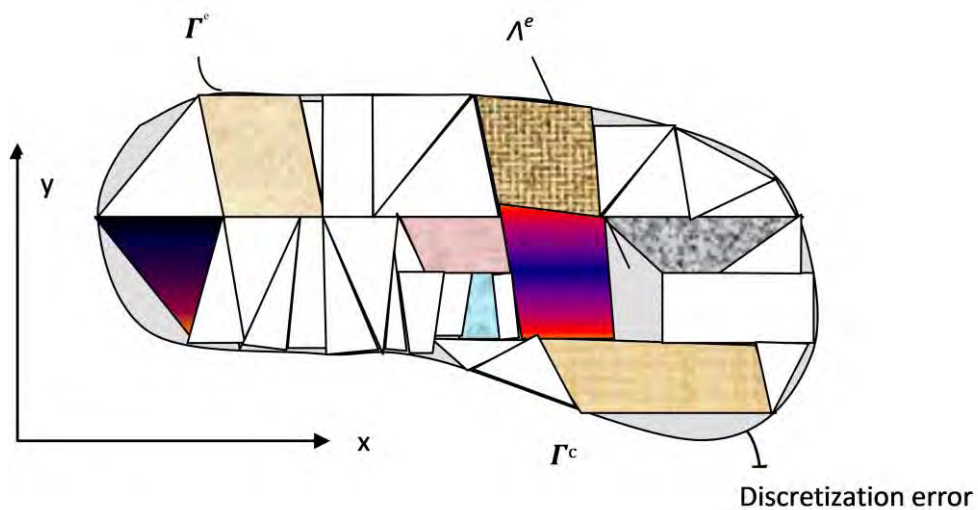
Figure 2.2: Finite element discretization of a domain

The computational domains with irregular geometries by using a set of finite elements make it a valuable practical tool for solving boundary value issues that arise in a wide range of engineering disciplines. The finite element mesh of the current physical domain is shown in Figure 2.3.
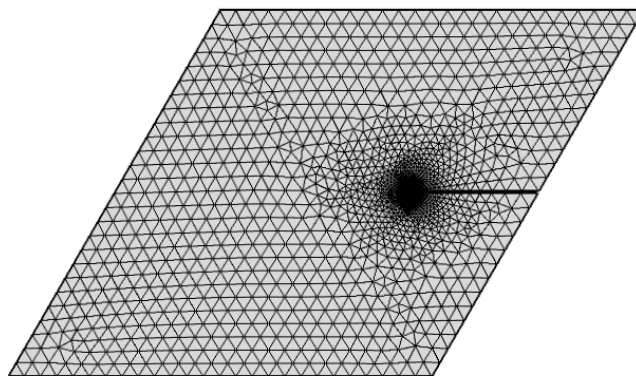
Figure 2.3: Mesh generation

2.3.8 Algorithm

The iterative Newton-Raphson method was the first to propose the algorithm; the discrete versions of the continuity, momentum, and energy equations are solved to obtain the value of the velocity and temperature. It is essential to make accurate predictions about the initial values of the variables. The numerical solutions for the variables are then produced while the convergent criteria are met. This is the last step. The flow chart (Figure 2.4) illustrates a simple algorithm.

Physical model

Governing equations

Boundary conditions

Mesh generation

Initial guess values of $U^*, V^*, \theta*$

Start

Forming 6x6 matrix against an element

Assemble all elements

Matrix factorization

U, V, θ

Converge

No

Yes

Stop
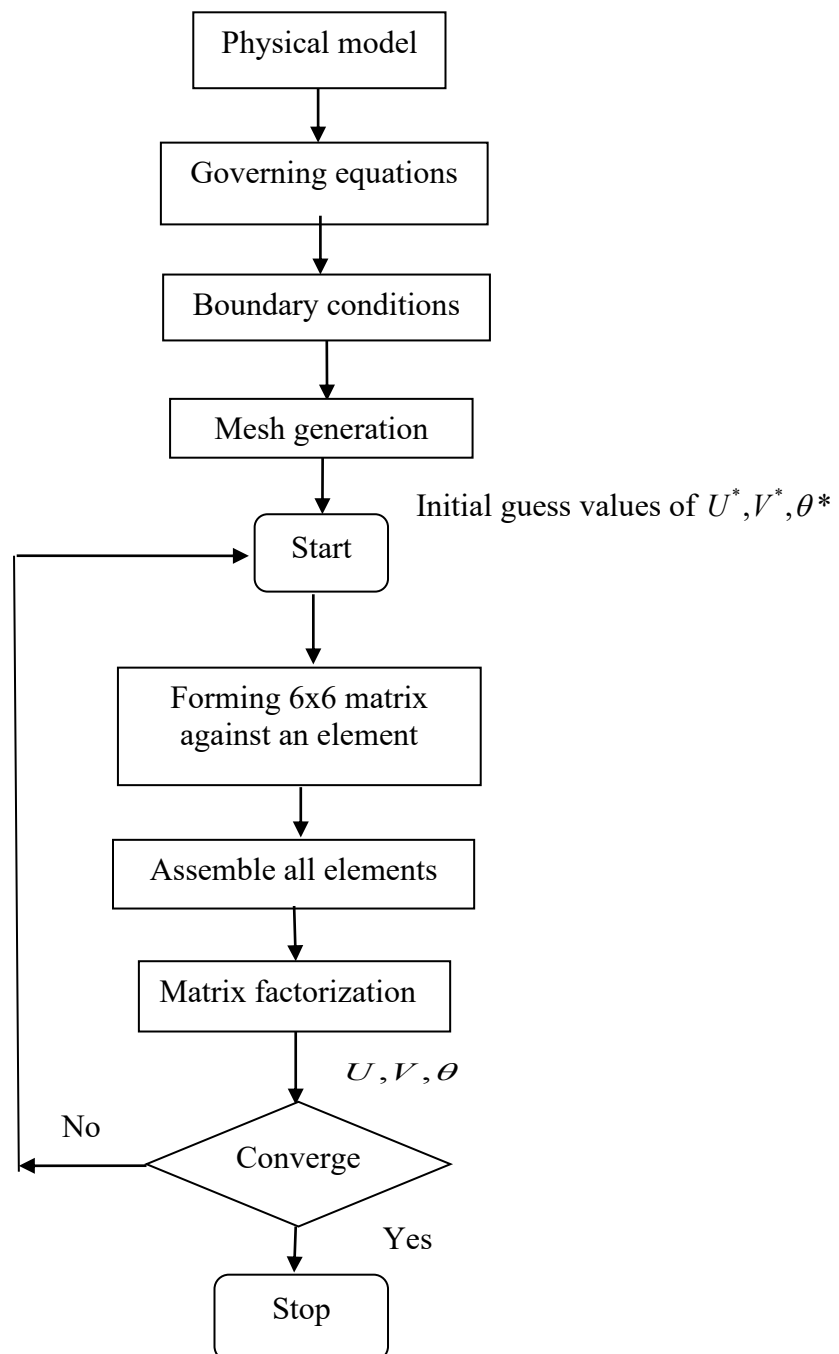
Figure 2.4: Flow chart of the computational procedure

2.4 GOVERNING EQUATIONS ALONG WITH BOUNDARY CONDITIONS

The following are the governing differential equations by Ambarita *et al.* [9] for natural convection flow are

$$\frac{\partial u}{\partial x} + \frac{\partial v}{\partial y} = 0 \tag{2.1}$$

$$u\frac{\partial u}{\partial x} + v\frac{\partial u}{\partial y} = -\frac{1}{\rho}\frac{\partial p}{\partial x} + \mu\nabla^2 u \tag{2.2}$$

$$u\frac{\partial v}{\partial x} + v\frac{\partial v}{\partial y} = -\frac{1}{\rho}\frac{\partial p}{\partial x} + \mu\nabla^2 v + \rho g\beta(T - T_c) \tag{2.3}$$

$$u\frac{\partial T}{\partial x} + v\frac{\partial T}{\partial y} = \alpha\nabla^2 T \tag{2.4}$$

where u and v are the velocity components along x and y axes, p is the pressure, ρ is the density, μ is the dynamic viscosity, β is the thermal expansion coefficient, T is the temperature and α is the thermal diffusivity.

2.4.1 Boundary conditions

All the boundaries have no-slip conditions, and the horizontal plane walls are adiabatically controlled in this system. The left inclined wall is kept at a sinusoidal condition by Varol *et al.* [34] as follows:

On the inclined left wall: $T(y) = T_{ref} \pm \nabla T \operatorname{Sin}\left(2\pi\frac{y}{S}\right)$ $\tag{2.5a}$

On the inclined right wall: $u = v = 0, T = T_h;$ $\tag{2.5b}$

On the top and bottom adiabatic wall: $u = v = \dfrac{\partial T}{\partial y} = 0;$ $\tag{2.5c}$

For the baffle: $u = v = 0, T = T_h;$ $\tag{2.5d}$

The governing equations (1)-(4) are resolved into non-dimensional forms by utilizing the dimensionless parameters:

$$X = \frac{x}{S}, Y = \frac{y}{S}, U = \frac{uS}{\alpha}, V = \frac{vS}{\alpha}, P = \frac{pS^2}{\rho\alpha^2}, \theta = \frac{T - T_c}{T_h - T_c}, D = \frac{d}{S}, L = \frac{l}{S}, B = \frac{b}{S} \tag{2.6}$$

The dimensionless governing equations are:

$$\frac{\partial U}{\partial X} + \frac{\partial V}{\partial Y} = 0 \tag{2.7}$$

$$U\frac{\partial U}{\partial X} + V\frac{\partial U}{\partial Y} = -\frac{\partial P}{\partial X} + \Pr \nabla^2 U \tag{2.8}$$

$$U\frac{\partial V}{\partial X} + V\frac{\partial V}{\partial Y} = -\frac{\partial P}{\partial X} + \Pr \nabla^2 V + Ra\,\Pr\,\theta \tag{2.9}$$

$$U\frac{\partial \theta}{\partial X} + V\frac{\partial \theta}{\partial Y} = \nabla^2 \theta \tag{2.10}$$

The parameters Ra and Pr are representing to be Rayleigh and Prandtl number are defined as follows:

$$Ra = \frac{g\beta(T_h - T_c)S^3}{\alpha v}, \; Pr = \frac{v}{\alpha}, \; \alpha = \frac{\kappa}{\rho C_p} \tag{2.11}$$

where v is the kinematic viscosity, κ denotes thermal conductivity and C_p denotes the specific heat.

The dimensionless boundary conditions for the transformed governing equations are:
On the inclined right wall: $U = V = 0, \theta = 1$ (2.12a)

On the upper and lower adiabatic walls: $U = V = \frac{\partial \theta}{\partial Y} = 0$ (2.12b)

On the inclined left wall: $U = V = 0, \theta = \lambda \sin(2\pi Y)$ (2.12c)

For the baffle: $U = V = 0, \theta = 1$ (2.12d)

Nusselt Number:
The performance rate of heat transport can be obtained by using the following equations of the Nusselt number,

$$Nu_{local} = -\left.\frac{\partial \theta}{\partial N}\right|_{surface} \tag{2.13}$$

The average Nusselt number on the sloping right inclined wall is examined in this section.

$$Nu_{avg} = \int_0^1 Nu_{local}\,dS \tag{2.14}$$

Effectiveness

Baffle effectiveness is a variable that measures the heat conversion augmentation inside an enclosure where the baffle is compared to a case without baffle, defined by Elatar *et al.* [17] as follows:

$$E_f = \frac{Q_{baffle}}{Q_{withoutbaffle}} \tag{2.15}$$

Angle effectiveness (A_{ef}) is the characteristic that measures the heat removal coefficient within the cavity when an angle is compared to a case $\alpha = 90^0$.

$$A_{ef} = \frac{Q_{\alpha<90^0<\alpha}}{Q_{\alpha=90^0}} \tag{2.16}$$

2.5 NUMERICAL ANALYSIS

The numerical solution of the governing equations and boundary conditions is accomplished using Galerkin weighted residual finite element techniques. This study has not presented the solution flow charts and specific computational processes because the fundamental numerical analysis has been preserved in the built-in function of COMSOL Multi-physics.

2.5.1 Finite Element Formulation and Computational Procedure

Natural convective heat alteration performance by linking Galerkin weighted residual (GWR) finite element process; the governing dimensionless equations (2.7) -(2.10) together with the non-dimensional boundary conditions (2.12a) -(2.12d) are solved numerically.

To derive the finite element equations, the method of weighted residuals Taylor and Hood [47] is applied to the equations (2.7) – (2.10) as

$$\int_A N_\alpha \left(\frac{\partial U}{\partial X} + \frac{\partial V}{\partial Y} \right) dA = 0 \tag{2.17}$$

$$\int_A N_\alpha \left(U \frac{\partial U}{\partial X} + V \frac{\partial U}{\partial Y} \right) dA = -\int_A H_\lambda \left(\frac{\partial P}{\partial X} \right) dA + Pr \int_A N_\alpha \left(\frac{\partial^2 U}{\partial X^2} + \frac{\partial^2 U}{\partial Y^2} \right) dA \qquad (2.18)$$

$$\int_A N_\alpha \left(U \frac{\partial V}{\partial X} + V \frac{\partial V}{\partial Y} \right) dA = -\int_A H_\lambda \left(\frac{\partial P}{\partial Y} \right) dA + Pr \int_A N_\alpha \left(\frac{\partial^2 V}{\partial X^2} + \frac{\partial^2 V}{\partial Y^2} \right) dA$$
$$+ Ra \, Pr \int_A N_\alpha \theta \, dA \qquad (2.19)$$

$$\int_A N_\alpha \left(U \frac{\partial \theta}{\partial X} + V \frac{\partial \theta}{\partial Y} \right) dA = \int_A N_\alpha \left(\frac{\partial^2 \theta}{\partial X^2} + \frac{\partial^2 \theta}{\partial Y^2} \right) dA \qquad (2.20)$$

where A is the element area, N_α (α = 1, 2, … …, 6) are the element interpolation functions for the velocity components and the temperature, and H_λ (λ = 1, 2, 3) are the element interpolation functions for the pressure.

Gauss's theorem is then applied to equations (2.18) -(2.20) to generate the boundary integral terms associated with the surface tractions and heat flux. Then equations (2.10) -(2.12) become,

$$\int_A N_\alpha \left(U \frac{\partial U}{\partial X} + V \frac{\partial U}{\partial Y} \right) dA + \int_A H_\lambda \left(\frac{\partial P}{\partial X} \right) dA$$
$$+ Pr \int_A \left(\frac{\partial N_\alpha}{\partial X} \frac{\partial U}{\partial X} + \frac{\partial N_\alpha}{\partial Y} \frac{\partial U}{\partial Y} \right) dA = \int_{S_0} N_\alpha S_x dS_0 \qquad (2.21)$$

$$\int_A N_\alpha \left(U \frac{\partial V}{\partial X} + V \frac{\partial V}{\partial Y} \right) dA + \int_A H_\lambda \left(\frac{\partial P}{\partial Y} \right) dA + Pr \int_A \left(\frac{\partial N_\alpha}{\partial X} \frac{\partial V}{\partial X} + \frac{\partial N_\alpha}{\partial Y} \frac{\partial V}{\partial Y} \right) dA$$
$$- Ra \, Pr \int_A N_\alpha \theta \, dA = \int_{S_0} N_\alpha S_y dS_0 \qquad (2.22)$$

$$\int_A N_\alpha \left(U \frac{\partial \theta}{\partial X} + V \frac{\partial \theta}{\partial Y} \right) dA + \int_A \left(\frac{\partial N_\alpha}{\partial X} \frac{\partial \theta}{\partial X} + \frac{\partial N_\alpha}{\partial Y} \frac{\partial \theta}{\partial Y} \right) dA = \int_{S_w} N_\alpha q_w dS_w \qquad (2.23)$$

Here (2.21) -(2.22) specifying surface tractions (S_x, S_y) along outflow boundary S_0 and (2.23) specifying velocity components and fluid temperature or heat flux (q_w) that flows into or out from domain along wall boundary S_w.

The basic unknowns for the above differential equations are the velocity components U, V the temperature, θ and the pressure, P. The six-node triangular element is used in this work for the development of the finite element equations. All six nodes are associated with velocities as well as temperature; only the corner nodes are associated with pressure. This means that a lower order polynomial is chosen for pressure, and which is satisfied through continuity equation. The velocity component and the temperature distributions and linear interpolation for the pressure distribution according to their highest derivative orders in the differential equations (2.7) -(2.10) as

$$U(X,Y) = N_\beta U_\beta \tag{2.24}$$

$$V(X,Y) = N_\beta V_\beta \tag{2.25}$$

$$\theta(X,Y) = N_\beta \theta_\beta \tag{2.26}$$

$$P(X,Y) = H_\lambda P_\lambda \tag{2.27}$$

where $\beta = 1, 2, \ldots \ldots, 6; \lambda = 1, 2, 3.$

Substituting the element velocity component distributions, the temperature distribution, and the pressure distribution from equations (2.24) -(2.27), the finite element equations can be written in the form,

$$K_{\alpha\beta^x} U_\beta + K_{\alpha\beta^y} V_\beta = 0 \tag{2.28}$$

$$K_{\alpha\beta\gamma^x} U_\beta U_\gamma + K_{\alpha\beta\gamma^y} V_\gamma U_\gamma + M_{\alpha\mu^x} P_\mu + Pr\left(S_{\alpha\beta^{xx}} + S_{\alpha\beta^{yy}}\right) U_\beta = U_{\alpha^u} \tag{2.29}$$

$$K_{\alpha\beta\gamma^x} U_\beta V_\gamma + K_{\alpha\beta\gamma^y} V_\beta V_\gamma + M_{\alpha\mu^y} P_\mu + Pr\left(S_{\alpha\beta^{xx}} + S_{\alpha\beta^{yy}}\right) V_\beta$$
$$- Ra\, Pr K_{\alpha\beta} \theta_\beta = Q_{\alpha^v} \tag{2.30}$$

$$K_{\alpha\beta\gamma^x} U_\beta \theta_\gamma + K_{\alpha\beta\gamma^y} V_\beta \theta_\gamma + \left(S_{\alpha\beta^{xx}} + S_{\alpha\beta^{yy}}\right) \theta_\beta = Q_{\alpha^\theta} \tag{2.31}$$

where the coefficients in element matrices are in the form of the integrals over the element area and along the element edges S_0 and S_w as

$$K_{\alpha\beta x} = \int_A N_\alpha N_{\beta,x} dA \tag{2.32a}$$

$$K_{\alpha\beta y} = \int_A N_\alpha N_{\beta,y} dA \tag{2.32b}$$

$$K_{\alpha\beta\gamma x} = \int_A N_\alpha N_\beta N_{\gamma,x} dA \tag{2.32c}$$

$$K_{\alpha\beta\gamma y} = \int_A N_\alpha N_\beta N_{\gamma,y} dA \tag{2.32d}$$

$$K_{\alpha\beta} = \int_A N_\alpha N_\beta dA \tag{2.32e}$$

$$S_{\alpha\beta xx} = \int_A N_{\alpha,x} N_{\beta,x} dA \tag{2.32f}$$

$$S_{\alpha\beta yy} = \int_A N_{\alpha,y} N_{\beta,y} dA \tag{2.32g}$$

$$M_{\alpha\mu x} = \int_A H_\alpha H_{\mu,x} dA \tag{2.32h}$$

$$M_{\alpha\mu y} = \int_A H_\alpha H_{\mu,y} dA \tag{2.32i}$$

$$Q_{\alpha\omega} = \int_{S_0} N_\alpha S_x dS_0 \tag{2.32j}$$

$$Q_{\alpha\psi} = \int_{S_0} N_\alpha S_y dS_0 \tag{2.32k}$$

$$Q_{\alpha\theta} = \int_{S_w} N_\alpha q_w dS_w \tag{2.32l}$$

These element matrices are evaluated in closed form ready for numerical simulation. Details of the derivation for these element matrices are omitted herein.

The derived finite element equations (2.28) -(2.31) are nonlinear. These nonlinear algebraic equations are solved by applying the Newton-Raphson iteration technique by first writing the unbalanced values from the set of the finite element equations (2.28) -(2.31) as,

$$F_{\alpha}{}^{p} = K_{\alpha\beta}{}^{x}U_{\beta} + K_{\alpha\beta}{}^{y}V_{\beta} \tag{2.33a}$$

$$\begin{aligned}
F_{\alpha}{}^{u} &= K_{\alpha\beta\gamma}{}^{x}U_{\beta}U_{\gamma} + K_{\alpha\beta\gamma}{}^{y}V_{\gamma}U_{\gamma} + M_{\alpha\mu}{}^{x}P_{\mu} \\
&\quad + Pr(S_{\alpha\beta}{}^{xx} + S_{\alpha\beta}{}^{yy})U_{\beta} - Q_{\alpha}{}^{u}
\end{aligned} \tag{2.33b}$$

$$\begin{aligned}
F_{\alpha}{}^{v} &= K_{\alpha\beta\gamma}{}^{x}U_{\beta}V_{\gamma} + K_{\alpha\beta\gamma}{}^{y}V_{\gamma}V_{\gamma} + M_{\alpha\mu}{}^{y}P_{\mu} + \\
&\quad Pr(S_{\alpha\beta}{}^{xx} + S_{\alpha\beta}{}^{yy})V_{\beta} - Q_{\alpha}{}^{v}
\end{aligned} \tag{2.33c}$$

$$F_{\alpha}{}^{\theta} = K_{\alpha\beta\gamma}{}^{x}U_{\beta}\theta_{\gamma} + K_{\alpha\beta\gamma}{}^{y}V_{\beta}U_{\gamma} + \left(S_{\alpha\beta}{}^{xx} + S_{\alpha\beta}{}^{yy}\right)\theta_{\beta} - Q_{\alpha}{}^{\theta} \tag{2.33d}$$

This leads to a set of algebraic equations with the incremental unknowns of the element nodal velocity components, temperatures, and pressures in the form,

$$\begin{bmatrix} K_{pu} & K_{pv} & 0 & 0 \\ K_{uu} & K_{uv} & 0 & K_{up} \\ K_{\theta u} & K_{\theta v} & K_{\theta\theta} & 0 \\ K_{vu} & K_{vv} & K_{v\theta} & K_{vp} \end{bmatrix} \begin{Bmatrix} \Delta p \\ \Delta u \\ \Delta\theta \\ \Delta v \end{Bmatrix} = - \begin{Bmatrix} F_{\alpha}{}^{p} \\ F_{\alpha}{}^{u} \\ F_{\alpha}{}^{\theta} \\ F_{\alpha}{}^{v} \end{Bmatrix} \tag{2.34}$$

where $K_{uu} = K_{\alpha\beta\gamma}{}^{x}U_{\beta} + K_{\alpha\gamma\beta}{}^{x}U_{\gamma} + K_{\alpha\beta\gamma}{}^{y}V_{\beta} + Pr\left(S_{\alpha\beta}{}^{xx} + S_{\alpha\beta}{}^{yy}\right)$

$K_{uv} = K_{\alpha\beta\gamma}{}^{y}U_{\gamma}$

$K_{u\theta} = 0$, $K_{up} = M_{\alpha\mu}{}^{x}$

$K_{vu} = K_{\alpha\beta\gamma}{}^{x}V_{\gamma}$

$K_{vv} = K_{\alpha\beta\gamma}{}^{x}U_{\beta} + K_{\alpha\gamma\beta}{}^{y}V_{\gamma} + K_{\alpha\beta\gamma}{}^{y}V_{\gamma} + Pr\left(S_{\alpha\beta}{}^{xx} + S_{\alpha\beta}{}^{yy}\right)$

$K_{v\theta} = -Ri\,K_{\alpha\beta}$, $K_{vp} = M_{\alpha\mu}{}^{y}$

$K_{\theta u} = K_{\alpha\beta\gamma}{}^{x}\theta_{\gamma}$, $K_{\theta v} = K_{\alpha\beta\gamma}{}^{y}\theta_{\gamma}$

$K_{\theta\theta} = K_{\alpha\beta\gamma}{}^{x}U_{\beta} + K_{\alpha\beta\gamma}{}^{y}V_{\beta} + (S_{\alpha\beta}{}^{xx} + S_{\alpha\beta}{}^{yy})$

$K_{\theta p} = 0$, $K_{pu} = K_{\alpha\beta}{}^{x}$, $K_{pv} = K_{\alpha\beta}{}^{y}$ and $K_{p\theta} = K_{pp} = 0$

The iteration process is terminated if the percentage of the overall change compared to the previous iteration is less than the specified value.

To solve the sets of the global nonlinear algebraic equations in the form of matrix, the Newton-Raphson iteration technique has been adapted through PDE solver with MATLAB interface. The convergence of solutions is assumed when the relative error for each variable between consecutive iterations is recorded below the convergence criterion ε such that $\left|\Phi^{n+1} - \Phi^n\right| < \varepsilon$, where n is number of iteration and $\Phi = U, V, \theta$. The convergence criterion was set to $\varepsilon = 10^{-5}$.

2.5.2 Grid Size Sensitivity Test

The current investigation makes use of a non-uniform free triangular and untagged grid structure. The significance of grid size on the precision of expected outcomes is investigated using five distinct grid structures of finite elements. The numerical findings are seen in Table 2.1 and in Figure 2.5; they indicate that there are no major improvements near the Grid - 8 and beyond. As a result, the Grid - 8 offered a suitable approach for all this investigation's computations.

Table 2.1: Grid testing for Nu_{avg} at various grid sizes for $\alpha = 60^{0}$ and $Ra = 10^{4}$

Grid size	Nodes	Elements	Nu_{avg}
Grid - 1	207	365	1.0147516836523418
Grid - 2	395	721	1.0520702553090469
Grid - 3	590	1090	1.0935497209932326
Grid - 4	890	1668	1.1052335134905118
Grid - 5	1590	3026	1.1237723365748096
Grid - 6	2639	5076	1.1482213550982552
Grid - 7	4940	9602	1.1621835303699541
Grid - 8	13178	25849	**1.1799940912535507**
Grid -9	41608	82294	1.1874665563900535
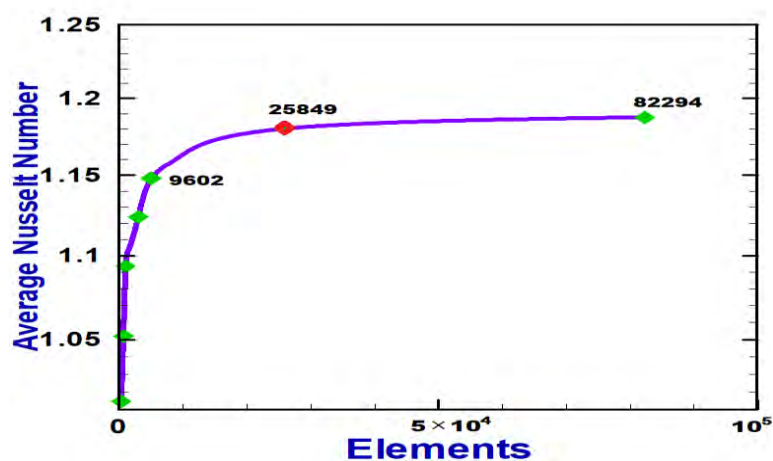
Figure 2.5: Grid testing for Nu_{avg} versus several elements

2.5.3 Validation of the Numerical Scheme

The current numerical code is validated by contrasting it to the previously reported work Elatar *et al.* [17], as shown in Figure 2.6. The variation of local Nusselt number are highly identical and can visualize the strong unification of present results with Elatar *et al.* [17], as viewed in Figure 2.6.

Elatar *et al.* [17]	Present work
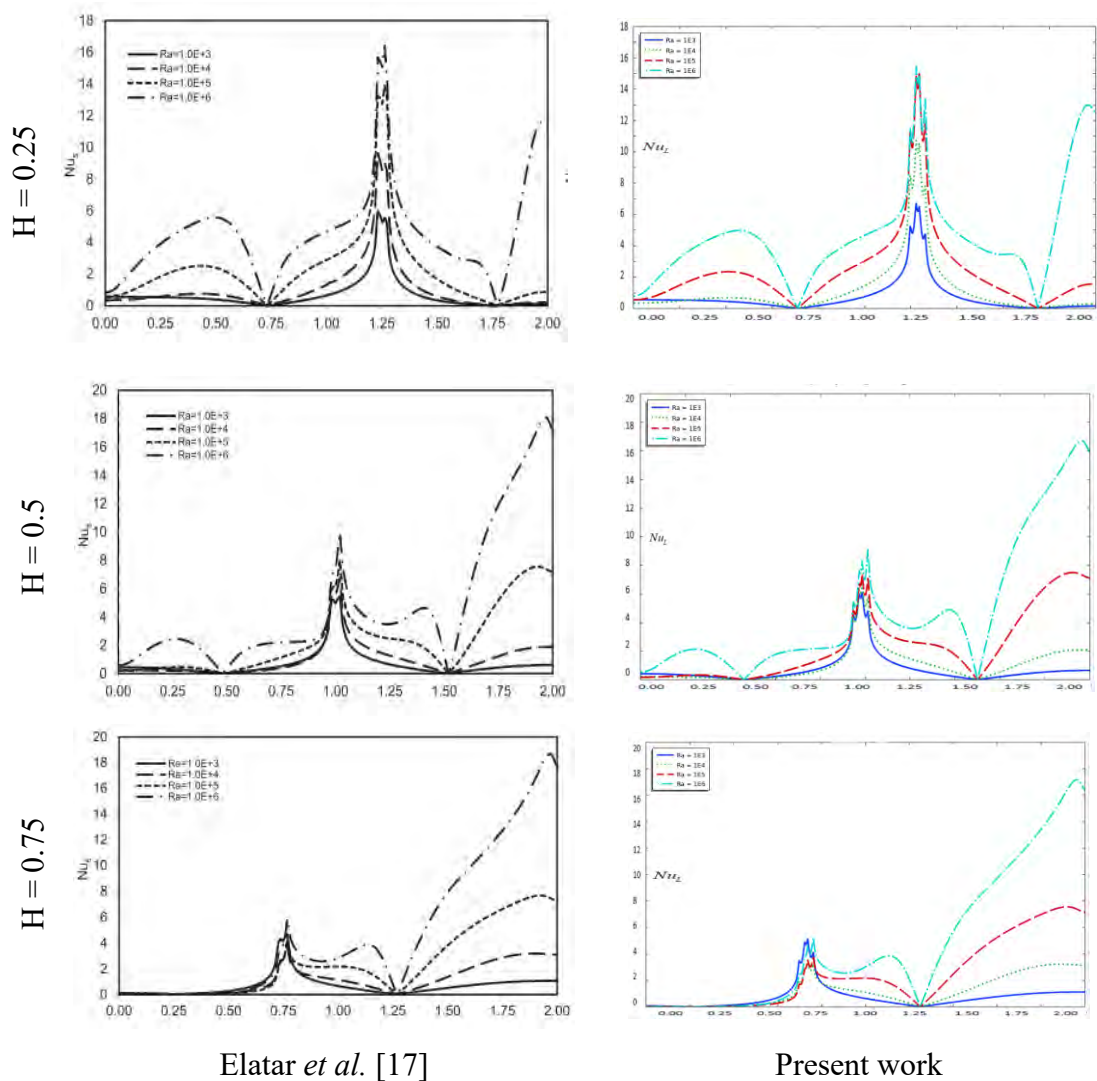
Figure 2.6: Comparisons between the outcome of Elatar *et al.* [17] and present work at $Ra = 10^4$, $L = 0.50$, $Pr = 0.71$.

Table 2.2: Comparisons of the average Nusselt number on cold wall among Elatar *et al.* [17], Nag *et al.* [11] and present work at $Ra = 10^6$, $L = 0.20$, and $Pr = 0.71$ is given in the following table:

B	0.02	0.04	0.1
Nag *et al* [11]	8.672	8.710	8.947
Elatar *et al.* [17]	8.861	8.888	9.033
present works	8.778	8.843	8.897

As shown in Table 2.2, the average Nusselt numbers are in good agreement with those reported by Nag *et al.* [11], and Elatar *et al.* [17]. These comprehensive validation efforts demonstrate the robustness and accuracy of the present numerical method.

1. Results and Discussions

This study examines the set of parameters for constant Prandtl number Pr = 1.41, skew angles $(15^0 \leq \alpha \leq 165^0)$. The length of the baffle (L = 0.20, 0.30, 0.50), the location of the baffle is set on the middle point of the right inclined wall, and the thickness of the baffle (D = 0.005) for the Rayleigh number $(10^3 \leq Ra \leq 10^6)$ are used for the investigation. The sinusoidal amplitude $\lambda = 0.50$ have been numerically analyzed for the temperature distribution and the flow sequence due to natural convection on the skewed cavity having an inclined left wall temperature varying sinusoidally. The results are shown graphically using velocity profiles, local Nusselt numbers, and heat transfer rates based on the average Nusselt number (Nu_{avg}) and the average fluid temperature. The baffle effectiveness (E_f) and angle effectiveness (A_{ef}) are shown as well as the measures of the baffle and skew angle performance. Results and the discussion are given using 3 cases starting with the effect of the skew angles for the fixed baffle length L = 0.20.

Case-I: (Effect of the skew angles for the baffle length L= 0.20)

Findings from streamlines:

Figure 3.1(a)-(f) show streamlines for different Rayleigh numbers $(10^3 \leq Ra \leq 10^6)$ with baffle lengths (L = 0.20), where the baffle is attached at the middle position of the inclined right wall inside the skewed enclosure. From Figure 3.1(a)-(f), it is found that the maximum velocities gradually increase with the increase of the Rayleigh number for all the cases of the skew angles. For different skew angles at a fixed baffle position, a larger principal cell was created, with its center roughly in the center of the cavity. Figure 3.1(a)-(f) illustrates that for higher Rayleigh number from $Ra = 10^5$ to $Ra = 10^6$, the center of the cell looks to get divided for all skew angles.

Moreover, all other values of the Rayleigh numbers at a constant baffle size and location produce one cell. Furthermore, at $Ra = 10^6$ for the skew angles ($\alpha = 90^0, \alpha = 120^0$, and $\alpha = 150^0$), the middle of the cell is separated into two cells. The flow structure becomes more substantial as the Rayleigh numbers increase, overlooking the moving vortices that climb the wall for baffle sizes and skew angles. The fluid flow is transmitted from the heated partition of inclined vertical wall in the cavity due to the buoyancy's effect.

The streamlines characterize how the strength of buoyancy inside the cavity is significant when Ra is between $Ra = 10^4$ and $Ra = 10^5$. There is also at least elliptic-shaped vortex inside the cavity. When $Ra = 10^6$, the strength of buoyancy inside the cavity is even more significant, and an elliptic-shaped cell appears inside the cavity once again. The schematic fact behind it is that the higher Rayleigh number increases the buoyancy force to influence the flow field. In the streamline of figure 3.1(a)-(f), we observed the maximum velocity progressively rising with increases in the skew angle up to $\alpha = 90^0$ for all the instances of the baffle lengths. After that, by raising the skew angle to $\alpha = 165^0$, the maximum velocity gradually decreases. Coincidently the skew angle $\alpha = 15^0$ and $\alpha = 165^0$ produces the same value which is 0.0018 ms^{-1} at $Ra = 10^3$ as expected. Furthermore, as previously stated, the maximum velocity increases as the Rayleigh number rises. In clockwise and counterclockwise rotating directions, two small cells are formed in the left and right corners, respectively. Finally, for the baffle length $L = 0.20$ the maximum velocity at $\alpha = 90^0$ is $49ms^{-1}$ with $Ra = 10^6$.
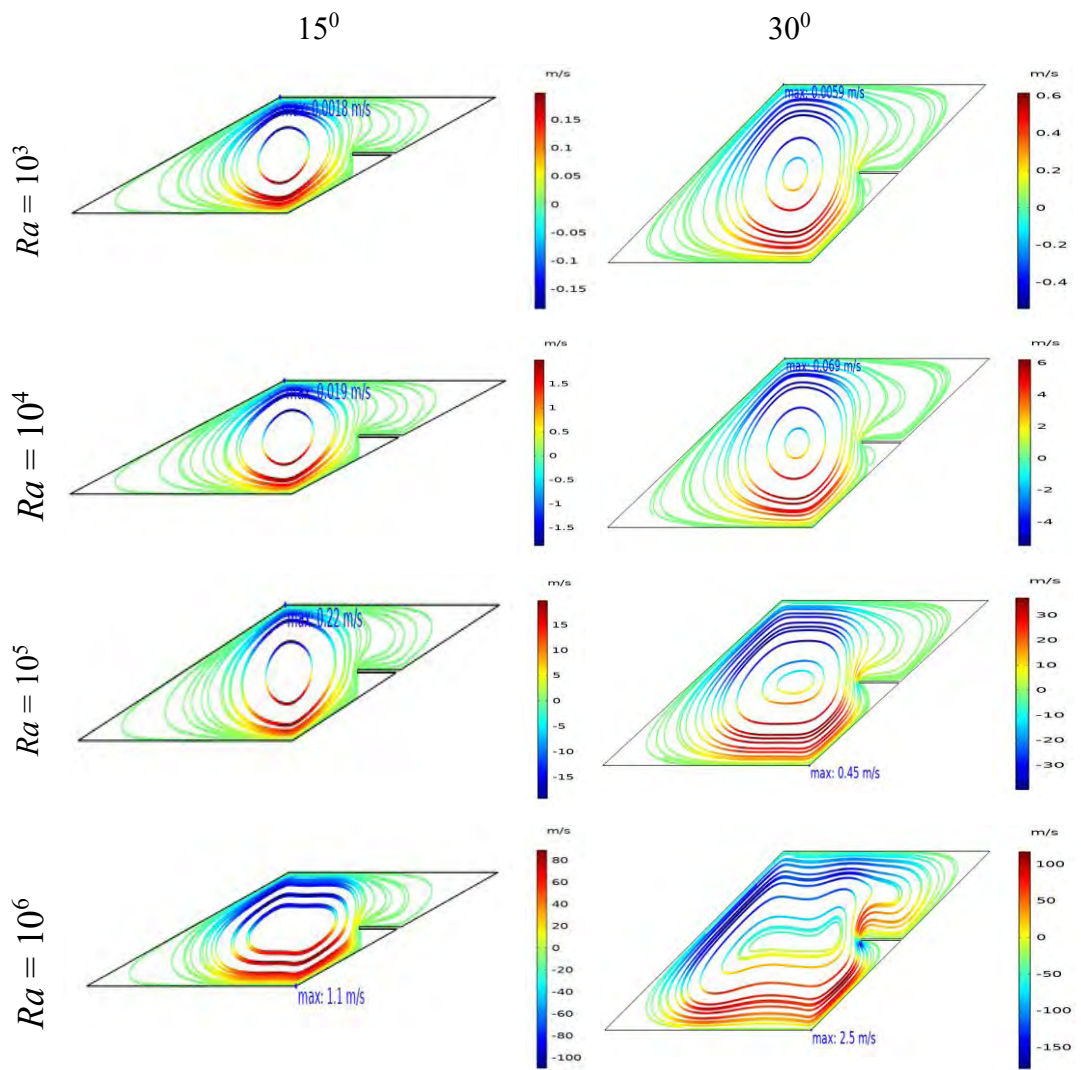
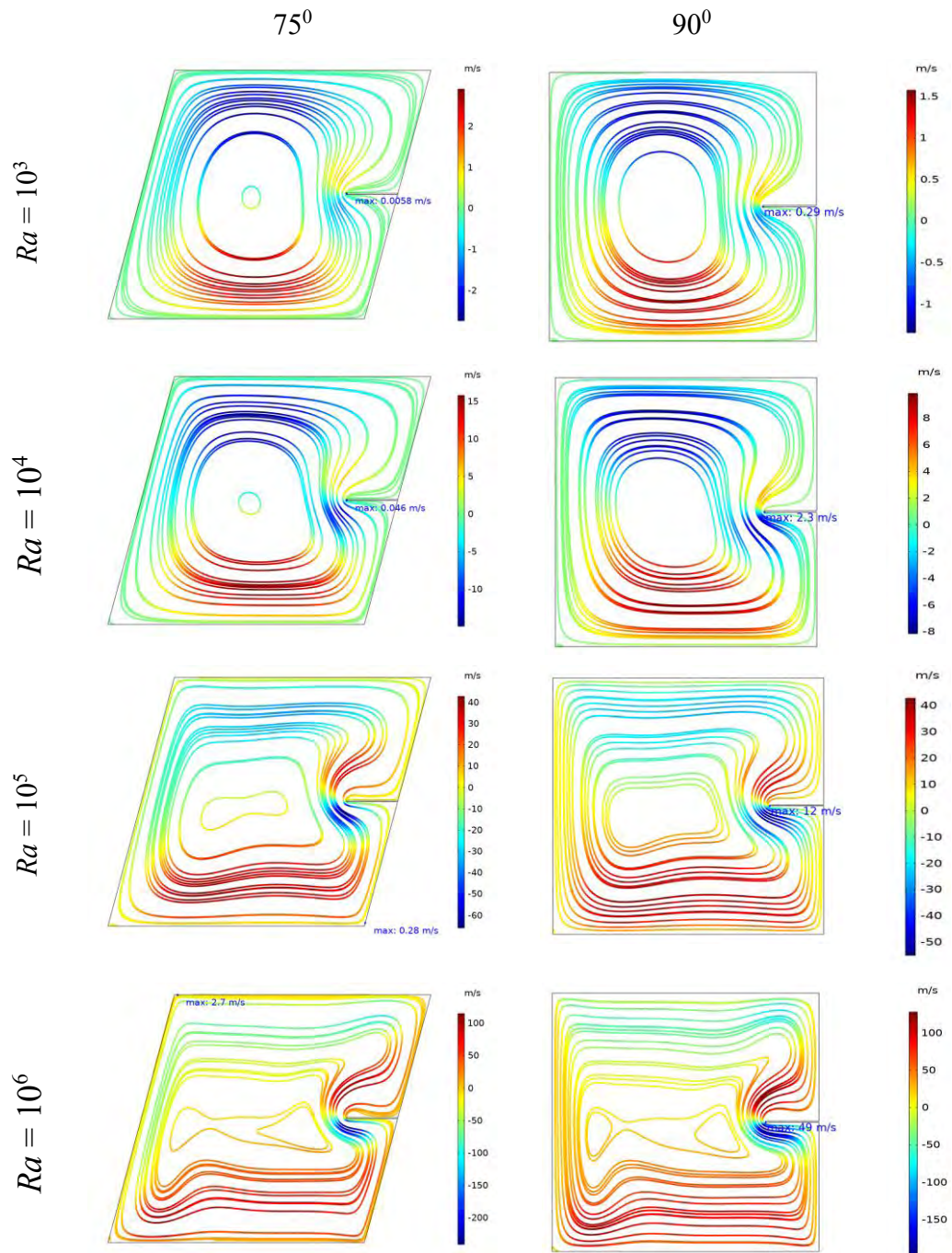**Figure 3.1 (a):** Streamline variations for various skew angles ($\alpha = 15^0, and\ \alpha = 30^0$) at $L = 0.20$.
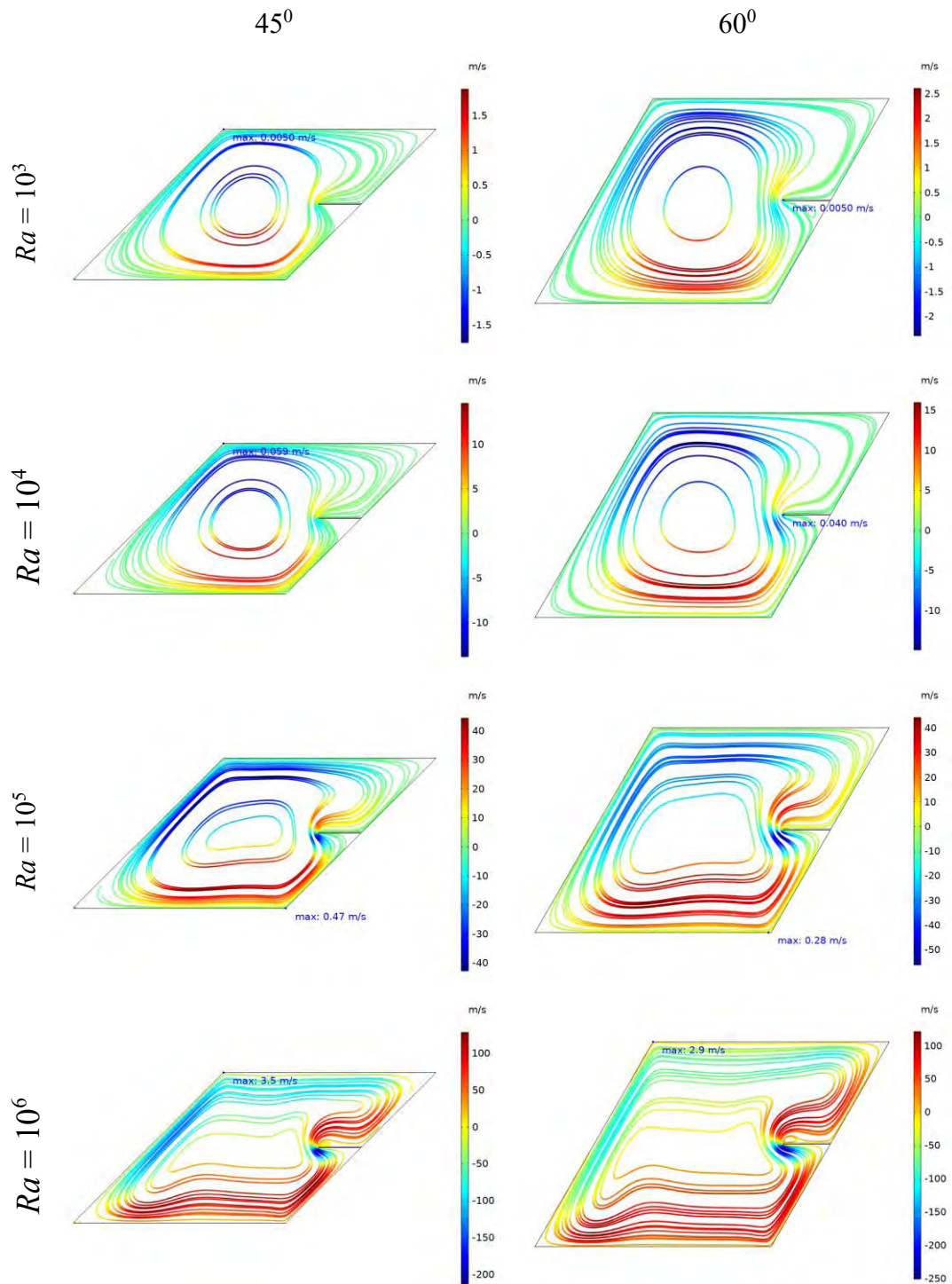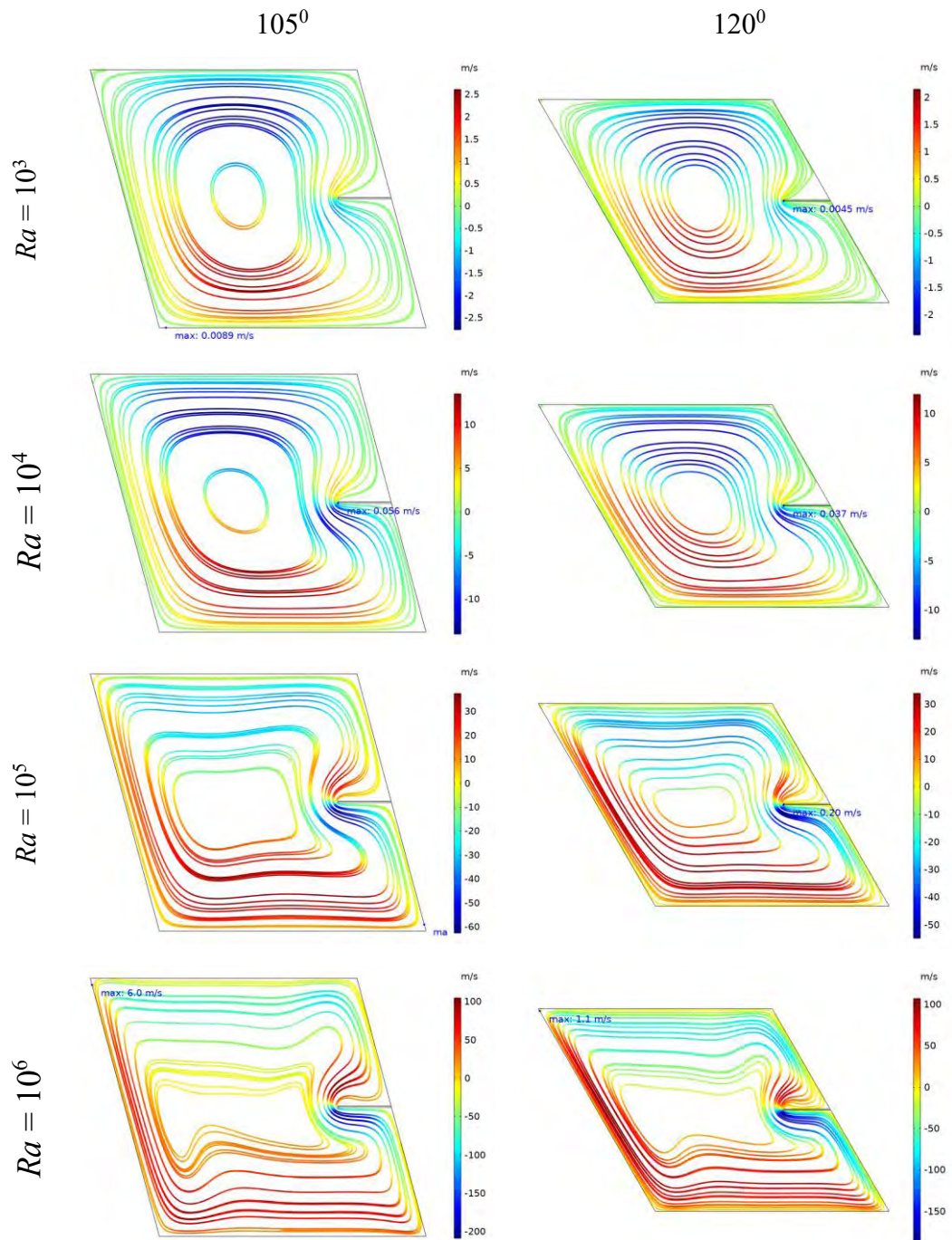
Figure 3.1(b): Streamline variations for various skew angles ($\alpha = 45^0, and\ \alpha = 60^0$) at $L = 0.20$.

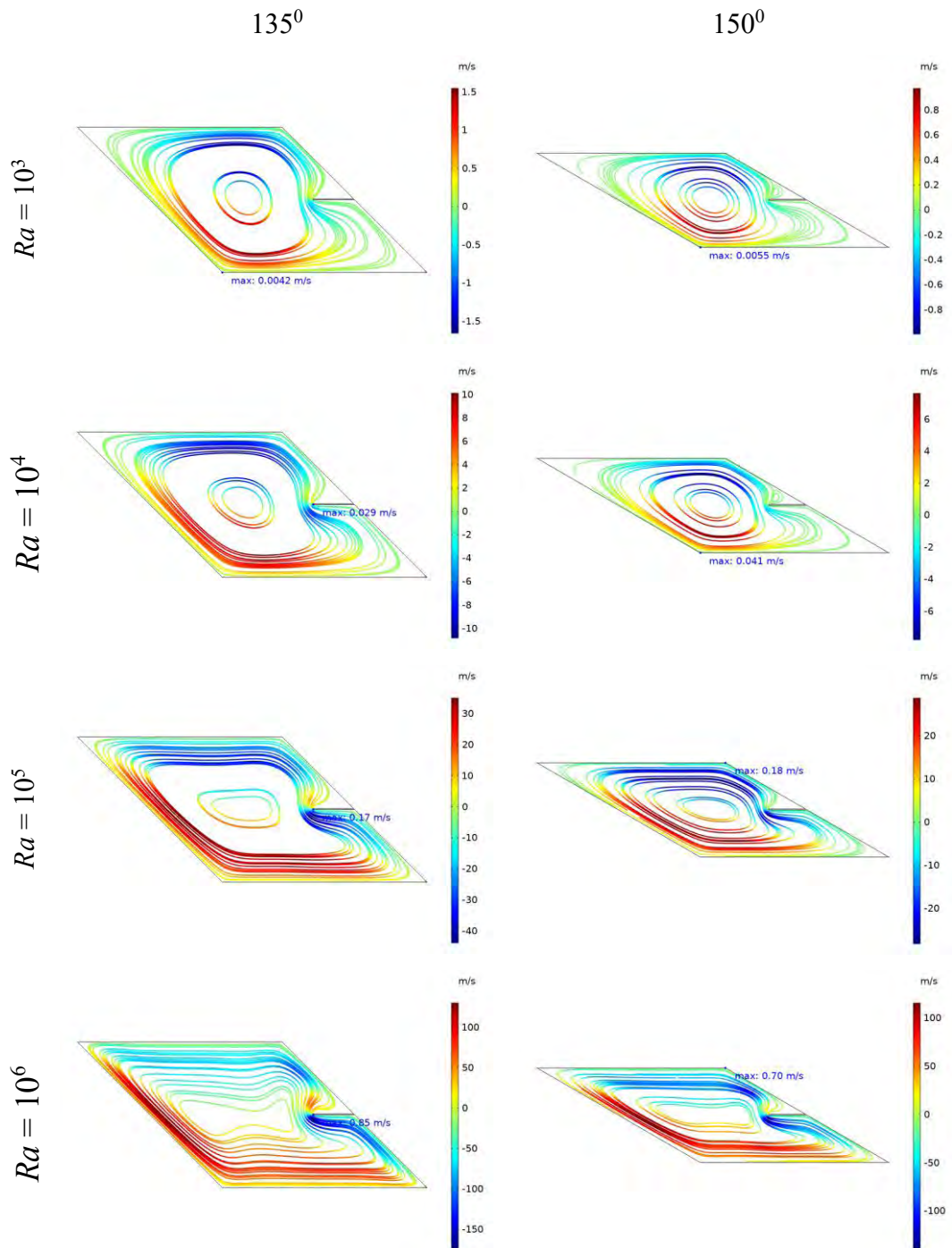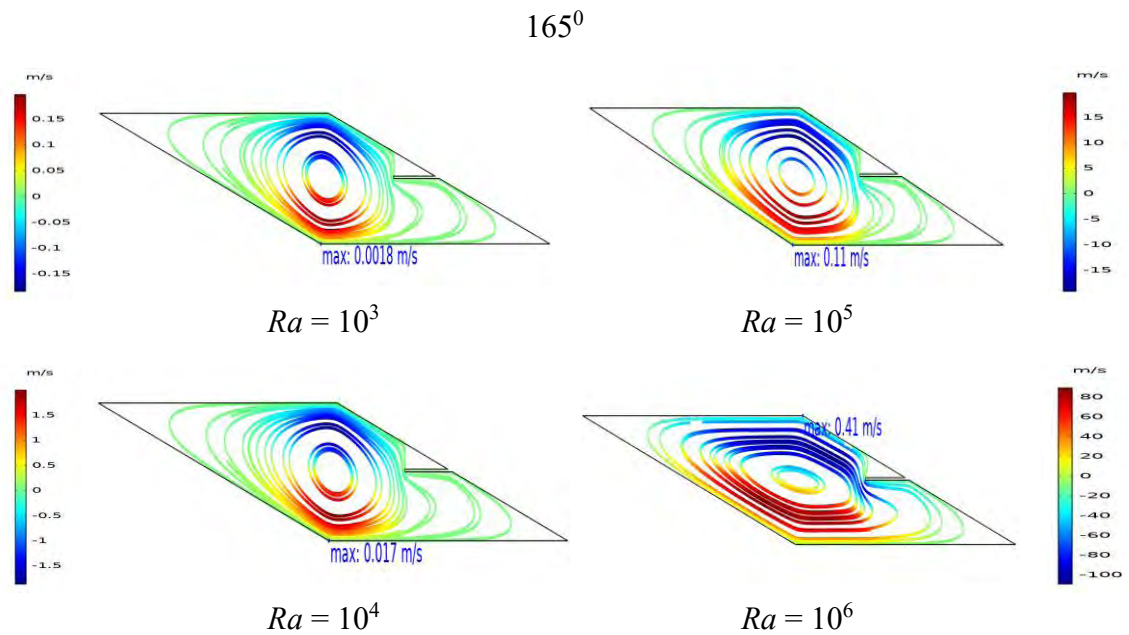**Figure 3.1(c):** Streamline variations for various skew angles ($\alpha = 75^0, and\ \alpha = 90^0$)

at $L = 0.20$.

105^0 120^0

$Ra = 10^3$

$Ra = 10^4$

$Ra = 10^5$

$Ra = 10^6$

Figure 3.1(d): Streamline variations for skew angles ($\alpha = 105^0, and \ \alpha = 120^0$)

at L = 0.20.

135^0 150^0

Figure 3.1 (e): Streamline variations for skew angles ($\alpha = 135^0, and\ \alpha = 150^0$)

at $L = 0.20$.

165^0

$Ra = 10^3$

$Ra = 10^5$

$Ra = 10^4$

$Ra = 10^6$

Figure 3.1 (f): Streamline variations for skew angles ($\alpha = 165^0$) at $L = 0.20$.

Findings from isotherms:

The conduction dominant heat transfer is demonstrated in Figure 3.2 (a)-(f), the results in the form of isotherms, which include for various Rayleigh number $(10^3 \le Ra \le 10^6)$, for various skew angles $(15^0 \le \alpha \le 165^0)$ at a constant baffle length and position. From Figure 3.2(a)-(c), the isotherm lines inside the enclosures become even more significant for all the values of Rayleigh number $(10^3 \le Ra \le 10^6)$ at $\alpha = 45^0$. Again, from Figure 3.2 (d)-(f), the isotherm lines within the enclosure become significant and the curvature get densed on the lower side of the baffle and top corner of left inclined surfaces for all skew angles and the Rayleigh numbers for constant baffle size and location. Also found that the isotherm lines exhibit variability for the Rayleigh number $(10^3 \le Ra \le 10^6)$. The curve of the isotherms augments with increasing Ra, and got thickened to the inclined side walls and at the baffle surfaces, which means growing heat transfer through convection.

15^0 30^0

$Ra = 10^3$

$Ra = 10^4$

$Ra = 10^5$

$Ra = 10^6$
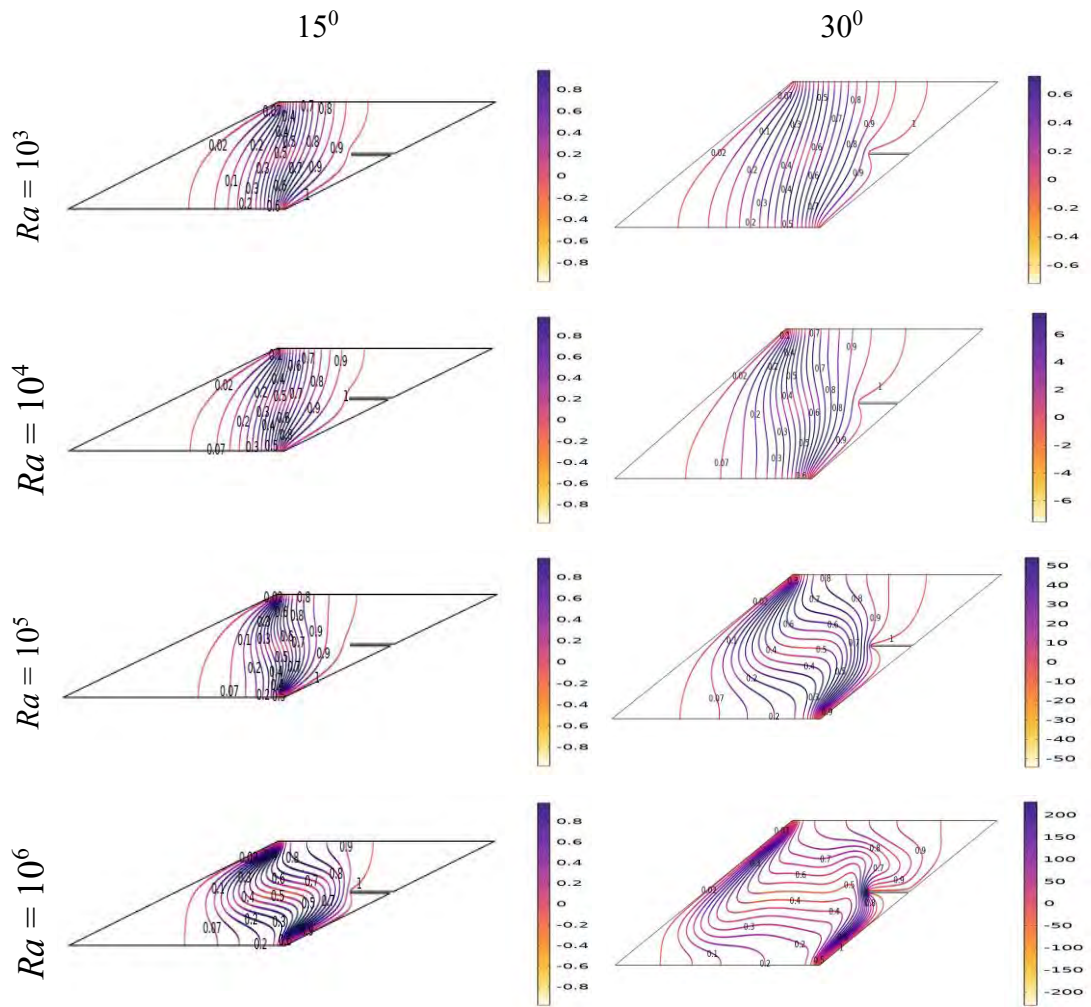
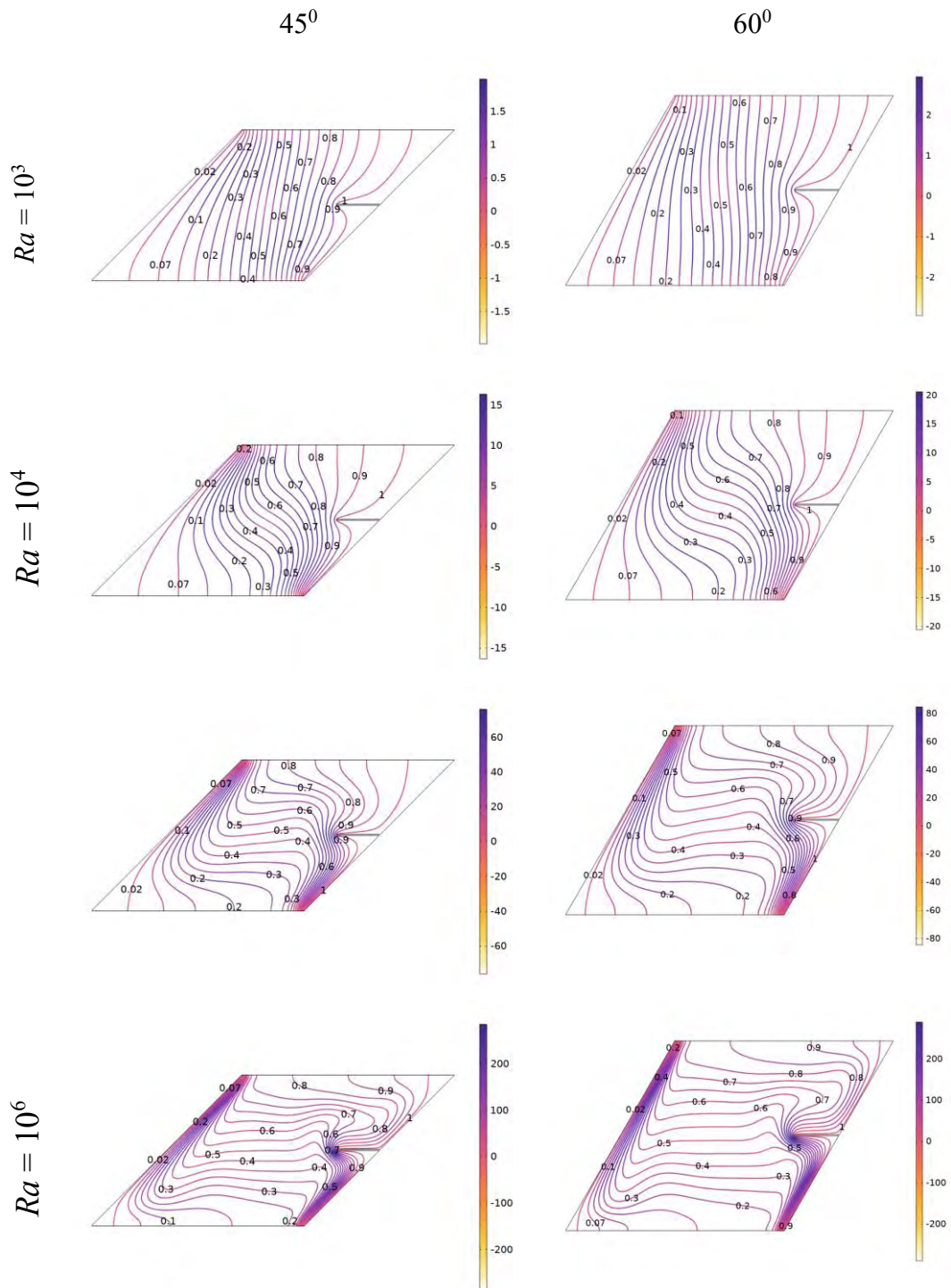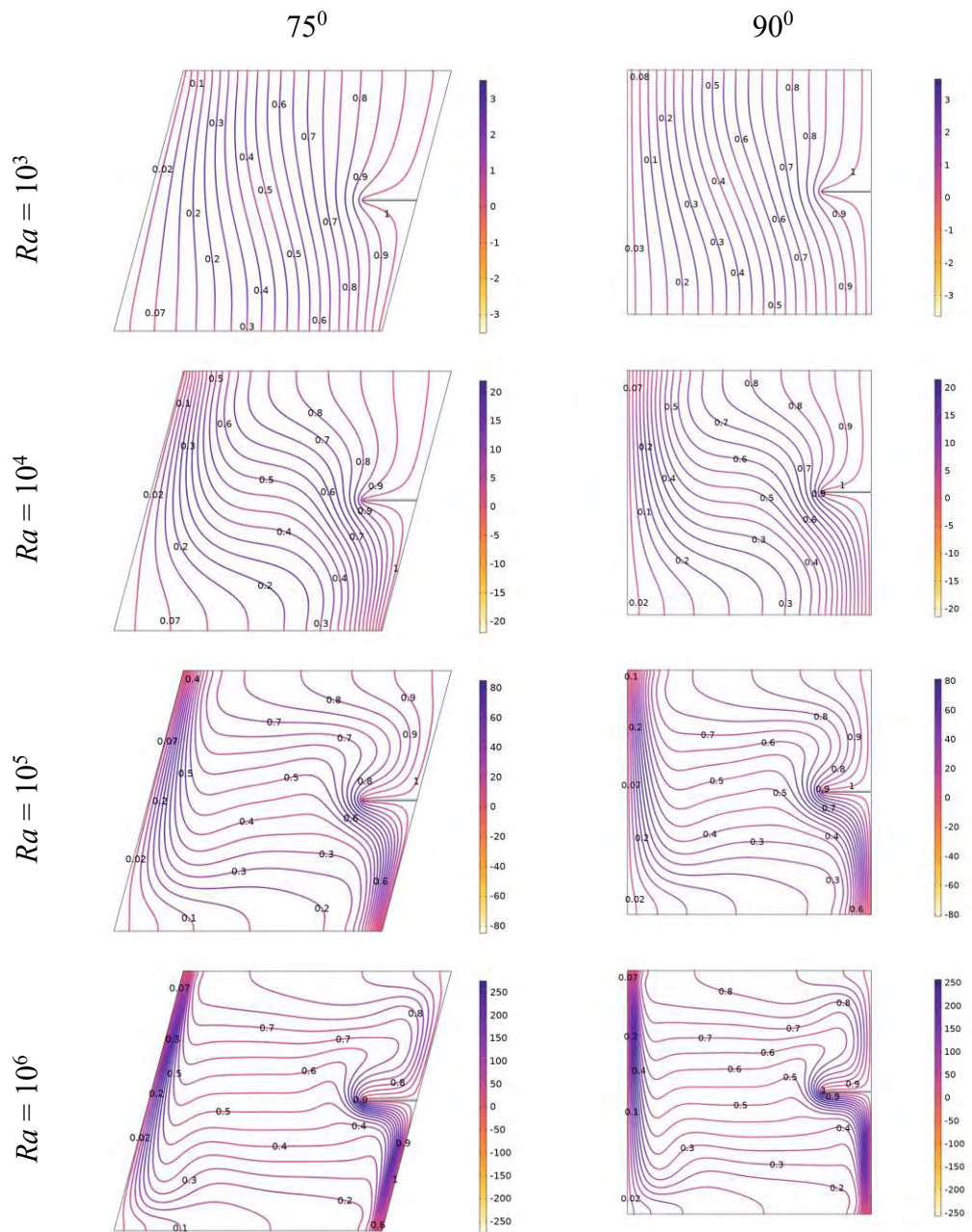**Figure 3.2 (a):** Isotherm variations for skew angles ($\alpha = 15^0$, *and* $\alpha = 30^0$) at $L = 0.20$.

Figure 3.2 (b): Isotherm variations for skew angles ($\alpha = 45^0, and\ \alpha = 60^0$) at $L = 0.20$.

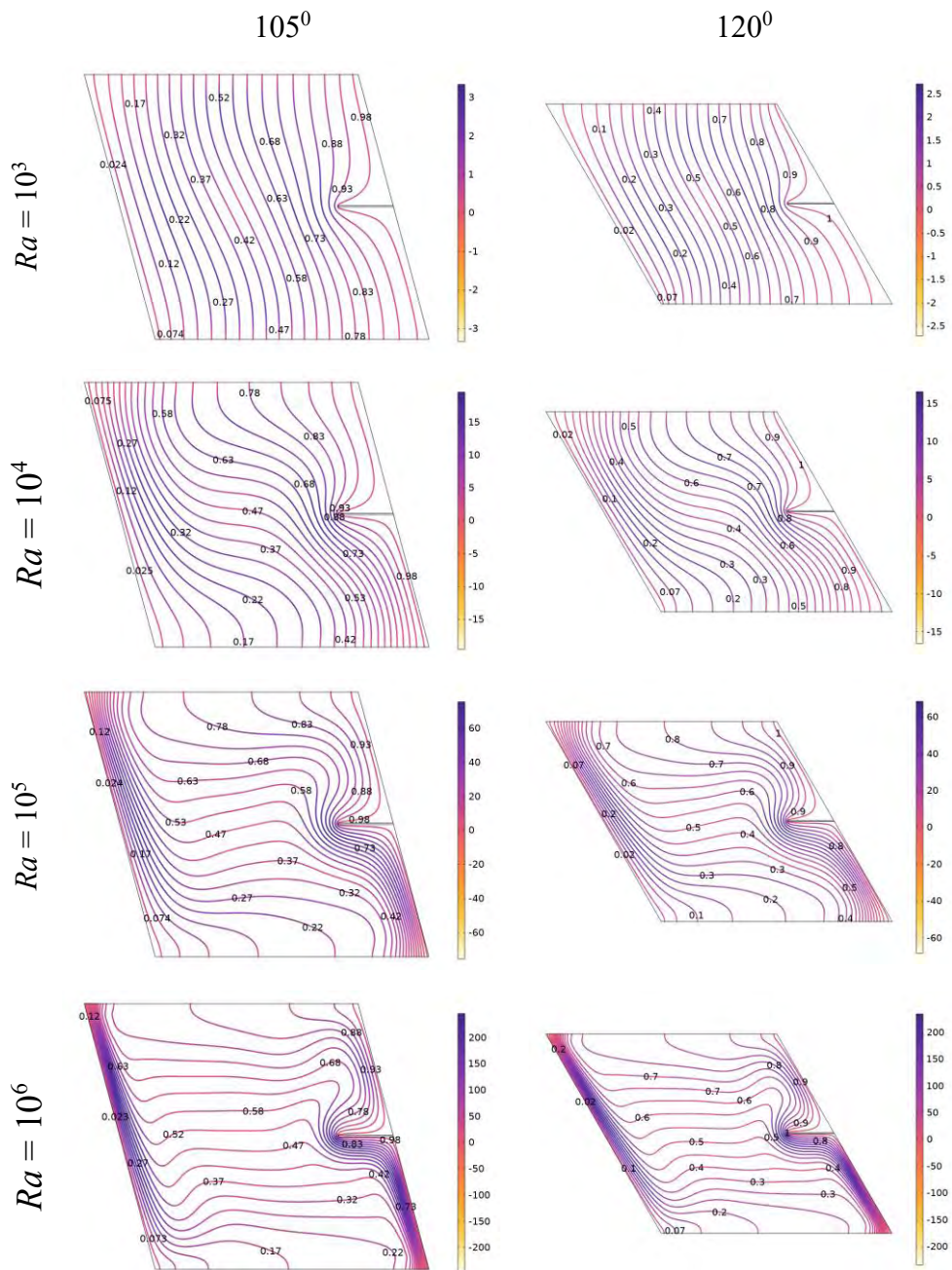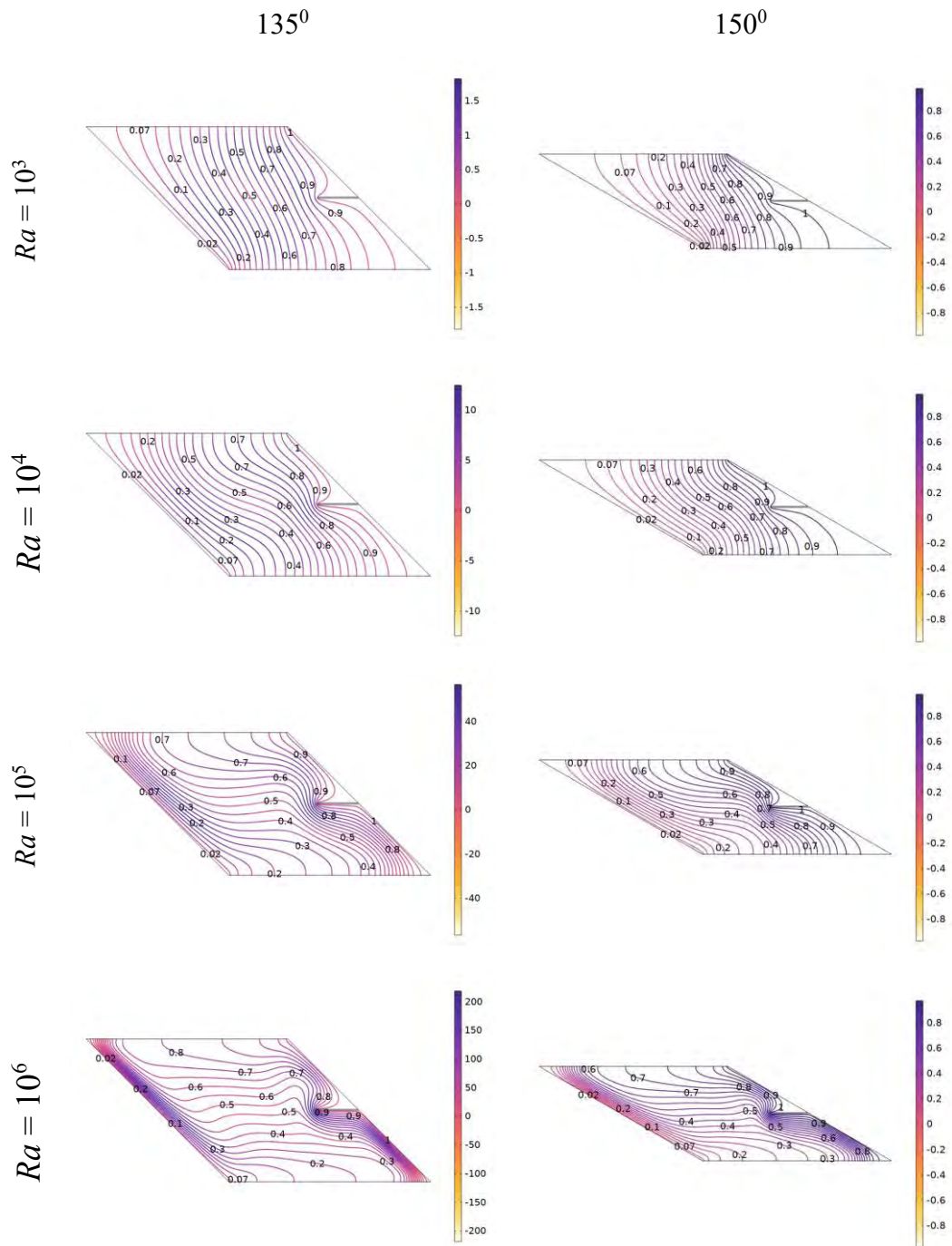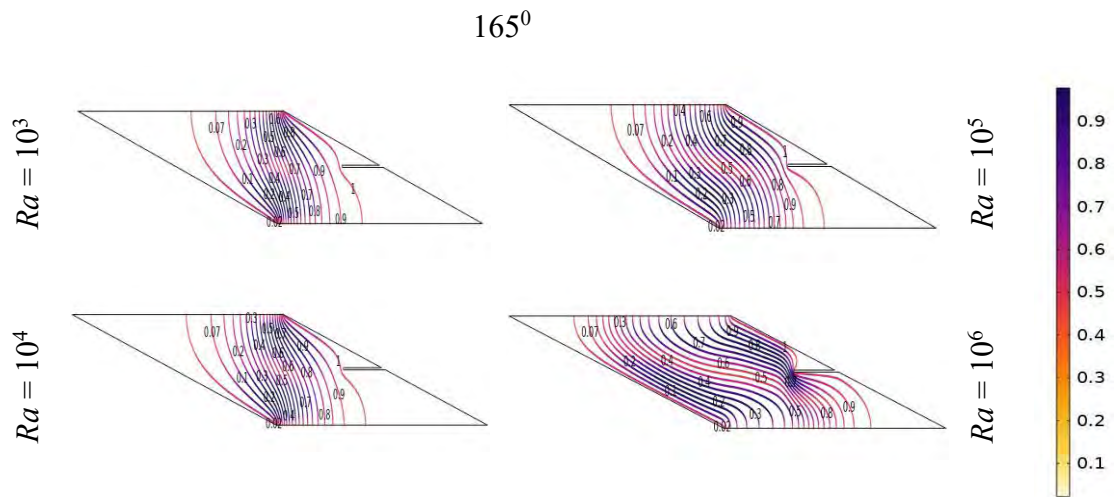**Figure 3.2 (c):** Isotherm variations for skew angles ($\alpha = 75^0, and\ \alpha = 90^0$) at $L = 0.20$.

Figure 3.2 (d): Isotherm variations for skew angles ($\alpha = 105^0$, and $\alpha = 120^0$) at $L = 0.20$.

**Figure 3.2 (e):** Isotherm variations for skew angles ($\alpha = 135^0$, and $\alpha = 150^0$) at $L = 0.20$.

165^0

Figure 3.2 (f): Isotherm variations for skew angles ($\alpha = 165^0$) at $L = 0.20$.

Velocity profiles for *L* = 0.20 at *Pr* = 1.41.

Figure 3.3(a)-(b), show the effect of Rayleigh number on velocity profile along the horizontal centerline for different skew angles $(15^0 \leq \alpha \leq 165^0)$ with a constant baffle length $L = 0.20$, baffle thickness $D = 0.005$, Rayleigh number $(10^3 \leq Ra \leq 10^6)$ at a fixed position of the baffle inside the cavity. From Figure 3.3(a)-(b), For $Ra = 10^3$ and $Ra = 10^4$ the dimensionless velocity changes are insignificant. For higher Ra values the velocity changed significantly for all the skew angles. In general, for the higher Rayleigh number; the magnitude of the maximum and minimum velocity increased.
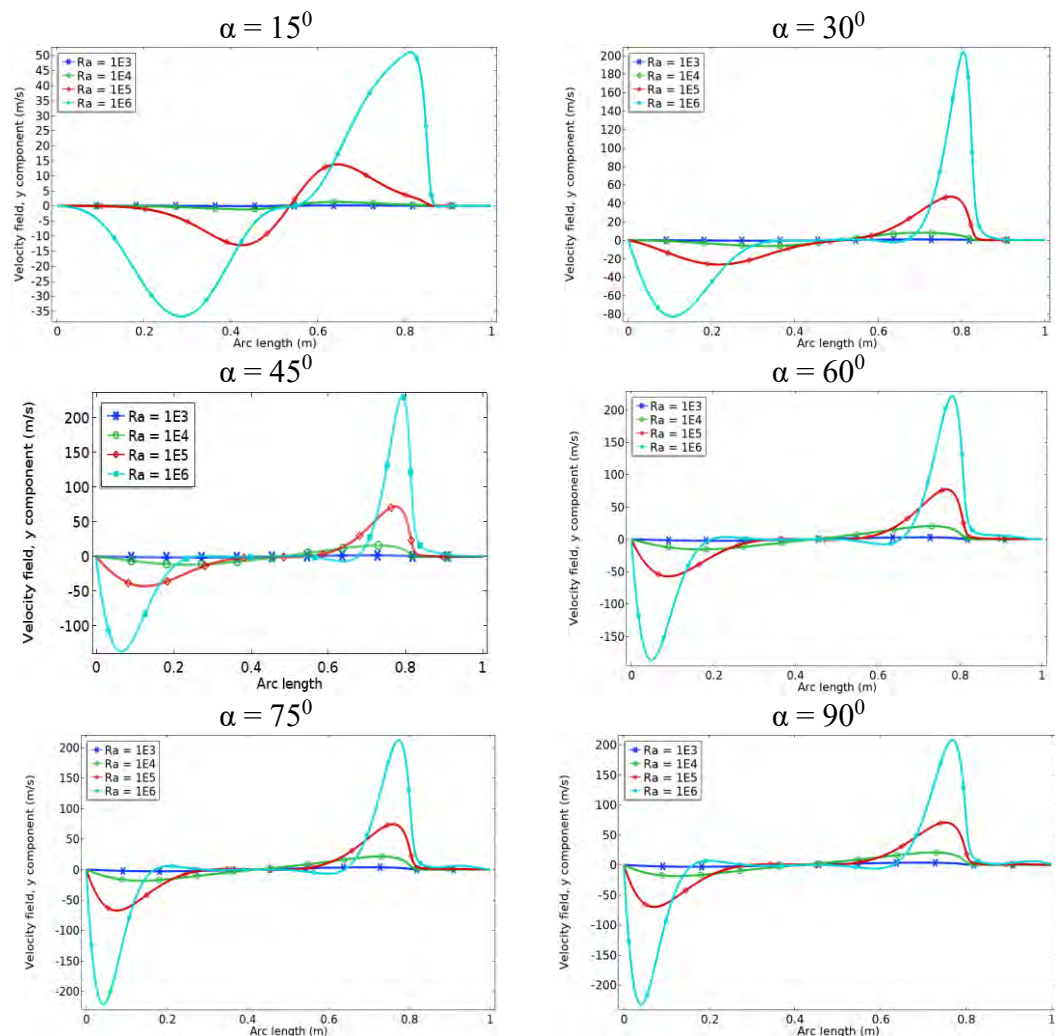
Figure 3.3 (a): Effect of Rayleigh number on **velocity profile** along the horizontal centerline for different skew angles $(15^0 \leq \alpha \leq 90^0)$ with $L = 0.20$.

$$\alpha = 105^0$$

$$\alpha = 120^0$$
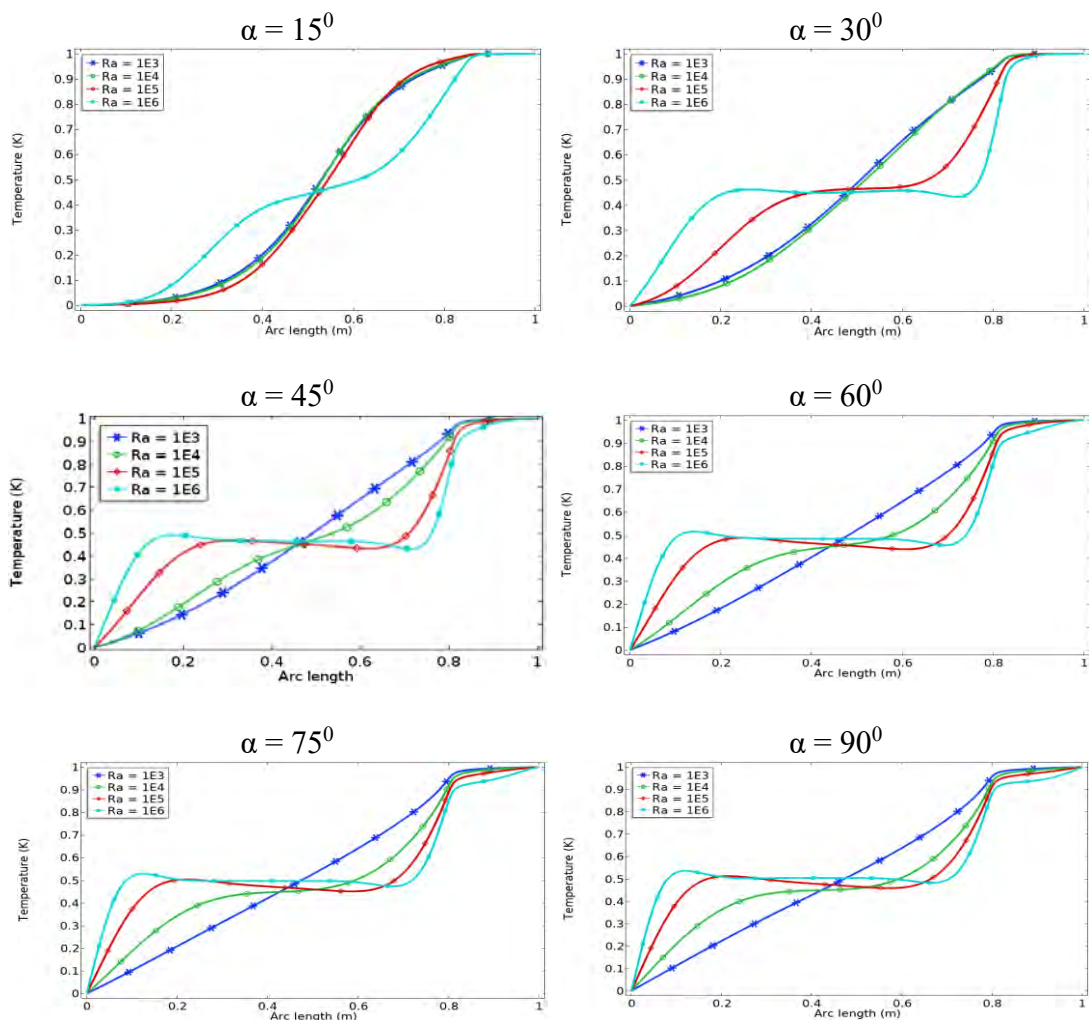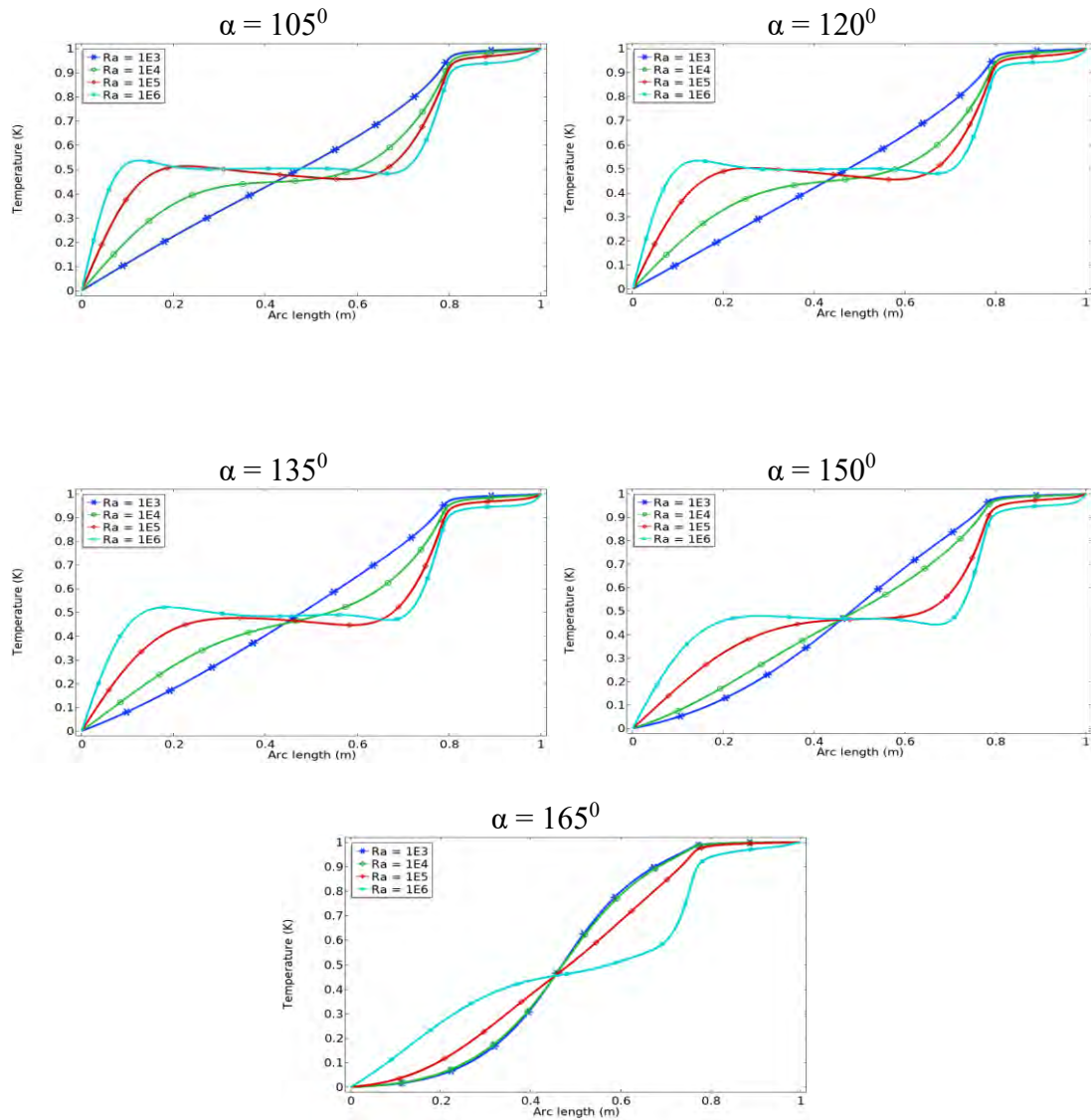
$$\alpha = 135^0$$

$$\alpha = 150^0$$

$$\alpha = 165^0$$
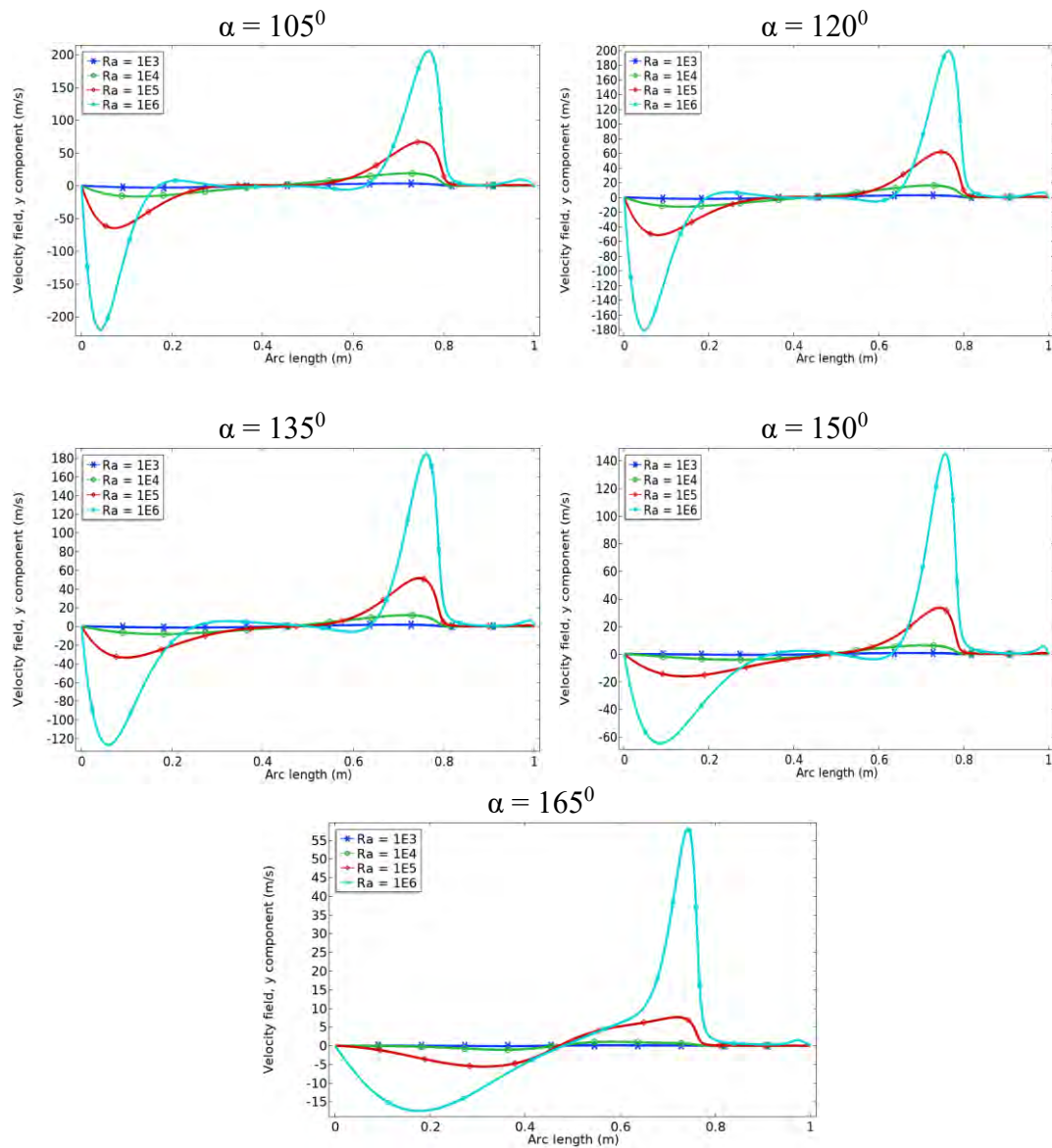
Figure 3.3 (b): Effect of Rayleigh number on **velocity profile** along the horizontal centerline for different skew angles $(105^0 \leq \alpha \leq 165^0)$ with $L = 0.20$.

Temperature profiles for *L* = 0.20 at *Pr* = 1.41.

Figure 3.4(a)-(b) demonstrates the effect of Rayleigh number on temperature profile along the horizontal centerline for different skew angles $(15^0 \leq \alpha \leq 90^0)$ with a constant baffle length *L* = 0.20, baffle thickness *D* = 0.005, and Rayleigh number $(10^3 \leq Ra \leq 10^6)$ with the sinusoidal heat transfer magnitude. When the Rayleigh number increases, temperature rises sharply close to the left and right walls, but temperature variation becomes insignificant around the central-most region of the cavity for skew angles $(30^0 \leq \alpha \leq 150^0)$. Somewhat similar trend of temperature variations are observed for skew angles $\alpha = 15^0$ and $\alpha = 165^0$ as expected.

Figure 3.4 (a): Effect of Rayleigh number on **temperature profile** along the horizontal centerline for different skew angles $(15^0 \leq \alpha \leq 90^0)$ with *L* = 0.20.

$$\alpha = 105^0$$

$$\alpha = 120^0$$

$$\alpha = 135^0$$

$$\alpha = 150^0$$

$$\alpha = 165^0$$
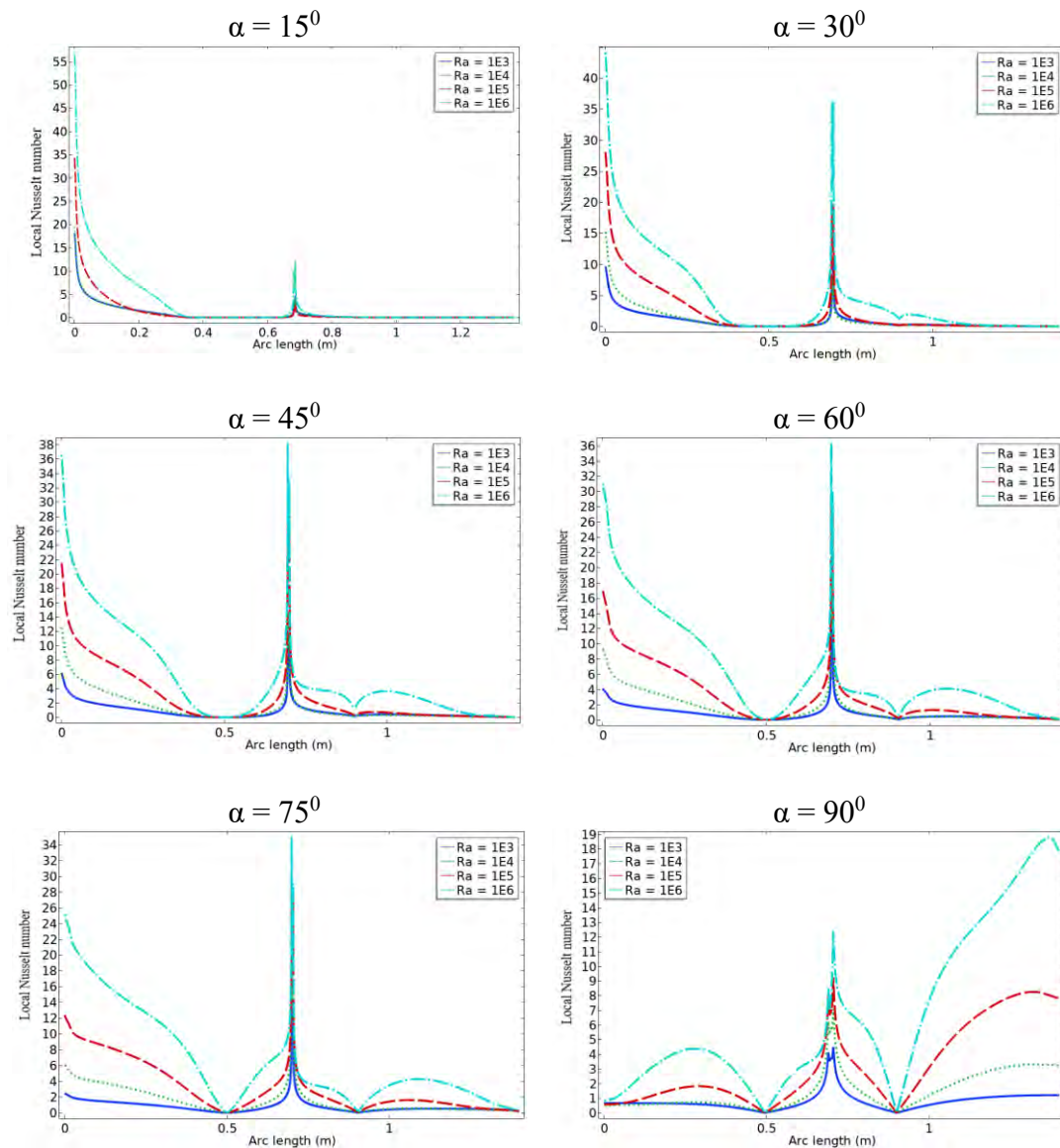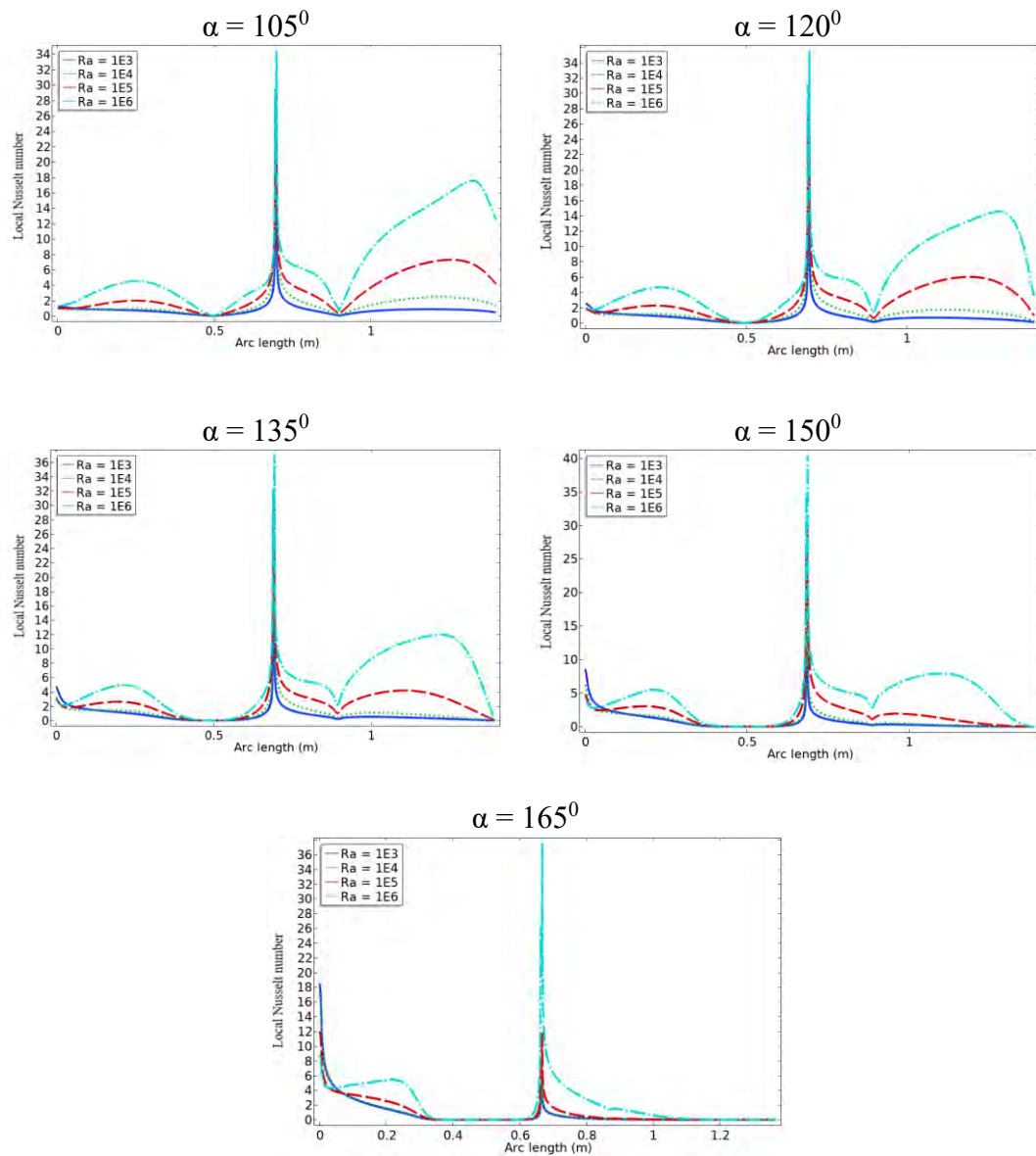

Figure 3.4(b): Effect of Rayleigh number on **temperature profile** along the horizontal centerline for different skew angles $(105^0 \leq \alpha \leq 165^0)$

Local Nusselt number for *L* = 0.20 at *Pr* = 1.41.

Figure 3.5(a)-(b) depicts the local Nusselt number (Nu_L) on the heated right inclined wall, including baffle exteriors at the value of baffle length (*L* = 0.20), baffle thickness *D* = 0.005 and Rayleigh number ($10^3 \leq Ra \leq 10^6$) at $\lambda = 0.50$. It remarked that the sketches of the Nu_L is more significant top side of the baffle for all the Rayleigh numbers at all the skew angles. It also demonstrates that the curves of the Nu_L are significantly changed with the increase of Rayleigh number.

$\alpha = 15^0$ $\alpha = 30^0$

$\alpha = 45^0$ $\alpha = 60^0$

$\alpha = 75^0$ $\alpha = 90^0$

Figure 3.5 (a): Effect of Rayleigh number on **local Nusselt number** on heated right inclined wall for different skew angles ($15^0 \leq \alpha \leq 90^0$) with *L* = 0.20.

$\alpha = 105^0$

$\alpha = 120^0$

$\alpha = 135^0$

$\alpha = 150^0$

$\alpha = 165^0$

Figure 3.5 (b): Effect of Rayleigh number on **local Nusselt number** on heated right inclined wall for different skew angles $(105^0 \le \alpha \le 165^0)$ with $L = 0.20$.
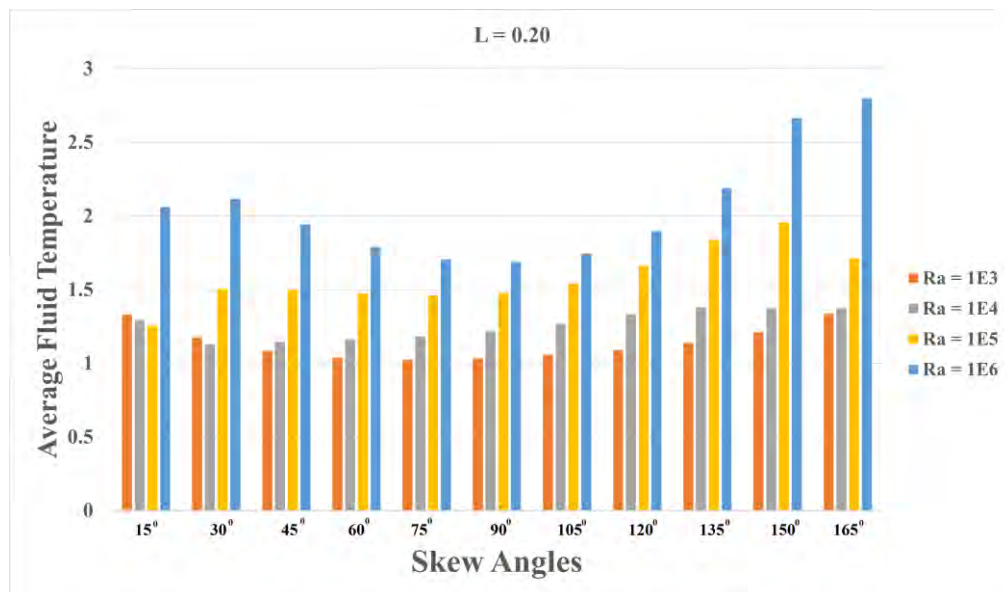
The average fluid temperature and Average Nusselt number for varying skew angles and Rayleigh number (Ra) at a constant baffle location (B) while the values of the other parameters are kept at their default values examined by Figure 3.6, Figure 3.7 and quantitative data in Table 3.1, Table 3.2 respectively.

Average fluid temperature for *L* = 0.20 at *Pr* = 1.41.

From Figure 3.6, the average fluid temperature decreases gradually with increasing skew angle up to $\alpha = 90^0$, and then increases except for the Rayleigh number $Ra = 10^4$ at the baffle size *L* = 0.20 while the other parameters are kept constant.

In Figure 3.6 and the numerical value in Table 3.1, increasing the Ra causes the average fluid temperature to increase continuously for all baffle sizes at the fixed position of the baffle. Furthermore, according to Table 3.1, the greatest average fluid temperature within the cavity was **2.799003281896193**, which was discovered at $Ra = 10^6$ in this case.
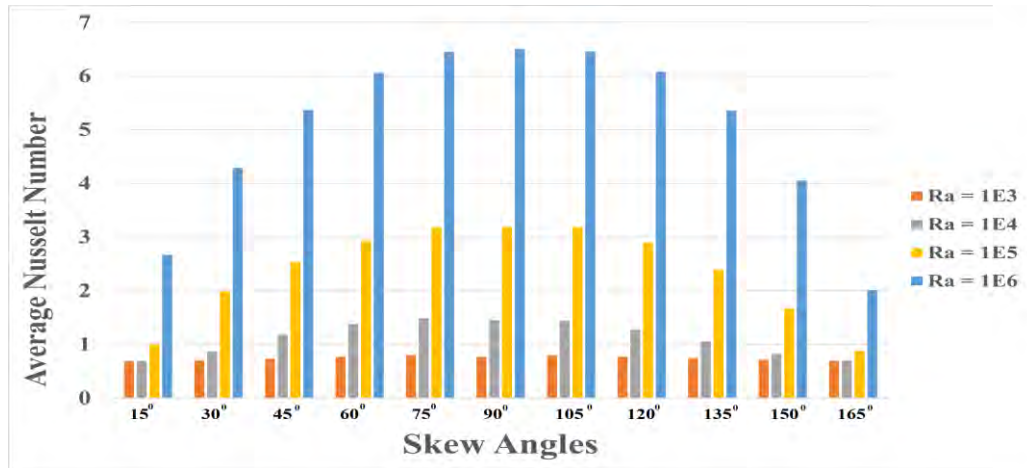

Figure 3.6: Effect of Rayleigh number on **average fluid temperature** on the cavity surface for different skew angles ($15^0 \leq \alpha \leq 165^0$) with *L* = 0.20.

Table 3.1: Average fluid temperature variations for various skew angles at L = 0.20.

Angles	Average Fluid Temperature			
	$Ra = 10^3$	$Ra = 10^4$	$Ra = 10^5$	$Ra = 10^6$
$\alpha = 15^0$	1.3298282093	1.2952472424	1.2549578733	2.0614891956
$\alpha = 30^0$	1.1748430123	1.1269059735	1.5079010577	2.1167123586
$\alpha = 45^0$	1.0834959011	1.1464622006	1.4991251635	1.9416687104
$\alpha = 60^0$	1.0381491351	1.1628759564	1.4738770770	1.7894931933
$\alpha = 75^0$	1.0249120773	1.1828520783	1.4597295681	1.7041112916
$\alpha = 90^0$	1.0332856116	1.2182915054	1.4775736024	1.6893000820
$\alpha = 105^0$	1.0564201368	1.2704036890	1.5399988866	1.7465116907
$\alpha = 120^0$	1.0915034152	1.3317389480	1.6620960320	1.8982433289
$\alpha = 135^0$	1.1393406878	1.3788837668	1.8373984405	2.1867930812
$\alpha = 150^0$	1.2099394659	1.3757958678	1.9577202041	2.6644465995
$\alpha = 165^0$	1.3365827926	1.3741960259	1.7136847496	**2.7990032818**

Average Nusselt number for *L* = 0.20 at *Pr* = 1.41

Figure 3.7 depicts the arrangement of the Nu_{avg} on the right inclined wall, which includes a baffle surface with the impact of Rayleigh numbers (*Ra*) and the skew angles. The value of the remaining parameters are constant. The mean Nusselt number increases in proportion to the increase of Rayleigh number for a given baffle size. when the Rayleigh number is increased at a uniform baffle length, the buoyancy force increases, and heat transfer improves. Table 3.2 shown the numerical value of a mean Nusselt number on the right inclined wall, including the baffle surface with multiple *Ra.* Furthermore, according to Table 3.2, the maximum Nu_{avg} was **6.504006769659389** on the heated area exposed for the skew angle $\alpha = 90^0$ and $Ra = 10^6$.

Figure 3.7: Effect of Rayleigh number on **average Nusselt number** along the inclined right wall for different skew angles $(15^0 \leq \alpha \leq 165^0)$ with $L = 0.20$.

Table 3.2: Average Nusselt number variations for various angle at $L = 0.20$.

Angles	Average Nusselt number			
	$Ra = 10^3$	$Ra = 10^4$	$Ra = 10^5$	$Ra = 10^6$
$\alpha = 15^0$	0.6911928943	0.6923993507	1.0021230489	2.6728478277
$\alpha = 30^0$	0.7078622611	0.8638242266	1.9879864196	4.2906092015
$\alpha = 45^0$	0.7390572439	1.1849635416	2.5318009894	5.3701602683
$\alpha = 60^0$	0.7732729137	1.3872335798	2.9350310378	6.0566975748
$\alpha = 75^0$	0.7988776454	1.4899013973	3.1801586522	6.4498470552
$\alpha = 90^0$	0.7684292872	1.4468817554	3.1888141155	**6.5040067696**
$\alpha = 105^0$	0.7965396170	1.4381447312	3.1862041144	6.4587367229
$\alpha = 120^0$	0.7729924647	1.2782138324	2.8942667098	6.0848609959
$\alpha = 135^0$	0.7420212383	1.0587499572	2.3914321738	5.3520693411
$\alpha = 150^0$	0.7118537042	0.8213948795	1.6706713596	4.0552398252
$\alpha = 165^0$	0.6949969893	0.7012709806	0.8794864498	2.0104456232

## Case-II: (Effect of the skew angles for the baffle length L= 0.30)

In this case, the numerical investigation of natural convection heat transfer in presence of sinusoidal boundary condition within the skewed cavity having horizontal baffle are numerically presented. The results obtained by the variations of Rayleigh numbers, different skew angles and the heat transfer rate at baffle length L = 0.30. The results of this study are shown in Figures 3.8- 3.15.

Findings from streamlines:

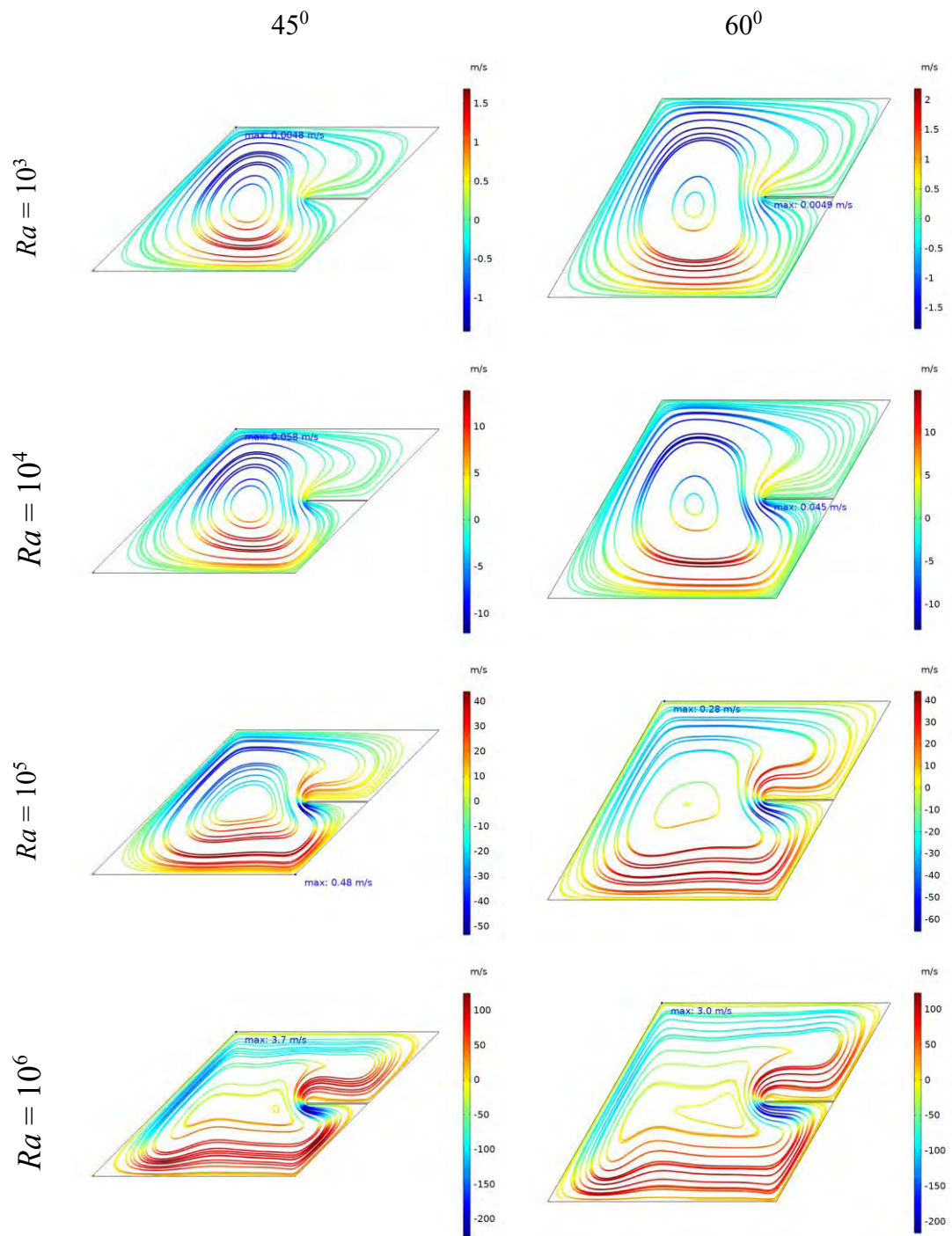Figure 3.8(a)-(f) show streamlines for different Rayleigh numbers $(10^3 \leq Ra \leq 10^6)$, skew angles $(15^0 \leq \alpha \leq 165^0)$. In this case, the baffle is connected to the inclined right wall within the skewed enclosure. Figure 3.8(a)-(f) shows that the maximum velocity in the streamline steadily increase with the increase of the Rayleigh number in the streamline for all the skew angles. For the different the skew angles, the maximum velocity increases steadily with increase the value of Rayleigh number. For the constant baffle length and location, a minor primary cell looks an oval was produced in the center of the cavity. The cell's center seems to split into different cells at all skew angles for the Rayleigh number $Ra = 10^6$ except at $\alpha = 165^0$ as seen in Figures 3.8. The flow structure becomes more significant, disregarding the moving vortices that ascend the wall as Rayleigh number and skew angles increase.

For all the cases of the Rayleigh number shown in figures 3.8(a)-(f), the maximum velocity rises gradually as the skew angle increases up to $\alpha = 90^0$. After then, the maximum velocity steadily lowers by progressively increase the skew angle. For completeness, it states that the skew angles of $\alpha = 15^0$ and $\alpha = 165^0$ both generate the same result, which is 0.0018 ms^{-1} at $Ra = 10^3$. Moreover, it is analogous to the preceding case.
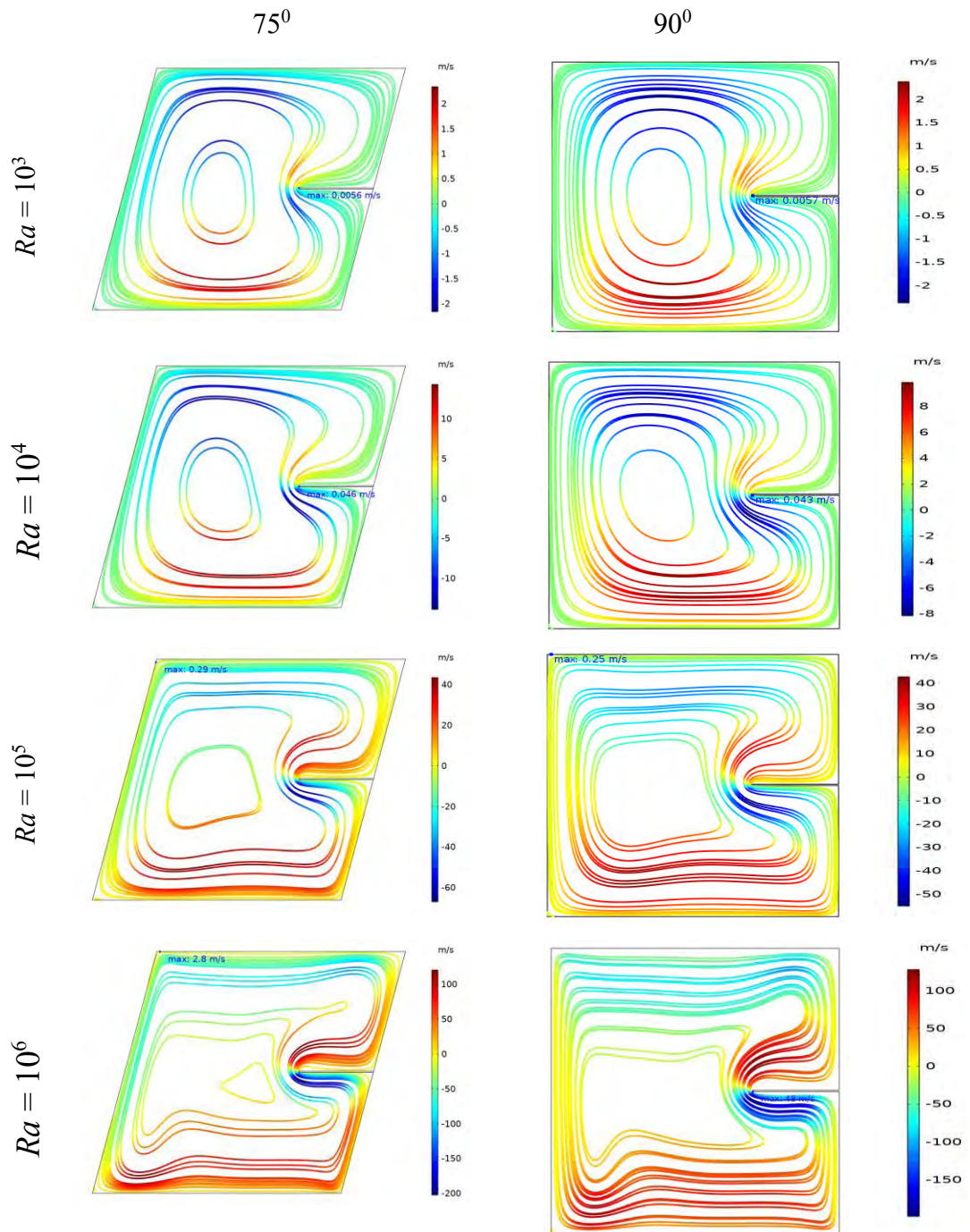
Aside from that, as previously mentioned, when the Rayleigh number rises, the maximum velocity increases as well. As a result, the maximum velocity is 48 ms^{-1} for $Ra = 10^6$ at an angle of $\alpha = 90^0$.

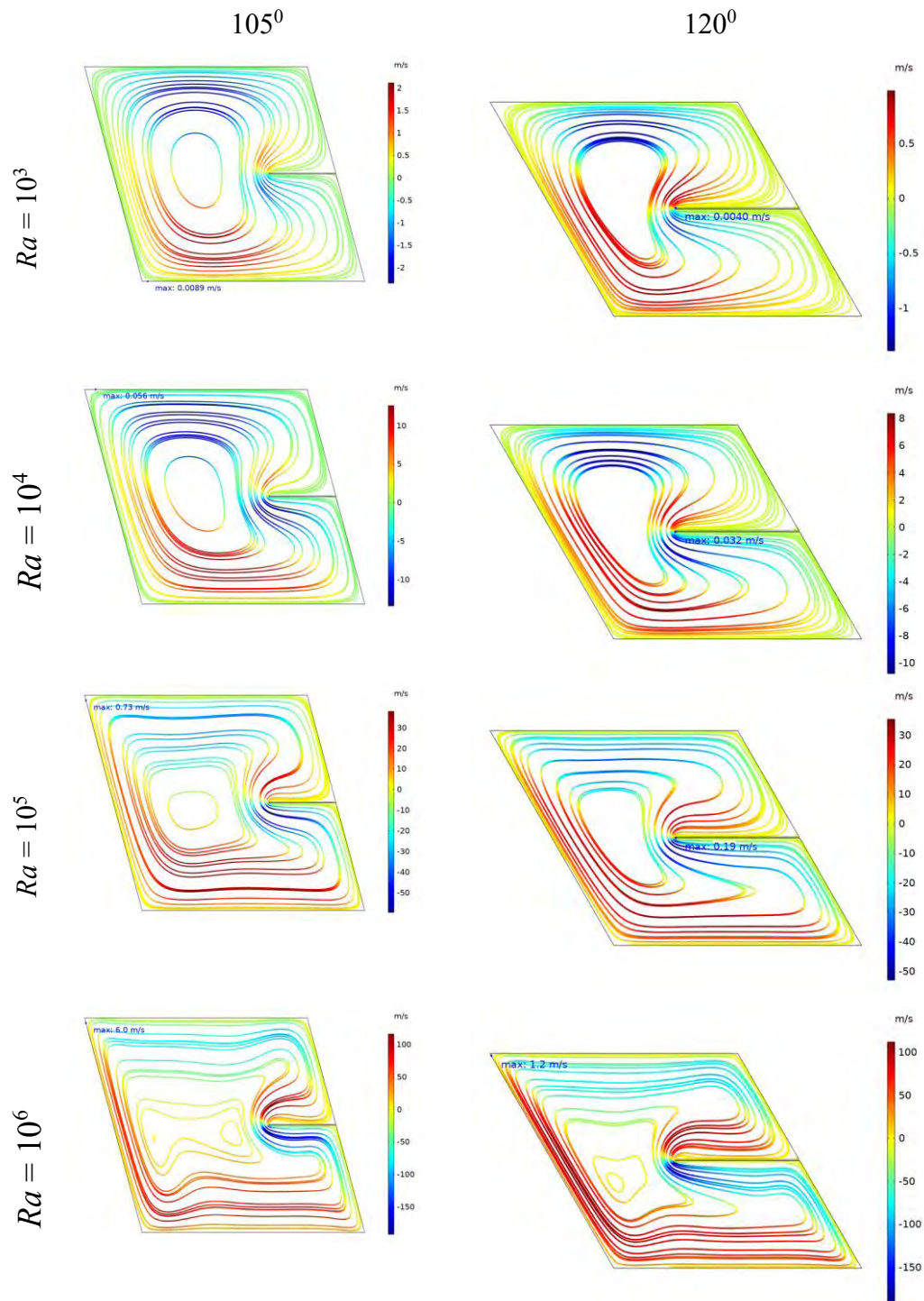15^0 30^0

$Ra = 10^3$

$Ra = 10^4$

$Ra = 10^5$

$Ra = 10^6$
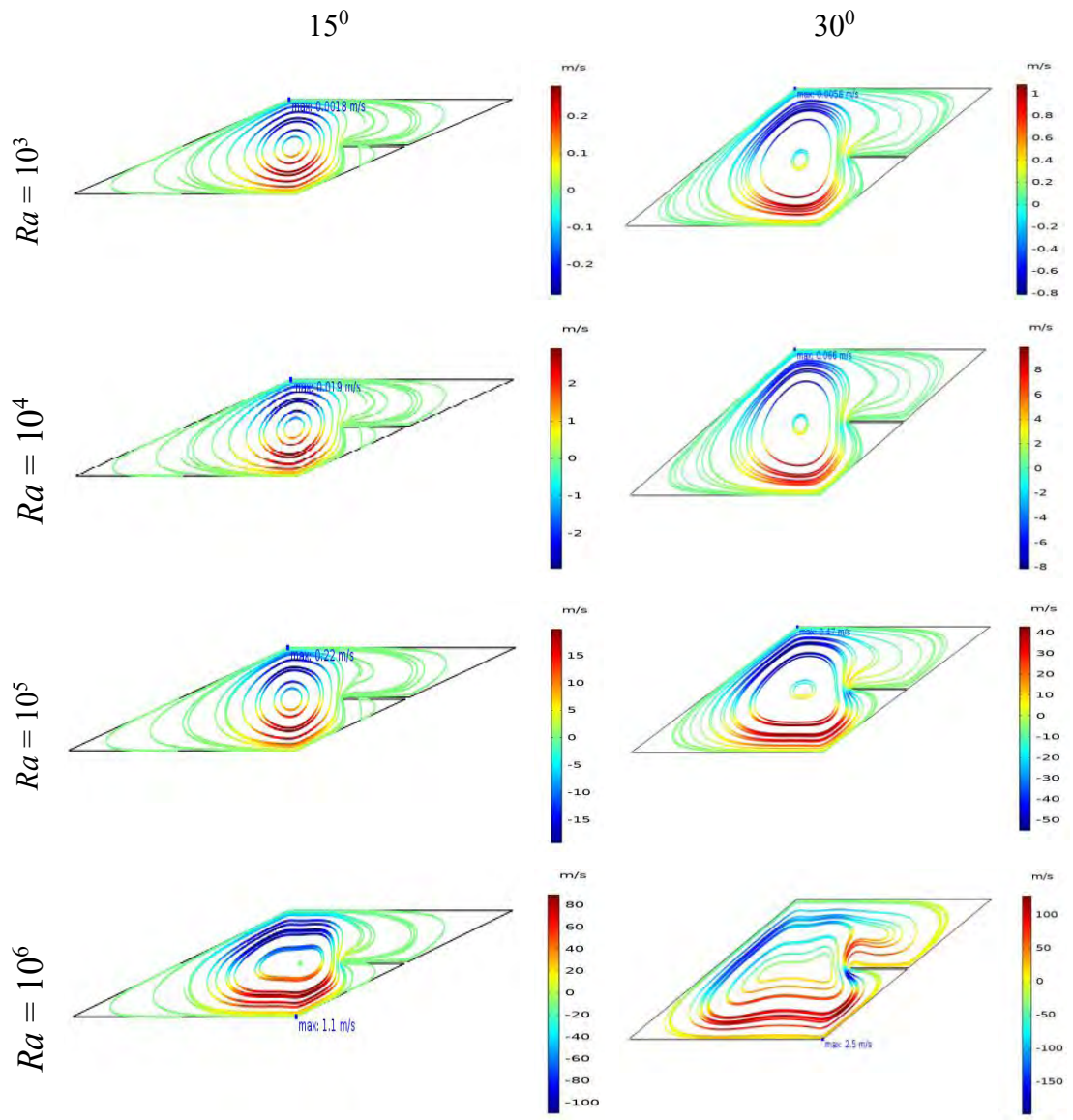
Figure 3.8(a): Streamline variations for the skew angles ($\alpha = 15^0$, and $\alpha = 30^0$) at *L=0.30.*

Figure 3.8(b): Streamline variations for various skew angles ($\alpha = 45^0$, and $\alpha = 60^0$) at $L = 0.30$.

Figure 3.8(c): Streamline variations for the skew angles ($\alpha = 75^0$, and $\alpha = 90^0$) at $L = 0.30$.

105^0 120^0

$Ra = 10^3$

$Ra = 10^4$

$Ra = 10^5$

$Ra = 10^6$

Figure 3.8 (d): Streamline variations for the skew angles ($\alpha = 105^0$, *and* $\alpha = 120^0$) at $L = 0.30$.

135^0 150^0
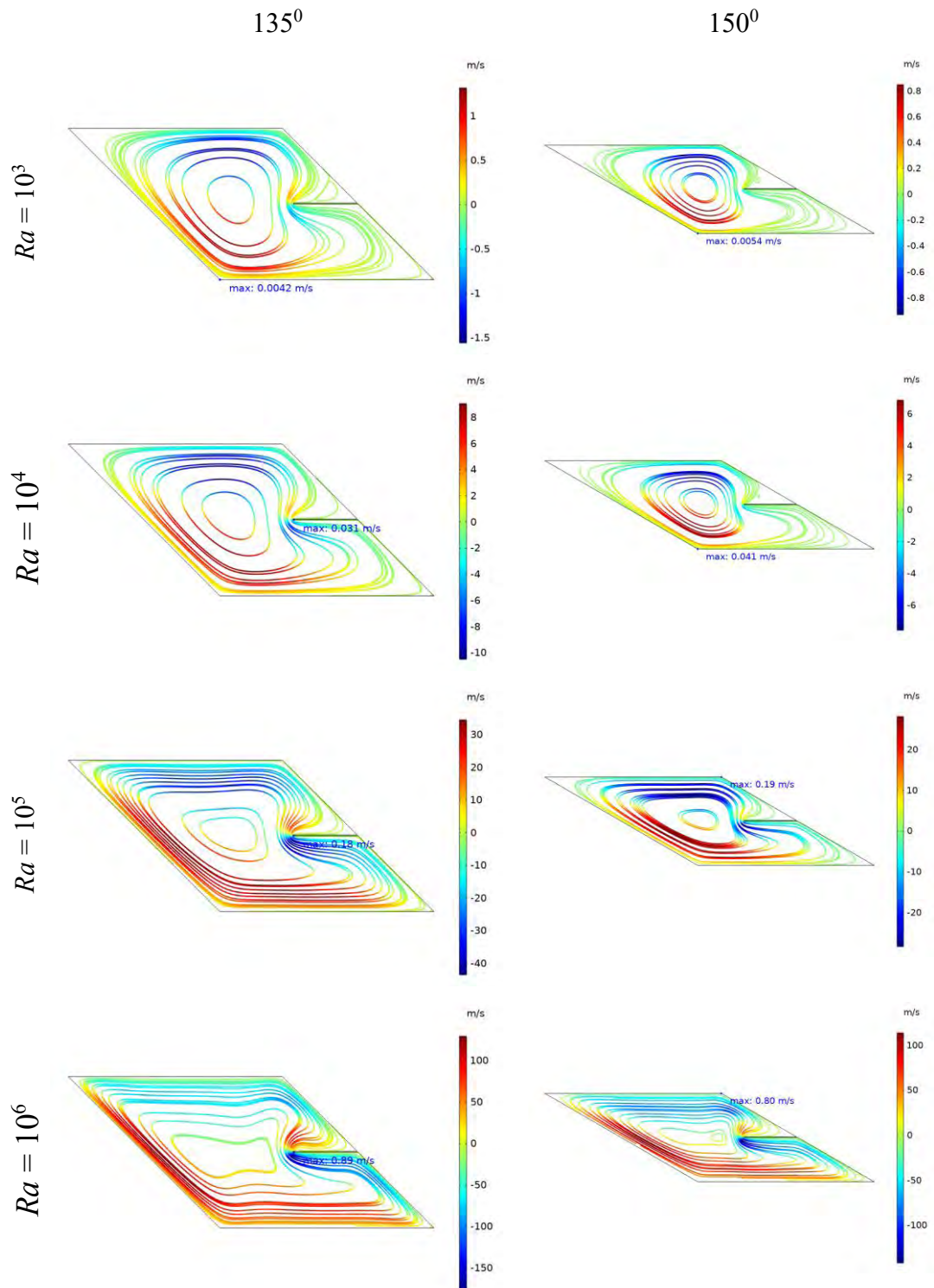
Figure 3.8(e): Streamline variations for skew angles ($\alpha = 135^0, and\ \alpha = 150^0$) at $L = 0.30$.

165^0

Ra = 10^3 Ra = 10^5

Ra = 10^4 Ra = 10^6
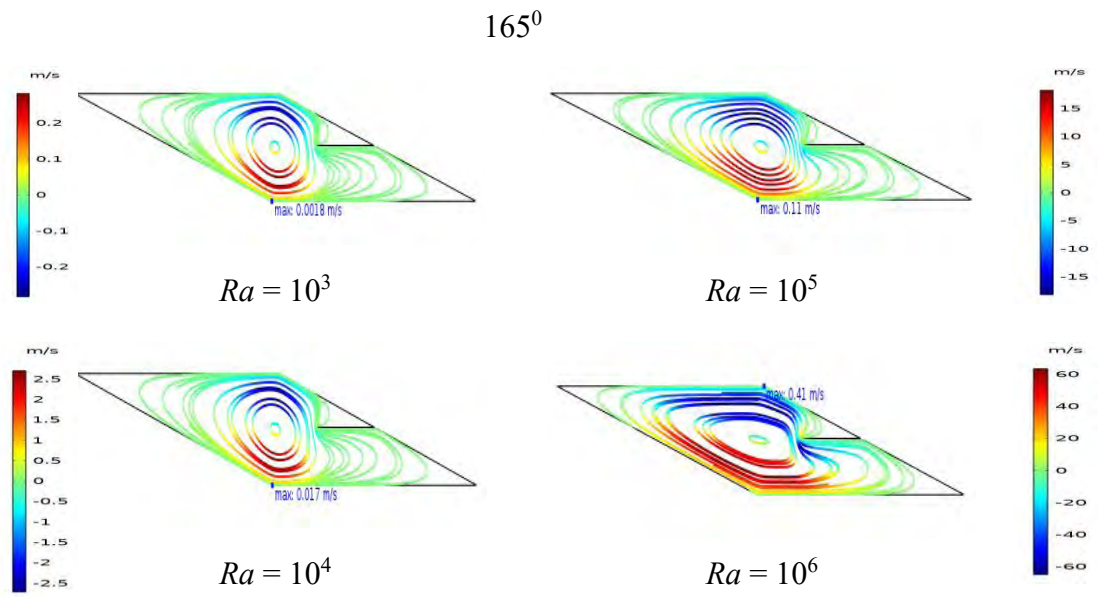
Figure 3.8(f): Streamline variations for the skew angles ($\alpha = 165^0$) at $L = 0.30$.

Findings from isotherms:

Figures 3.9(a)-(f) exhibits the prevalent heat transfer conductance; the findings are presented in isotherms containing multiple Rayleigh numbers ($15^0 \leq \alpha \leq 165^0$) at a constant baffle length (L = 0.30) and location. According to Figure 3.9, the isotherms lines within the enclosures become significantly more substantial for all the skew angles at $Ra = 10^6$. Figure 3.9(a)-(f) shows that for concentrate towards a left inclined surface and the lower side of the baffle surface are denser for all the variations of the skew angle and the Rayleigh numbers. When the Rayleigh number increase, the isotherm lines show more noticeable. And that the isotherm lines are influencing more inside the enclosure, resulting in increased heat transfer through convection.
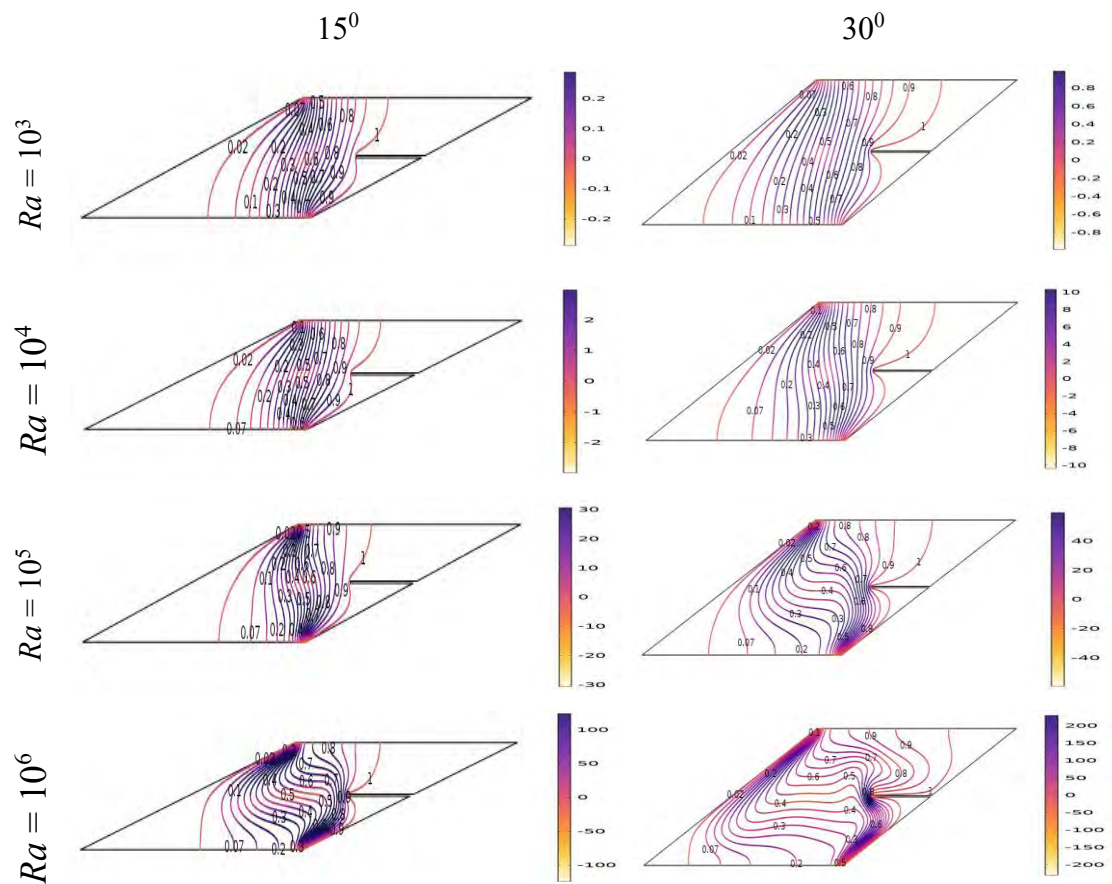
Figure 3.9(a): Isotherm variations for skew angles ($15^0 \leq \alpha \leq 90^0$) at $L = 0.30$.

Figure 3.9(b): Isotherm variations for skew angles ($\alpha = 45^0$, and $\alpha = 60^0$) at $L = 0.30$.

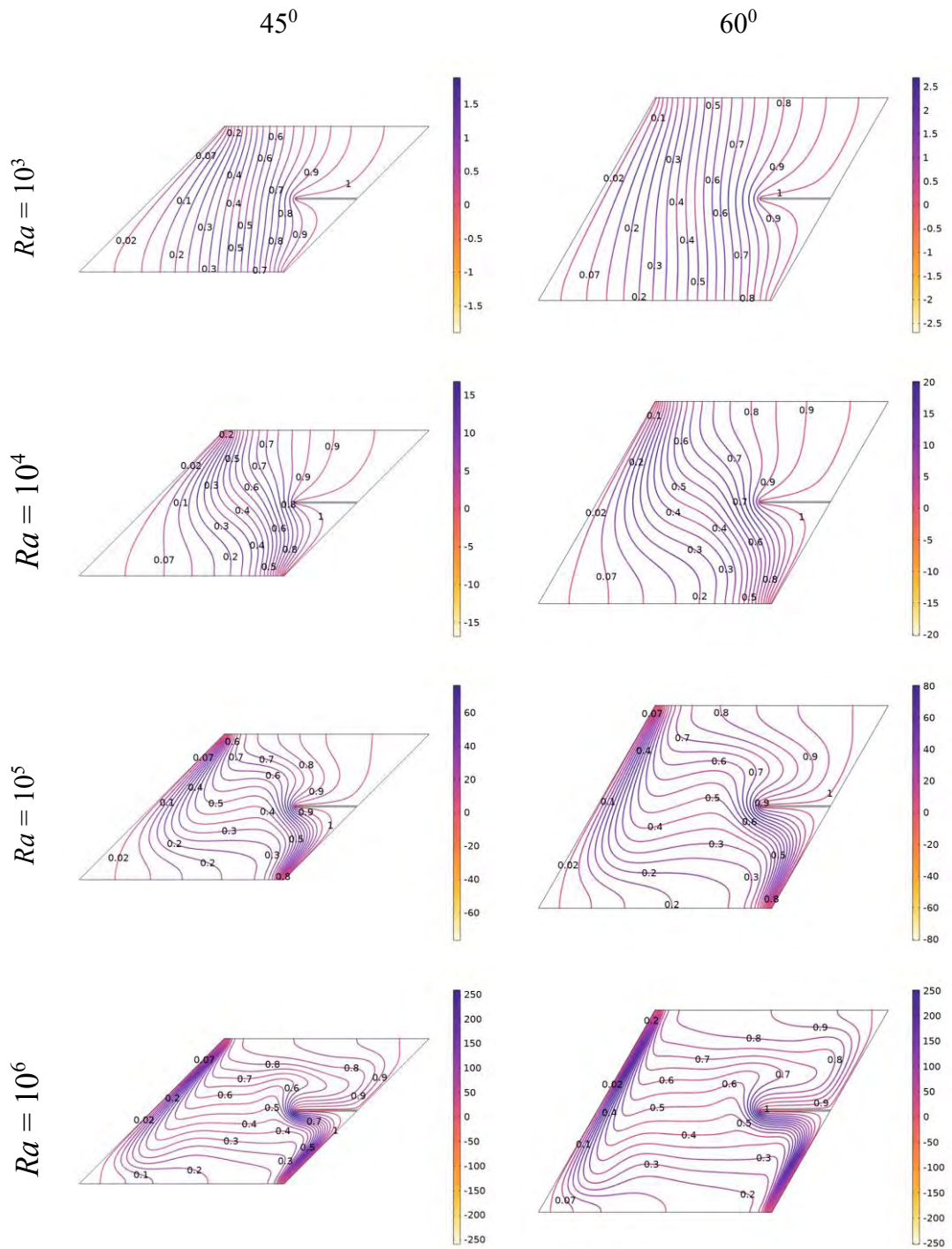**Figure 3.10 (c):** Isotherm variations for skew angles ($\alpha = 75^0$, and $\alpha = 90^0$) at $L = 0.30$.

105^0 120^0

Figure 3.9(d): Isotherm variations for skew angles ($\alpha = 105^0$, and $\alpha = 120^0$) at $L = 0.30$.

135^0 150^0

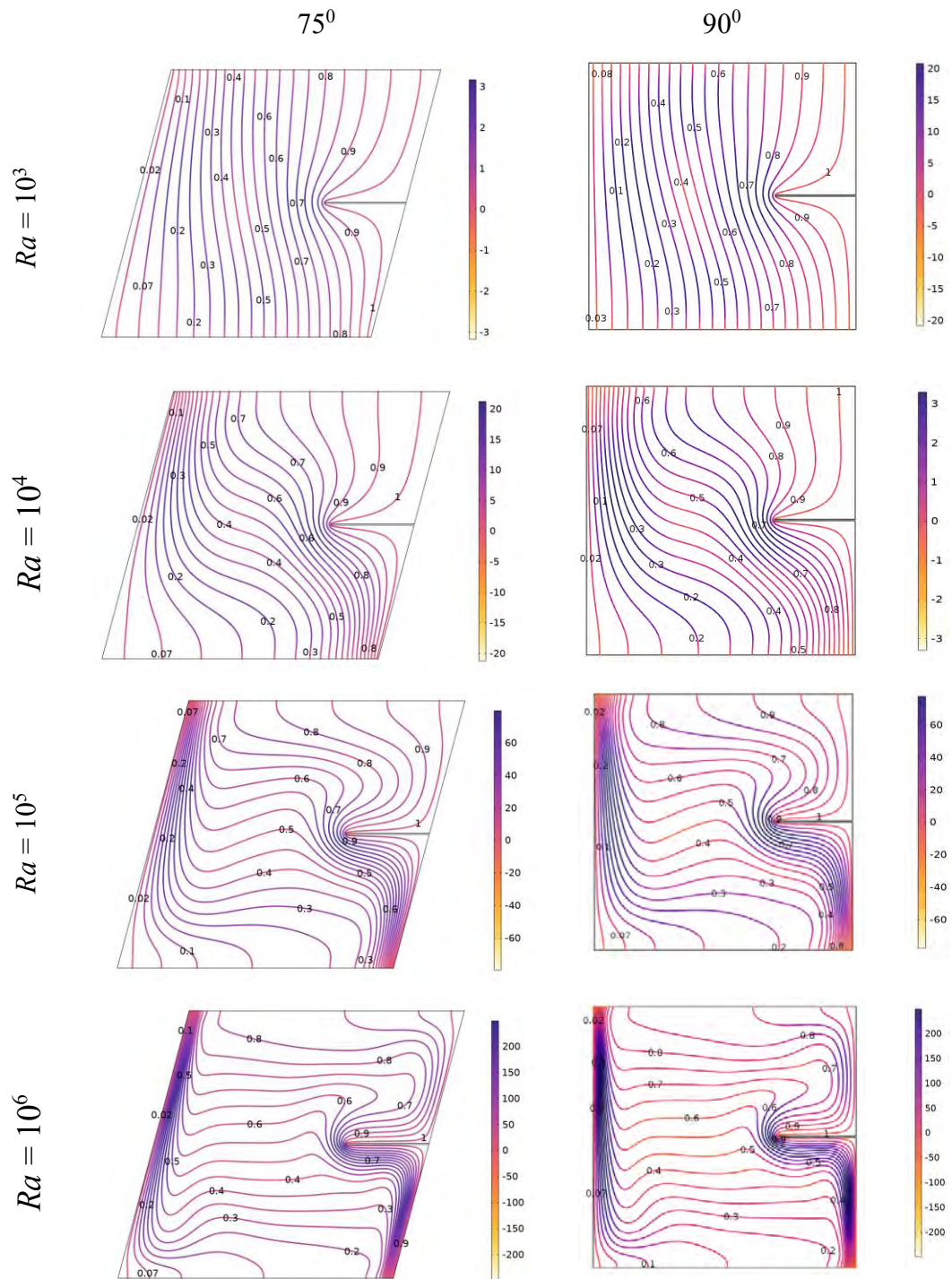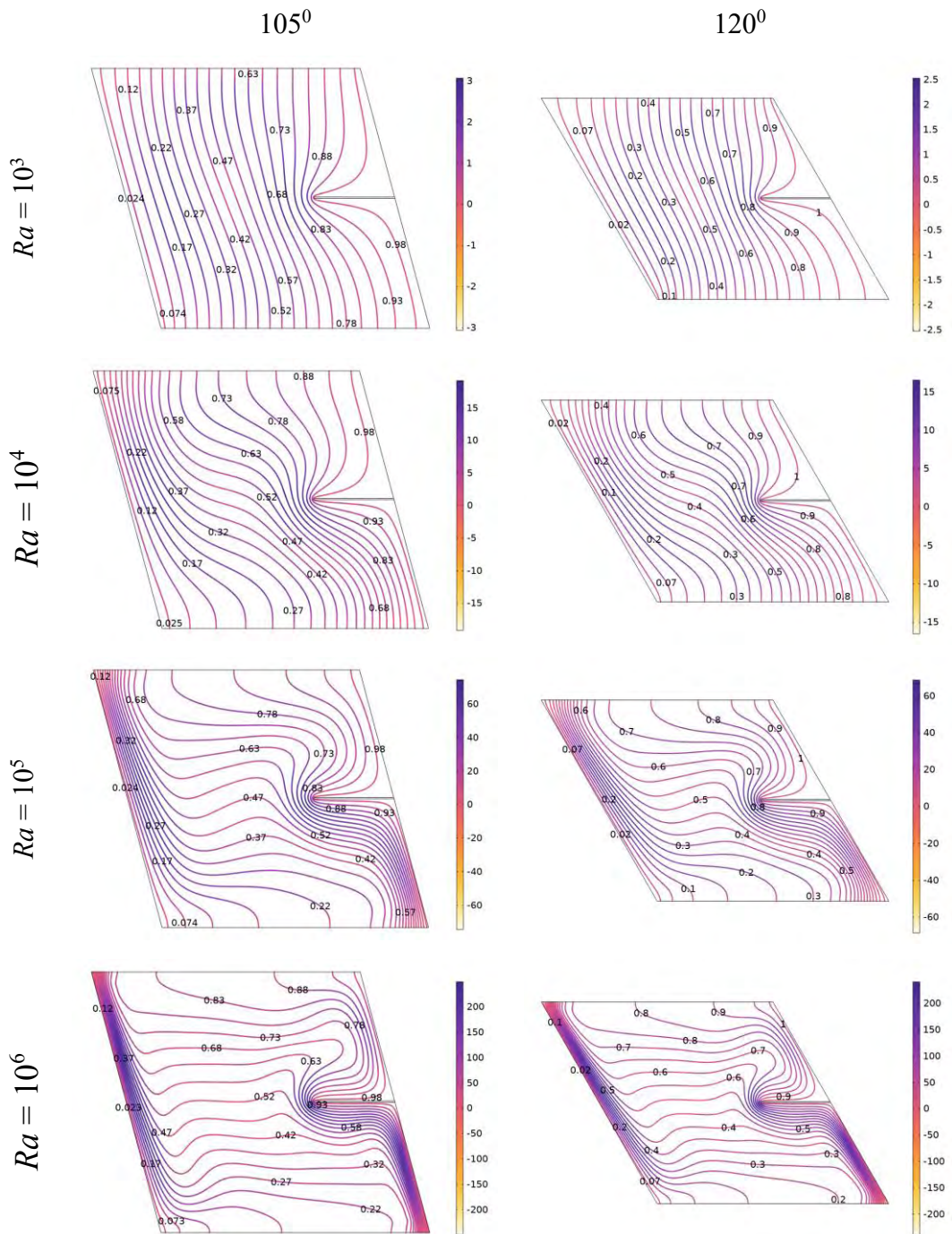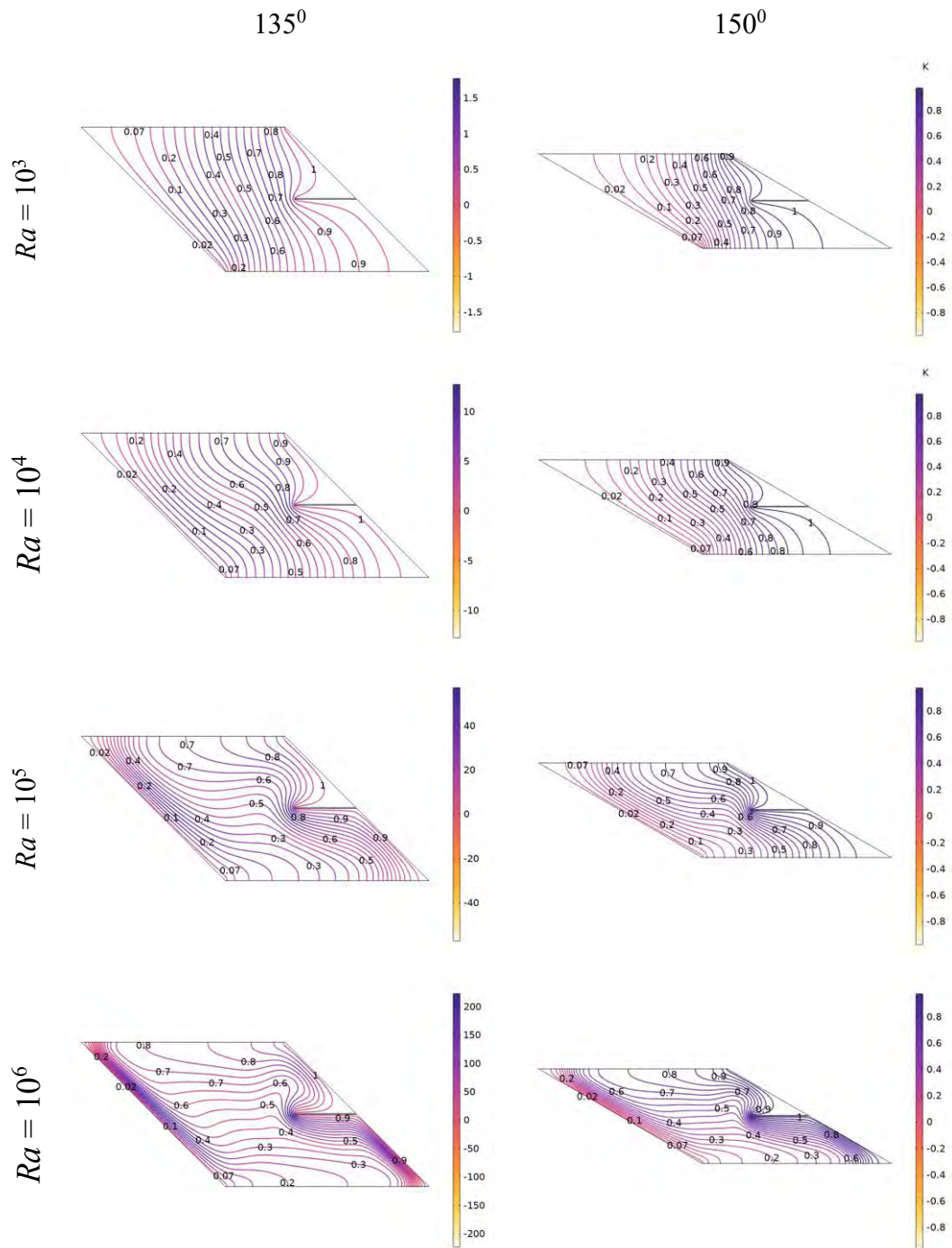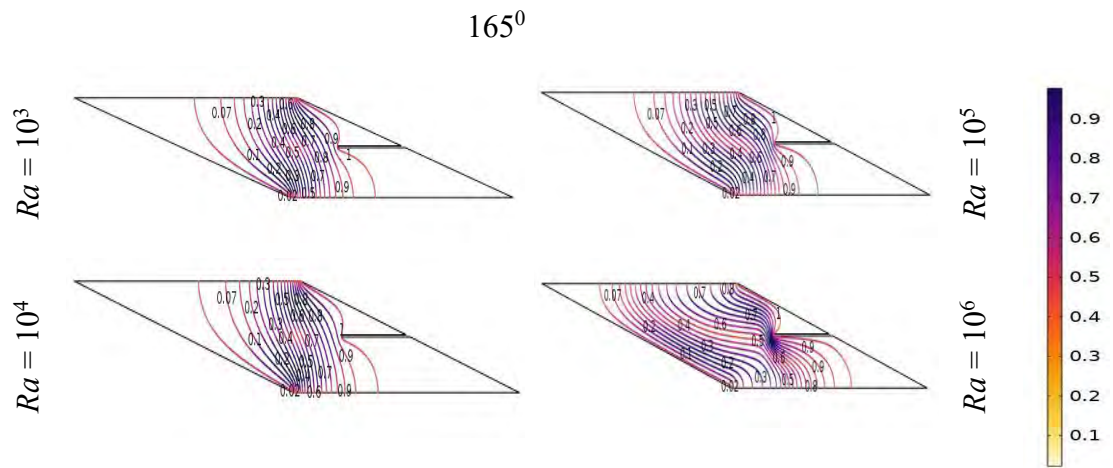**Figure 3.9(e):** Isotherm variations for skew angles ($\alpha = 135^0$, and $\alpha = 150^0$) at $L = 0.30$.

165^0

Figure 3.9(f): Isotherm variations for skew angle ($\alpha = 165^0$) at $L = 0.30$.

Velocity profiles for *L* = 0.30 at *Pr* = 1.41

Figure 3.10(a)-(b) exhibits the impact of various skew angles ($15^0 \leq \alpha \leq 165^0$), and Rayleigh number ($10^3 \leq Ra \leq 10^6$) on velocity profiles toward the horizontal centerline with baffle thickness D = 0.005, for constant baffle length and location inside the cavity. For the lowest Rayleigh number ($Ra = 10^3$ and $Ra = 10^4$) the dimensionless velocity increases insignificantly as seen in the Figure 3.10. On the contrary, for higher Rayleigh number the dimensionless velocity profiles transformed significantly for all the skew angles. The fundamental amplitude of the maximum and minimum velocities also augments for the Rayleigh number grows,
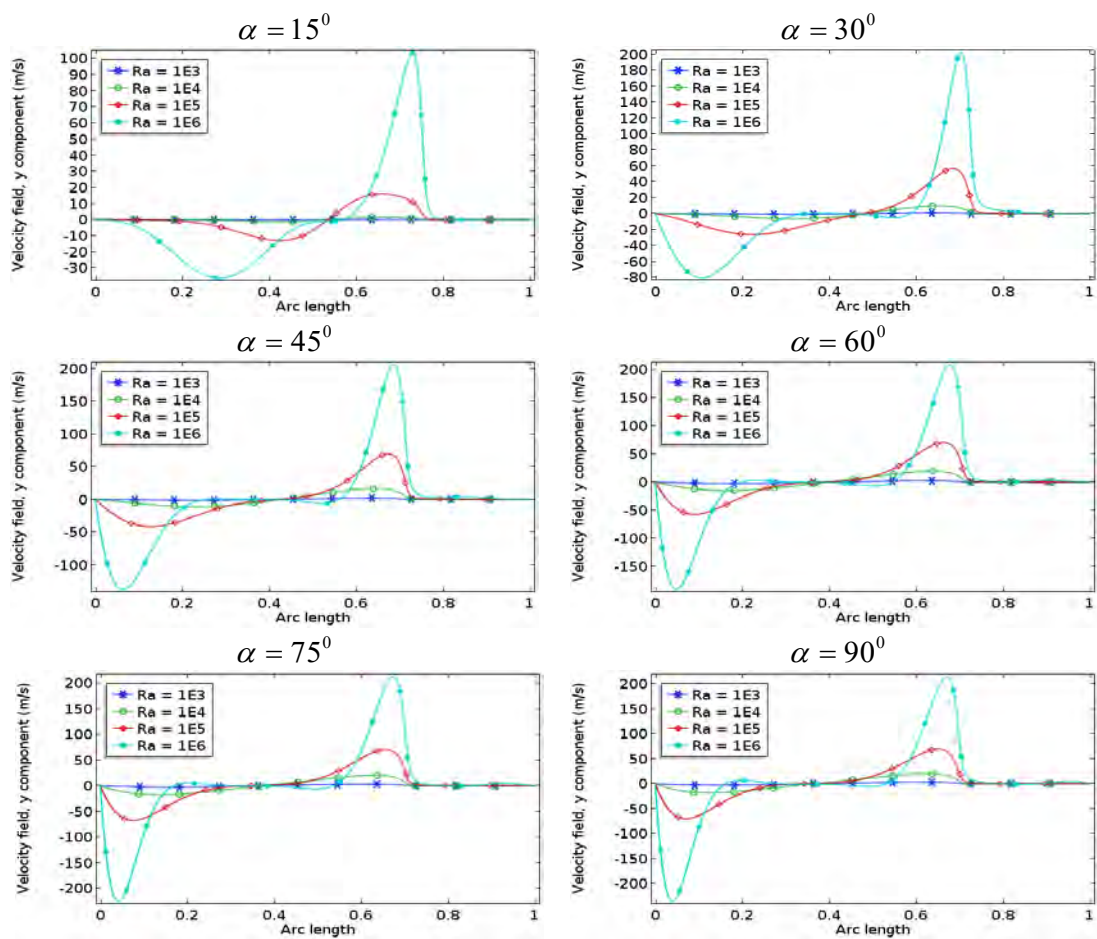
Figure 3.10 (a): Effect of Rayleigh number on **velocity profile** along the horizontal centerline for different skew angles ($15^0 \leq \alpha \leq 90^0$) with $L = 0.30$.

$$\alpha = 105^0$$

$$\alpha = 120^0$$

$$\alpha = 135^0$$

$$\alpha = 150^0$$

$$\alpha = 165^0$$
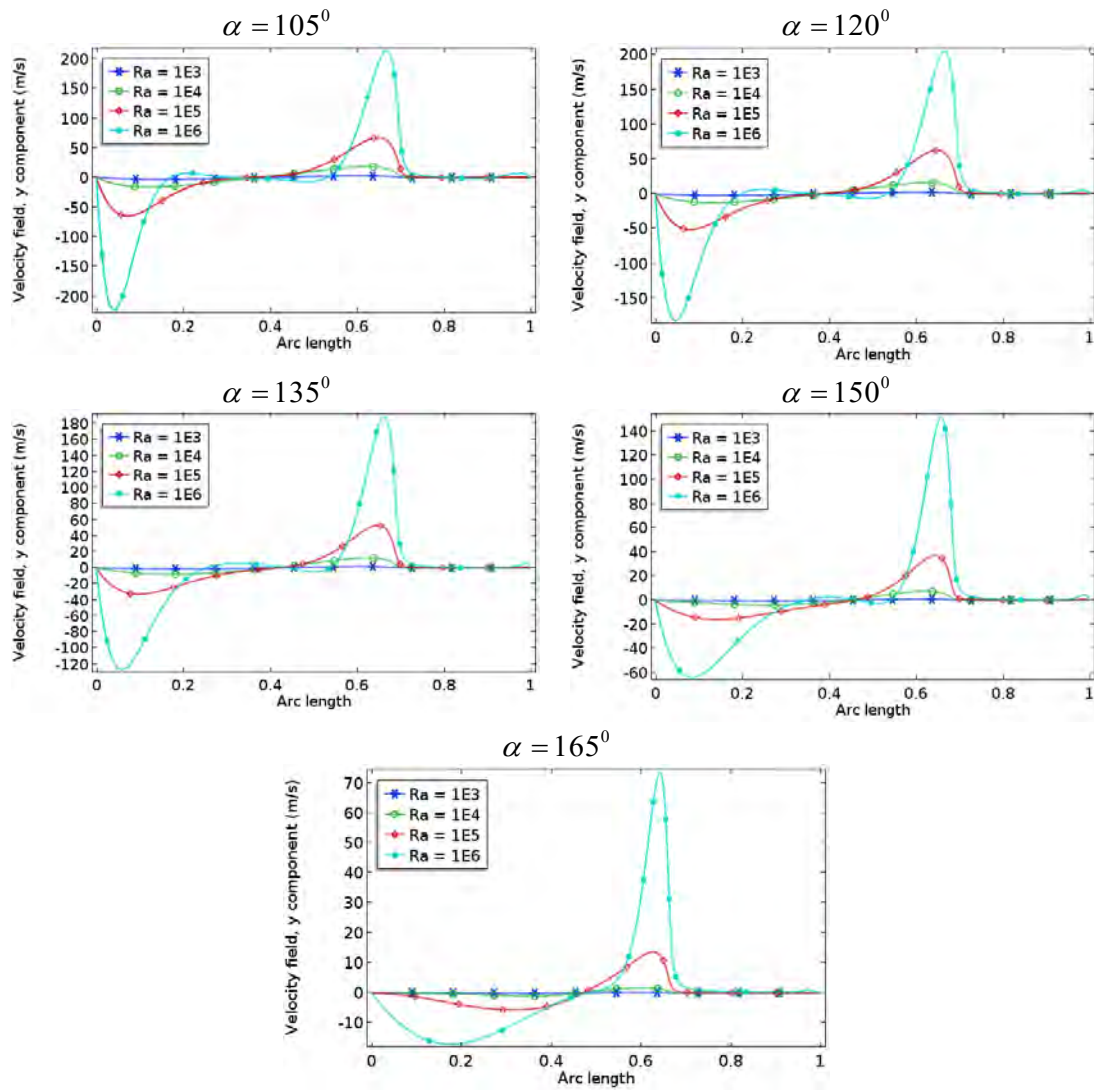
Figure 3.10 (b): Effect of Rayleigh number on **velocity profile** along the horizontal centerline for different skew angles $(105^0 \leq \alpha \leq 165^0)$ with $L = 0.30$.

Temperature profiles for *L* = 0.30 at *Pr* = 1.41

From Figure 3.11(a)-(b), the influence of the temperature profiles s along the horizontal centerline for different skew angles ($15^0 \leq \alpha \leq 165^0$) and Rayleigh number ($10^3 \leq Ra \leq 10^6$), baffle thickness D = 0.005 with sinusoidal heat transfer magnitude ($\lambda = 0.50$) shown in the plots. When the Rayleigh number increases, temperature become more crucial within the cavity. the curvature of the temperature lines becomes more prominent inside the enclosure due to the increased significance of the temperature. but temperature variation becomes insignificant around the central-most region of the cavity for skew angles ($30^0 \leq \alpha \leq 150^0$). As expected, a somewhat similar trend of temperature changes is scrutinized for skew angles $\alpha = 15^0$ and $\alpha = 165^0$.
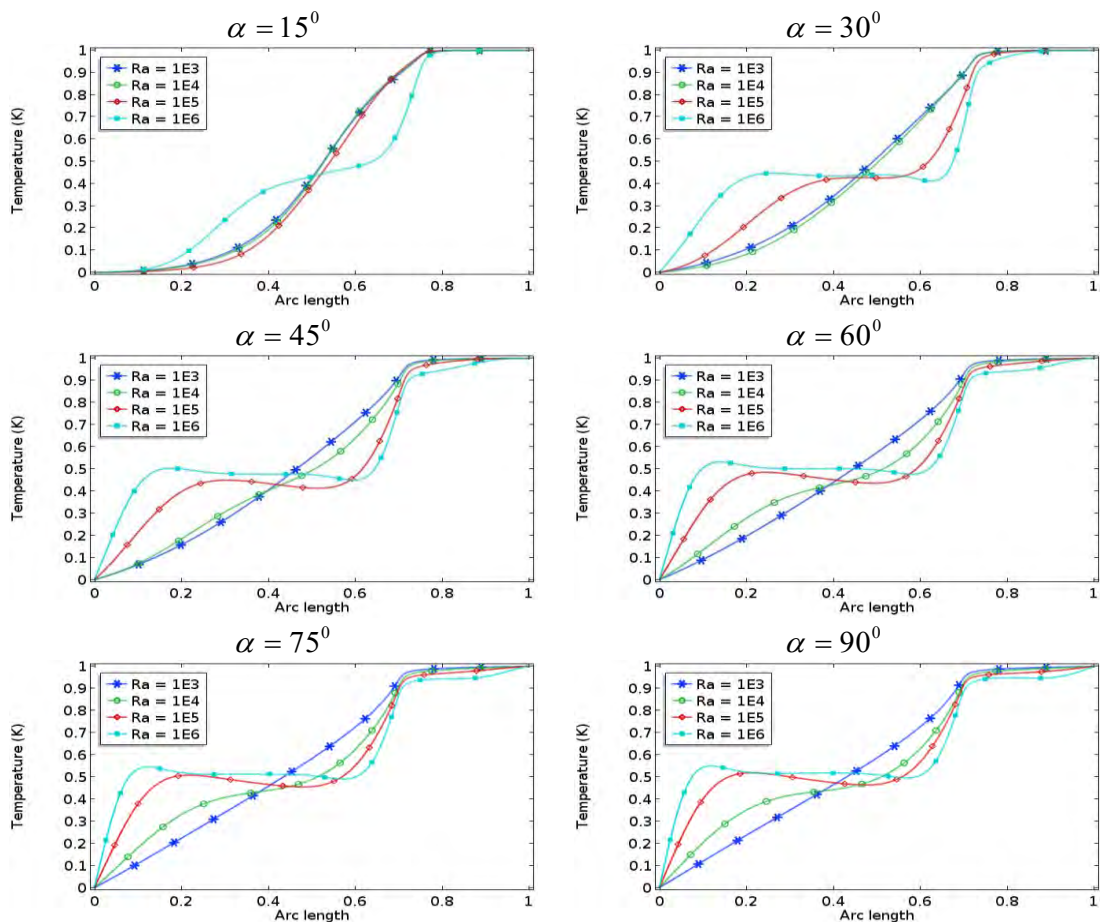
Figure 3.11 (a): Effect of Rayleigh number on **temperature profile** along the horizontal centreline for different skew angles ($15^0 \leq \alpha \leq 90^0$) with *L* = 0.30.
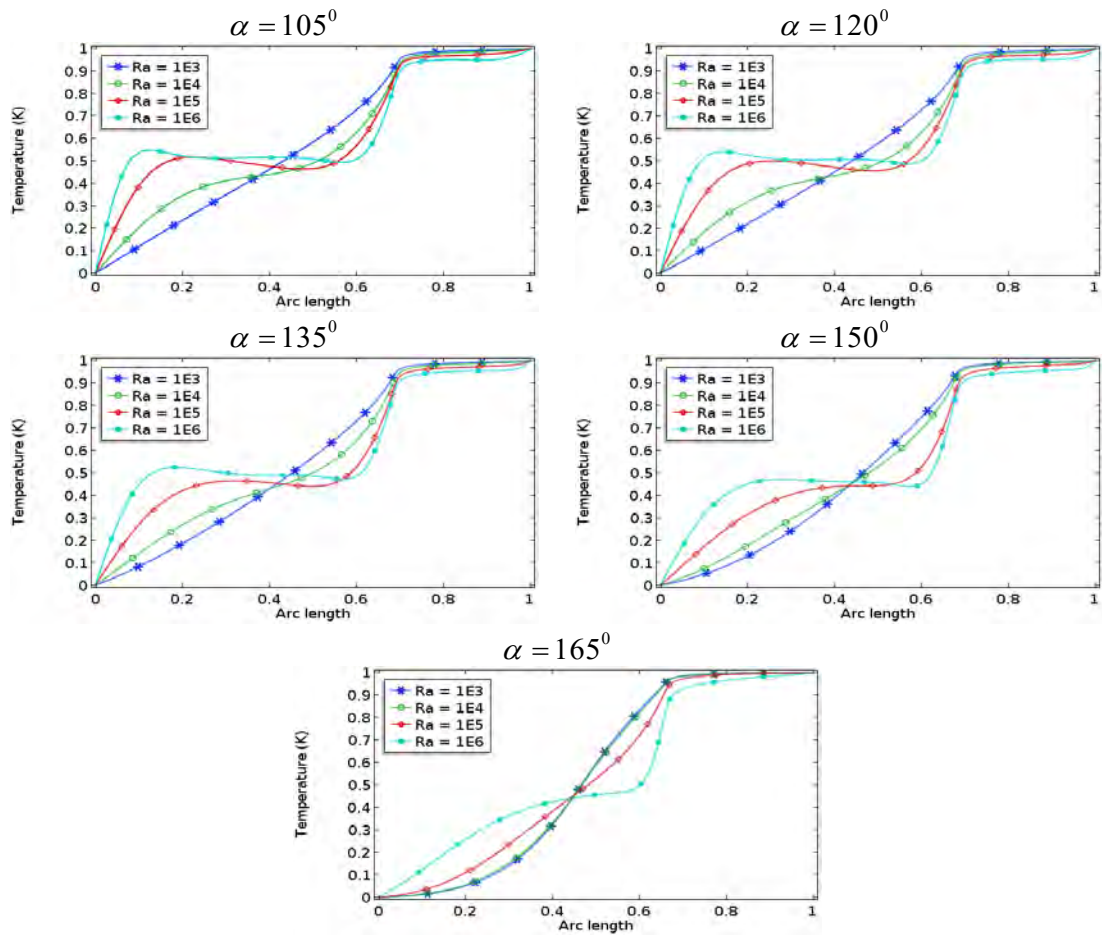
Figure 3.11 (b): Effect of Rayleigh number on **temperature profile** along the horizontal centreline for different skew angles $(105^0 \leq \alpha \leq 165^0)$ with $L = 0.30$.

Local Nusselt number for *L* = 0.30 at *Pr* = 1.41

Figure 3.16 displays the Effect of Rayleigh number $(10^3 \leq Ra \leq 10^6)$ on local Nusselt number along the inclined right wall for different skew angles $(15^0 \leq \alpha \leq 90^0)$, including baffle exteriors for the value of baffle length (*L* = 0.30) and baffle thickness (D = 0.005) at $(\lambda = 0.50)$. It was observed that the curvature of the local Nusselt number (Nu_L) substantial for all skew angles except at $\alpha = 15^0$. It also indicates that when the Rayleigh number increases, the curvature lines of the local Nusselt number rise in elevation.
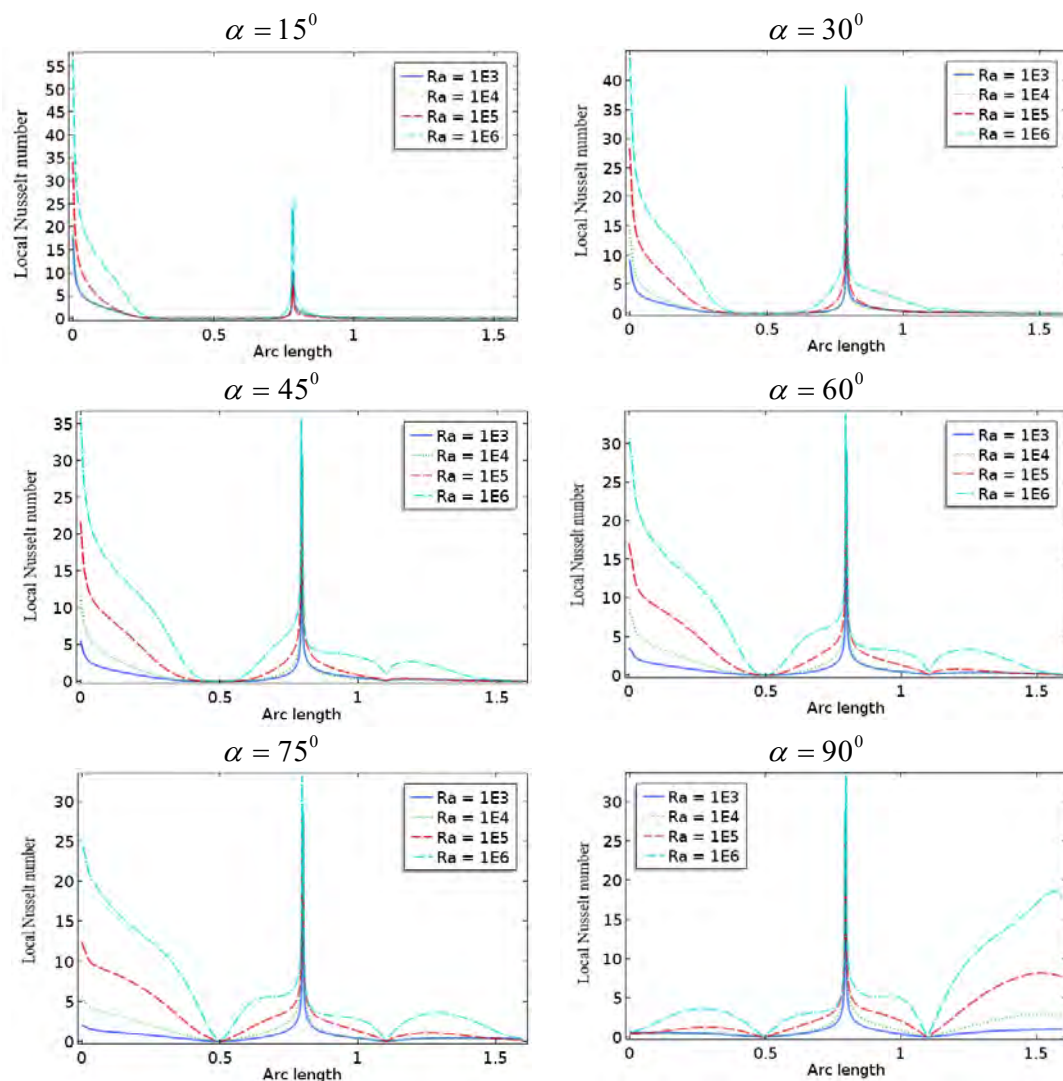
Figure 3.12 (a): Effect of Rayleigh number on **local Nusselt number** along the inclined right wall for different skew angles $(15^0 \leq \alpha \leq 90^0)$ with *L* = 0.30.

$$\alpha = 105^0 \qquad\qquad \alpha = 120^0$$

$$\alpha = 135^0 \qquad\qquad \alpha = 150^0$$

$$\alpha = 165^0$$
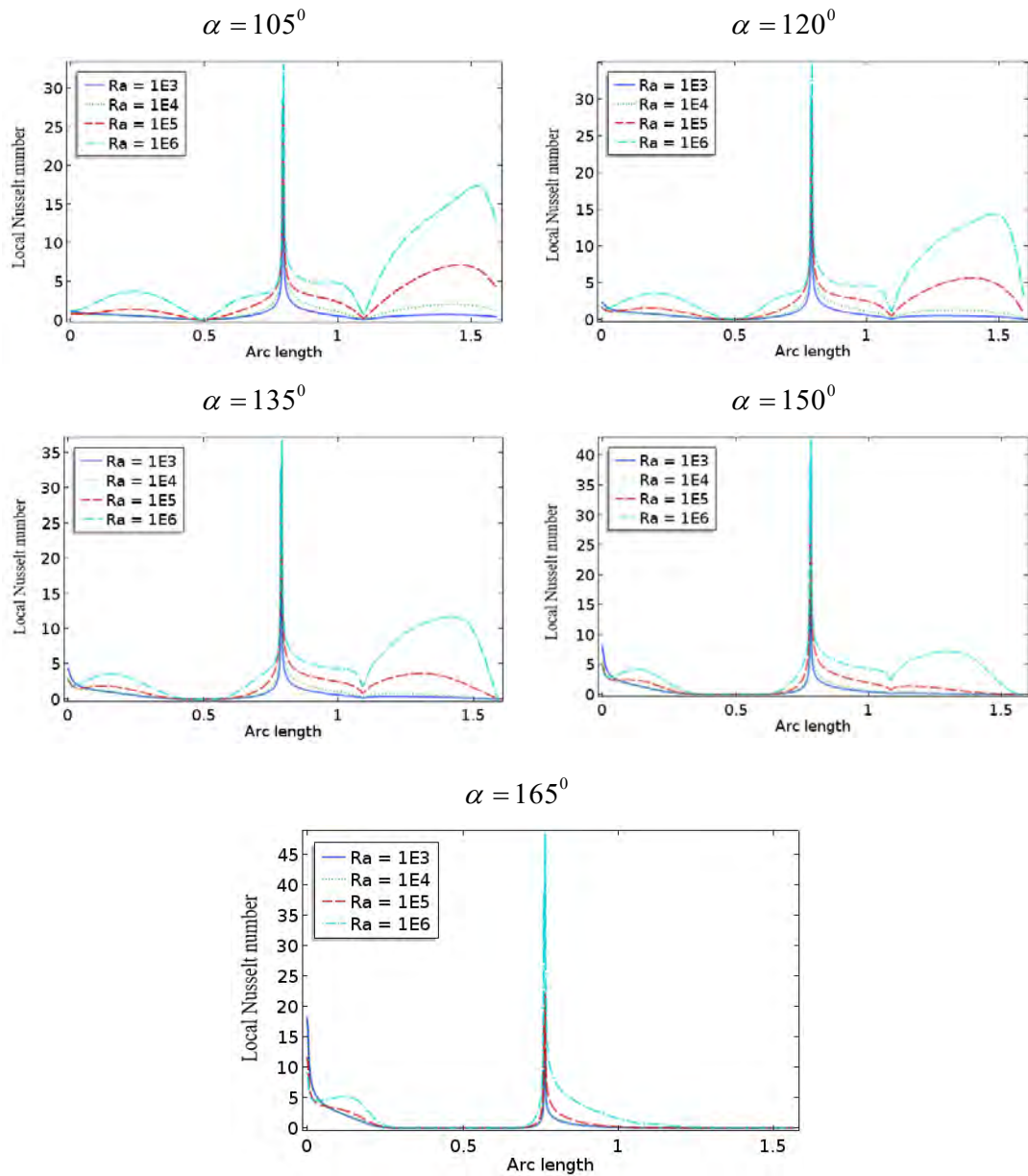
Figure 3.12 (b): Effect of Rayleigh number on **local Nusselt number** along the inclined right wall for different skew angles $(105^0 \leq \alpha \leq 165^0)$ with $L = 0.30$.

Figure 3.13 and Figure 3.14 represent the average fluid temperature and average Nusselt number for varying skew angles, as well as the Rayleigh number (*Ra*) at a constant baffle location (B). At the same time, the values of the other parameters are kept at their default values. The quantitative data in Table 3.3 and Table 3.4 show the magnitude of the average fluid temperature and average Nusselt number for varying skew angles and Rayleigh number (*Ra*) at a constant baffle length (L) and baffle location (B).

Average fluid temperature for *L* = 0.30 at *Pr* = 1.41

When the skew angle is increased to $\alpha = 90^0$, the average fluid temperature declines progressively, except at the skew angle $\alpha = 30^0$. Increased Ra causes the average fluid temperature to increase for all skew angles when the baffle is in the stationary position, as illustrated in Figure 3.13 and the numerical value in Table 3.3. Furthermore, according to Table 3.3, the highest mean fluid temperature inside the cavity is **2.6914052935736750** at $\alpha = 150^0$, which was observed in this instance.
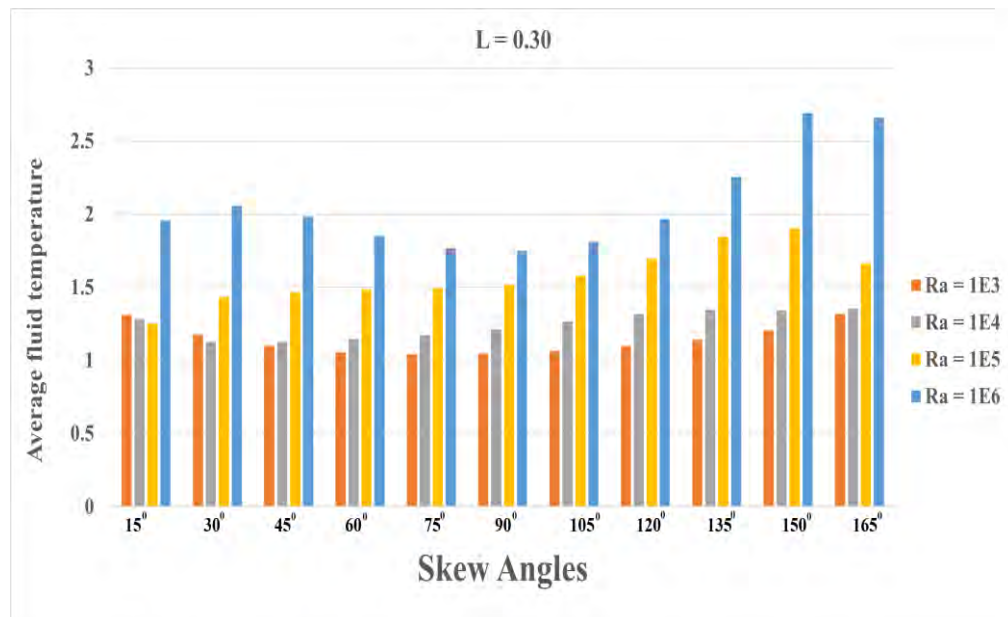

Figure 3.13: **Average fluid temperature** variations for skew angles and Ra at *L* = 0.30.

Table 3.3: Average fluid temperature variations for skew angles and Ra.

Angles	Average fluid temperature			
	$Ra=10^3$	$Ra=10^4$	$Ra=10^5$	$Ra=10^6$
$\alpha=15^0$	1.31334447305	1.2813186060	1.2519007691	1.9580465232
$\alpha=30^0$	1.17528847738	1.1276112087	1.4344542759	2.0580953665
$\alpha=45^0$	1.09865388408	1.1287291222	1.4651487470	1.9838041511
$\alpha=60^0$	1.05662046025	1.1472254175	1.4850104360	1.8511382210
$\alpha=75^0$	1.04105016589	1.1751397312	1.4924169790	1.7668503529
$\alpha=90^0$	1.04563778148	1.2152484750	1.5172122107	1.7511702997
$\alpha=105^0$	1.06531698757	1.2653800719	1.5804068444	1.8113724259
$\alpha=120^0$	1.09732039091	1.3154249032	1.6947023750	1.9658220469
$\alpha=135^0$	1.14159721168	1.3463270270	1.8442758195	2.2530562144
$\alpha=150^0$	1.20450229227	1.3417128368	1.9013777601	**2.6914052935**
$\alpha=165^0$	1.31822059694	1.3527676151	1.6641008997	2.6615099520

Average Nusselt number for *L* = 0.30 at *Pr* = 1.41

Figure 3.14-3.15 shows the arrangement of the average Nusselt number (Nu_{avg}) on the right inclined wall, including the baffle surface with the impact of skew angles ($15^0 \le \alpha \le 165^0$) within the skewed cavity for various values of Rayleigh numbers ($10^3 \le Ra \le 10^6$). The most significant investigation results are to Augment the heat transfer rate increasing the skew angle to $\alpha=90^0$ for all the Rayleigh numbers. After that, the heat transfer rate decreases for all the Rayleigh numbers by increasing the skew angle to $\alpha=165^0$. The mean Nusselt number augments with the increase of the Rayleigh number and varying skew angles at a regular baffle size and location. As a result, we can conclude that the heat transfer rate increases as the Rayleigh number increases. The buoyancy force rises, and heat transmission improves as the Rayleigh number grows at a uniform baffle length. Because of the convergence of these curves, it is easy to note that the influence of skew angles with the baffle placements on the heated wall is less evident. Table 3.4 shows the numerical value of a mean Nusselt number along the right inclined wall, including

baffle surface with different values of skew angles and Rayleigh numbers. Also, including Table 3.4, the highest Nu_{avg} is **5.954877283556091** along heated surface exposed at $\alpha = 90^0$, $Ra = 10^6$.

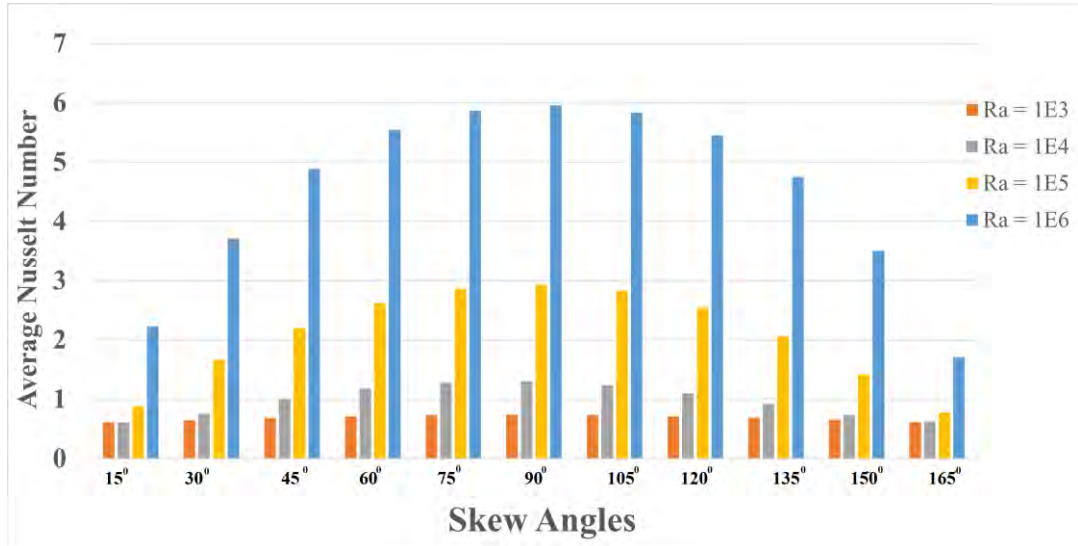**Figure 3.14:** Impact of Nu_{avg} for various skew angle and Ra for L = 0.30.

$$\alpha = 15^0 - 90^0 \qquad\qquad \alpha = 105^0 - 165^0$$
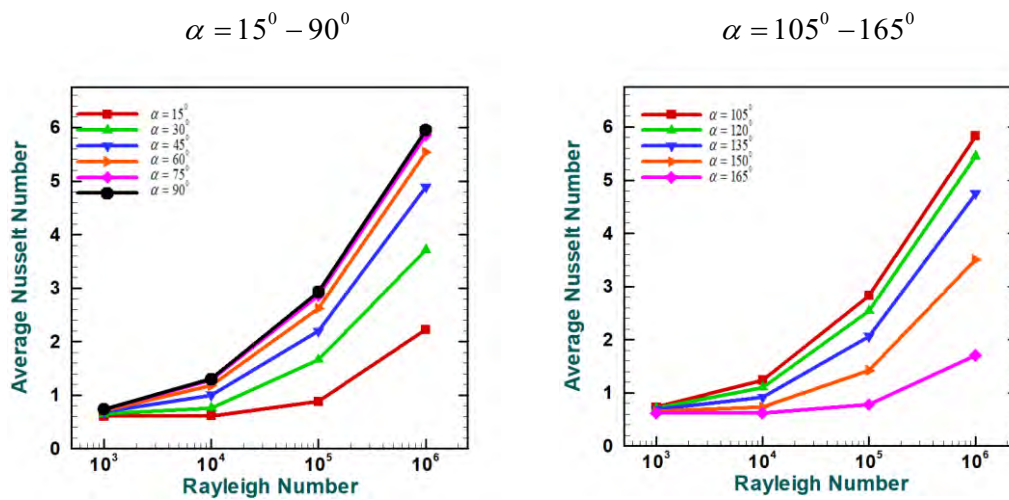
Figure 3.15: Impact of Nu_{avg} for various skew angle and Ra at $L = 0.30$.

Table 3.4: Average Nusselt number variations at $L = 0.30$ for several skew angles.

Angles	Average Nusselt number			
	$Ra = 10^3$	$Ra = 10^4$	$Ra = 10^5$	$Ra = 10^6$
$\alpha = 15^0$	0.6112808549	0.6124265266	0.8822105649	2.2262156937
$\alpha = 30^0$	0.6509568379	0.7588398532	1.6664389042	3.7123003808
$\alpha = 45^0$	0.6868521060	1.0014415932	2.1979866820	4.887453769
$\alpha = 60^0$	0.7151717554	1.1799940912	2.6224620731	5.537871649
$\alpha = 75^0$	0.7342273186	1.2810496176	2.8633059361	5.863326647
$\alpha = 90^0$	0.7409135400	1.3018375270	2.9298714450	**5.954877283**
$\alpha = 105^0$	0.7343268366	1.2389821991	2.8291725266	5.833615801
$\alpha = 120^0$	0.7164800346	1.1012491598	2.5434667240	5.450182766
$\alpha = 135^0$	0.6902587740	0.9193783588	2.0633616430	4.747949960
$\alpha = 150^0$	0.6561407152	0.7351962283	1.4239681852	3.505464552
$\alpha = 165^0$	0.6172627331	0.6227160443	0.7777603321	1.707626249

Case-III: (Effect of the skewed angle for the baffle length L = 0.50)

In this case, the numerical outputs of the natural convection heat transfer analysis in sinusoidal boundary conditions in a skewed cavity with a horizontal baffle. The required results were obtained by the variety of Rayleigh numbers, skew angles at the baffle length L = 0.30. In this case, the data are shown in Figures 3.16 - 3.25 was obtained by finite-element method.

Findings from streamlines:

For various Rayleigh numbers ($(10^3 \leq Ra \leq 10^6)$) and skew angles$(15^0 \leq \alpha \leq 165^0)$, Figures 3.16(a)-(f) depict streamlines for the baffle length maintained at L=0.50 is connected at the middle position of the inclined right wall inside the skewed enclosure. From the Figure 3.16, the maximum velocity gradually rises with increase of the Rayleigh numbers for all the skew angles. Furthermore, the maximum velocity gradually rises with the increase of the skew angles. For different skew angles at a fixed baffle position, a larger principal cell was created, with its center roughly in the center of the cavity. There is at least one irregular elliptic-shaped vortex inside the cavity. When the buoyancy strength inside the cavity becomes even more remarkable, an elliptic-shaped cell emerges within the cavity once again. From the Figure 3.16, we can see that the maximum velocity gradually augments for the skew angle increase up to $\alpha = 90^0$ for all the Rayleigh numbers. By increasing the skew angles to $\alpha = 165^0$, the maximum velocity drops steadily. As previously mentioned, the maximum velocity increases as the Rayleigh number grows.

Finally, with the baffle length L= 0.50, the maximum velocity at $\alpha = 90^0$ and $Ra = 10^6$ is $49 ms^{-1}$.
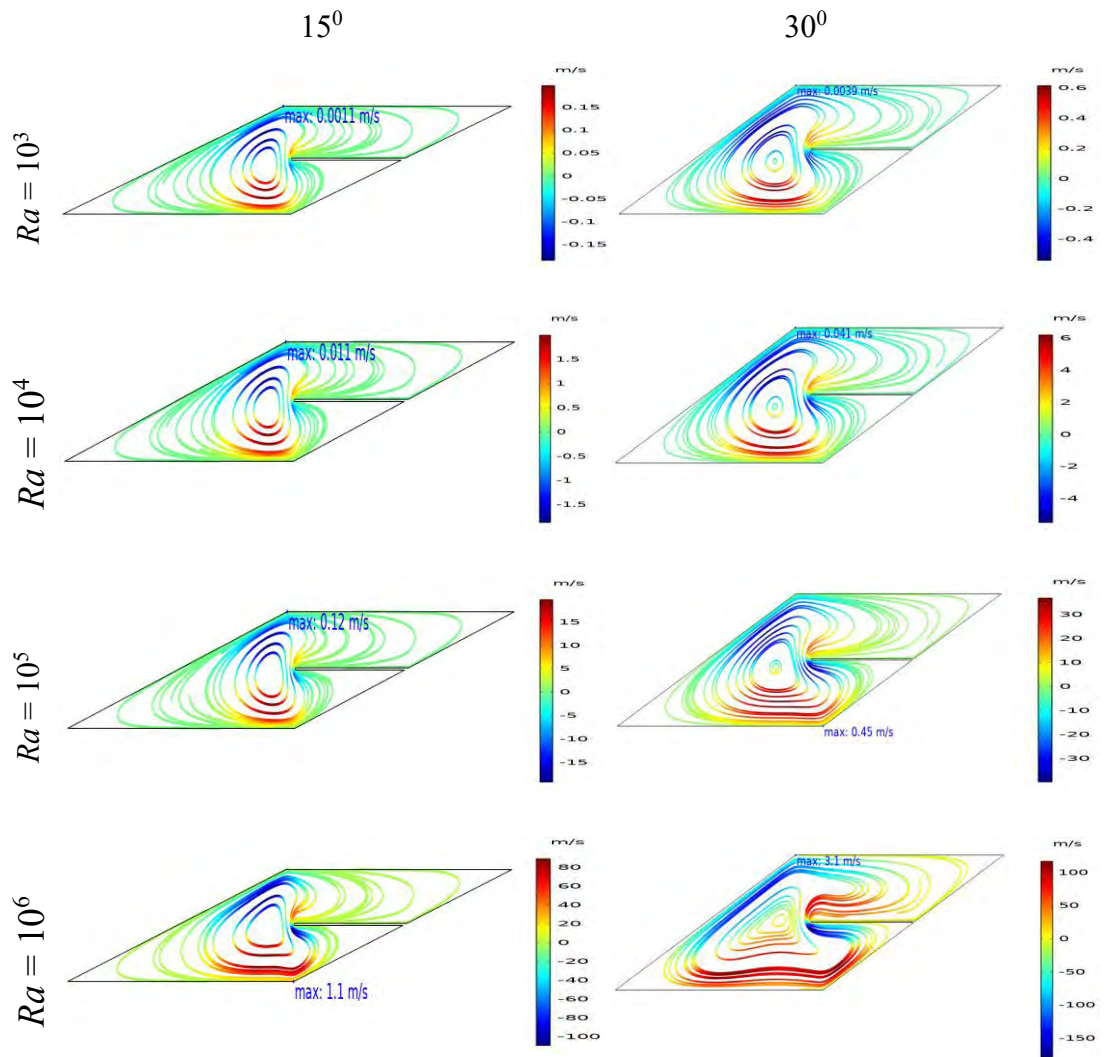
Figure 3.16(a): Streamline variations for the skew angles ($\alpha = 15^0$, *and* $\alpha = 30^0$) at $L = 0.50$

45^0 60^0

$Ra = 10^3$

$Ra = 10^4$

$Ra = 10^5$

$Ra = 10^6$
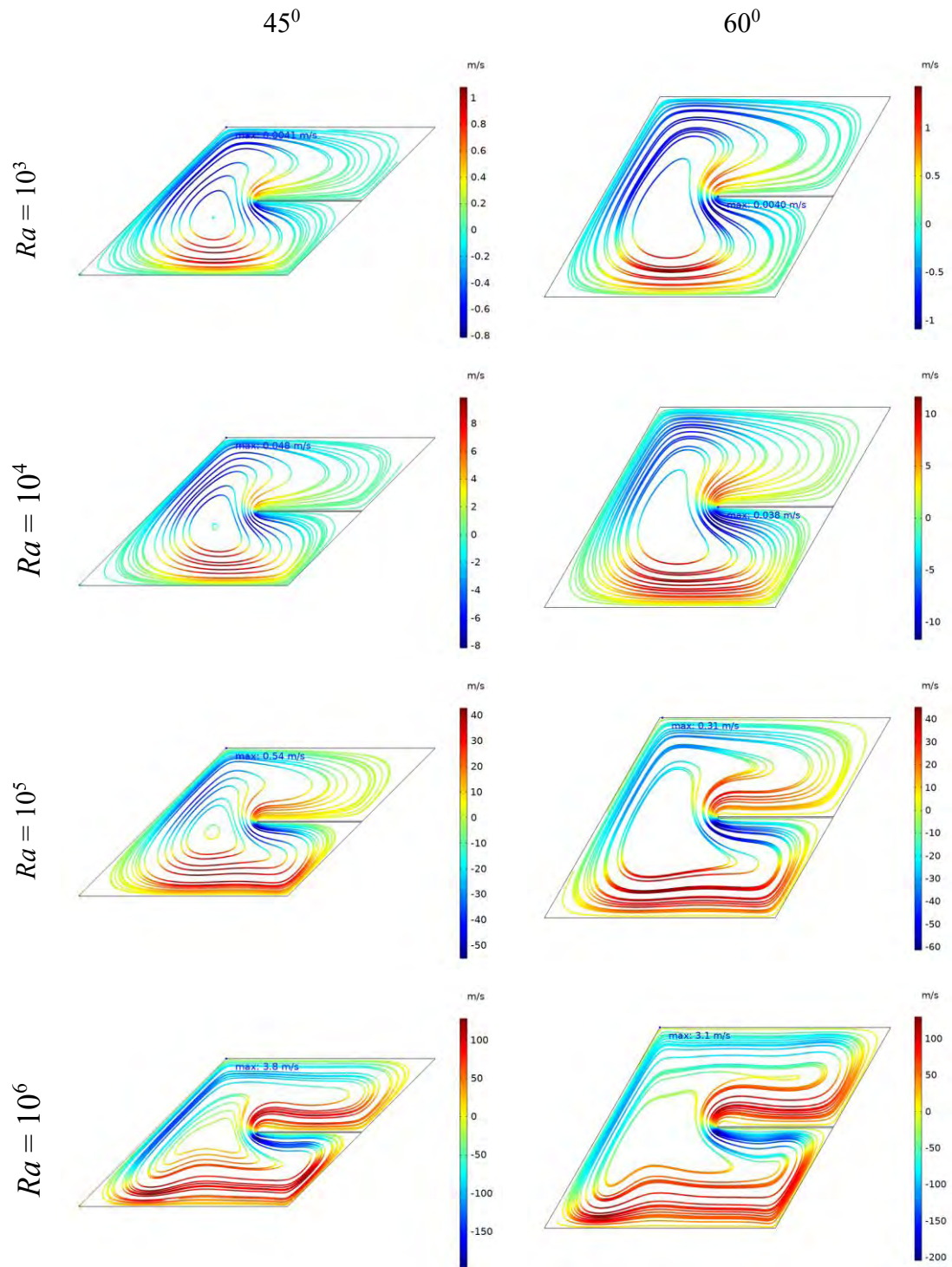
Figure 3.16(b): Streamline variations for the skew angles ($\alpha = 45^0$, *and* $\alpha = 60^0$) at $L = 0.50$

75⁰ 90⁰

$Ra = 10^3$

$Ra = 10^4$

$Ra = 10^5$

$Ra = 10^6$
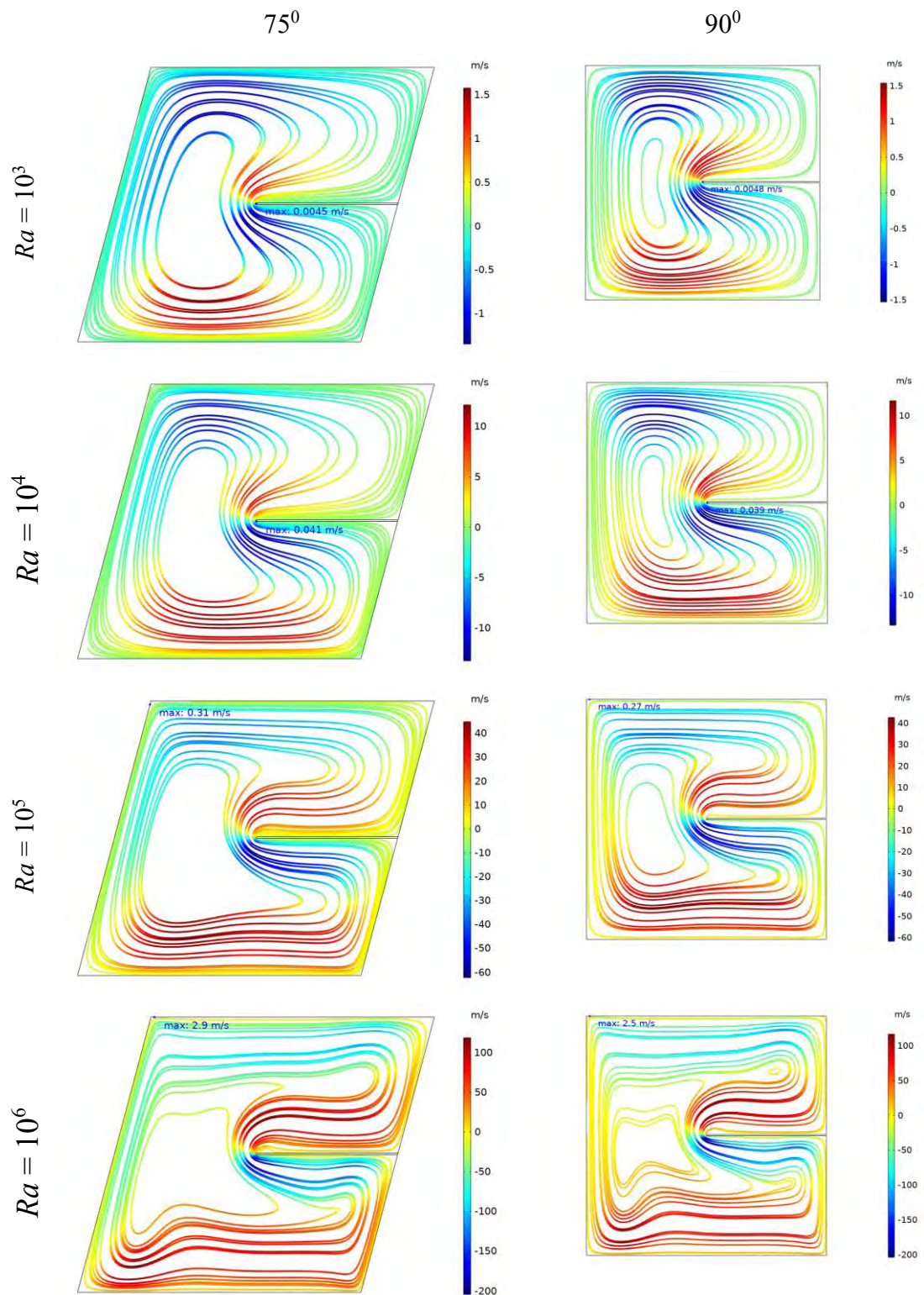
Figure 3.16(c): Streamline variations for the skew angles ($\alpha = 75^0$, and $\alpha = 90^0$) at $L = 0.50$

Figure 3.16(d): Streamline variations for the skew angles ($\alpha = 105^0$, and $\alpha = 120^0$) at $L = 0.50$.

135⁰   150⁰

Ra = 10³

Ra = 10⁴

Ra = 10⁵

Ra = 10⁶
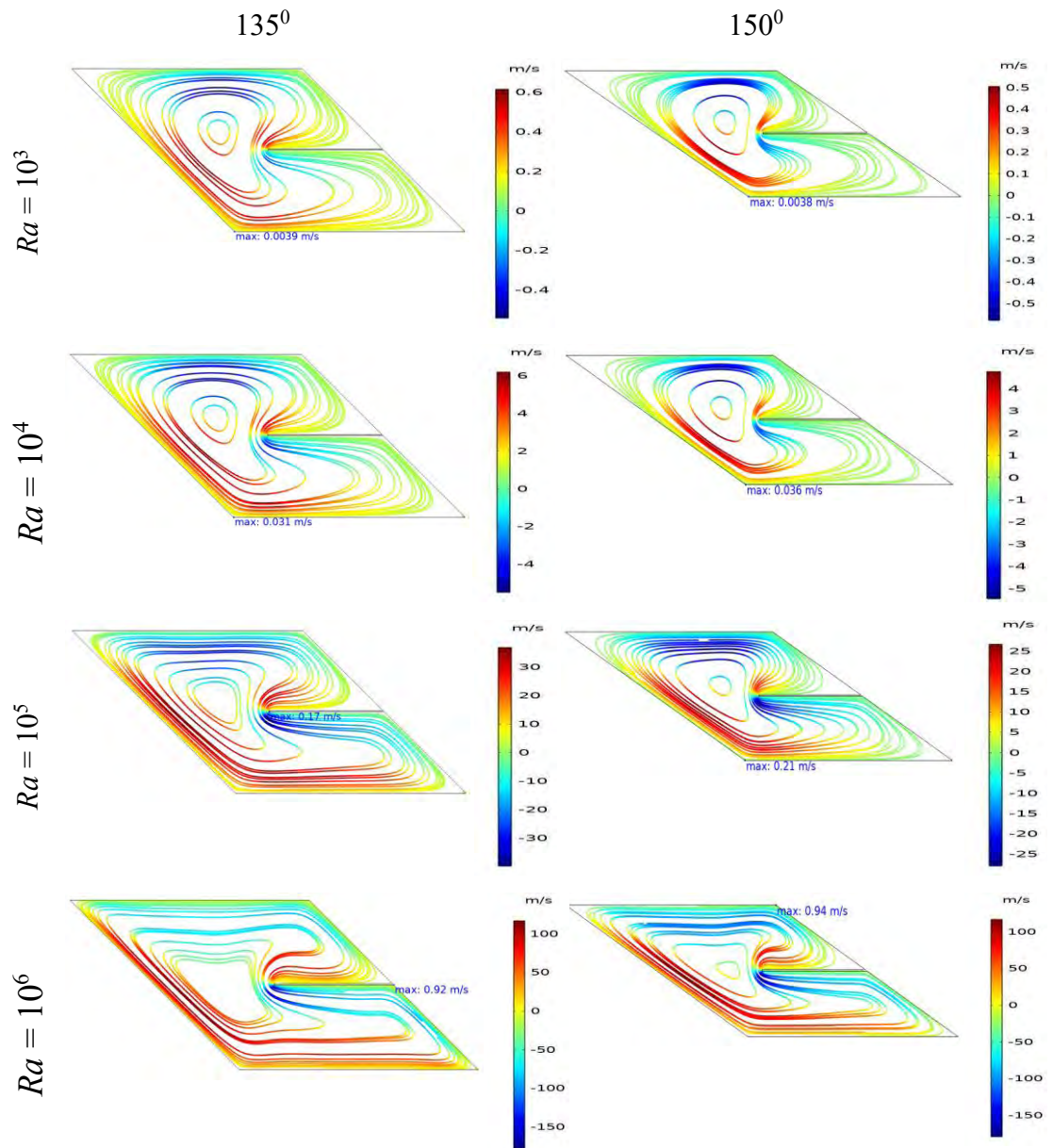
Figure 3.16(e): Streamline variations for the skew angles ($\alpha = 135^0$, *and* $\alpha = 150^0$) at $L = 0.50$

165⁰

$Ra = 10^3$ $Ra = 10^5$

$Ra = 10^4$ $Ra = 10^6$
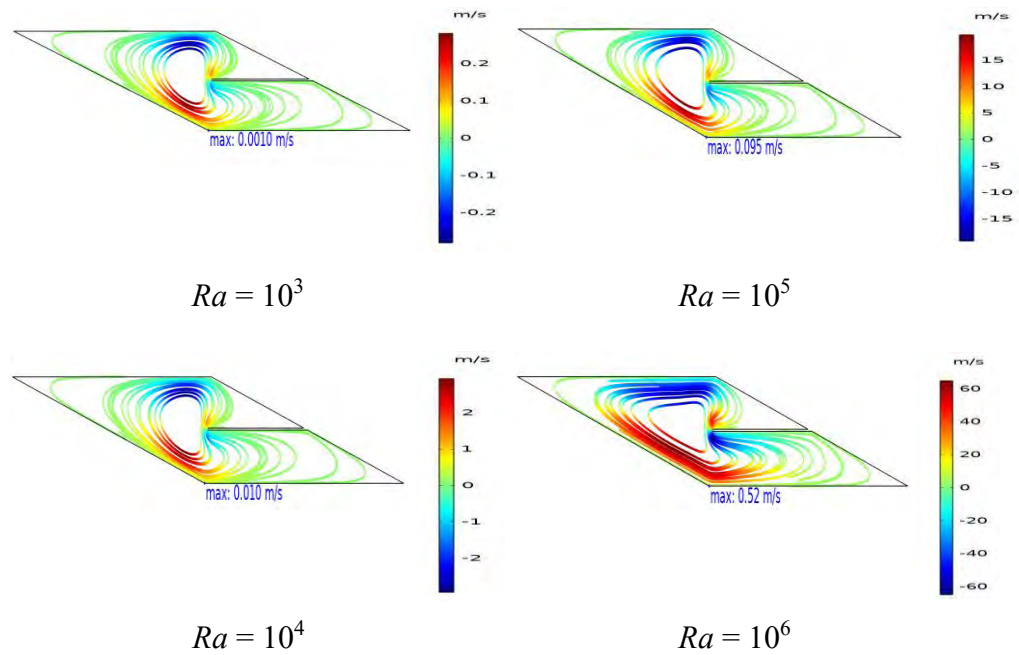
Figure 3.16(f): Streamline variations for the skew angle ($\alpha = 165^0$) at $L = 0.50$

Findings from isotherms:

At a fixed baffle length ($L = 0.50$) and position B = 0.50, figures 3.17(a)-(f) show the predominant heat transfer conductance. The findings are provided in isotherms with multiple Rayleigh numbers ($15^0 \le \alpha \le 165^0$) and skew angles ($15^0 \le \alpha \le 165^0$). The top and lower side of the baffle and left-inclined surface are denser for all skew angles and Rayleigh numbers. In addition, the isotherm lines exert more significant influence within the enclosure, increasing heat transfer through convection. Findings from isotherms in this case highly similar to the other cases as described before.
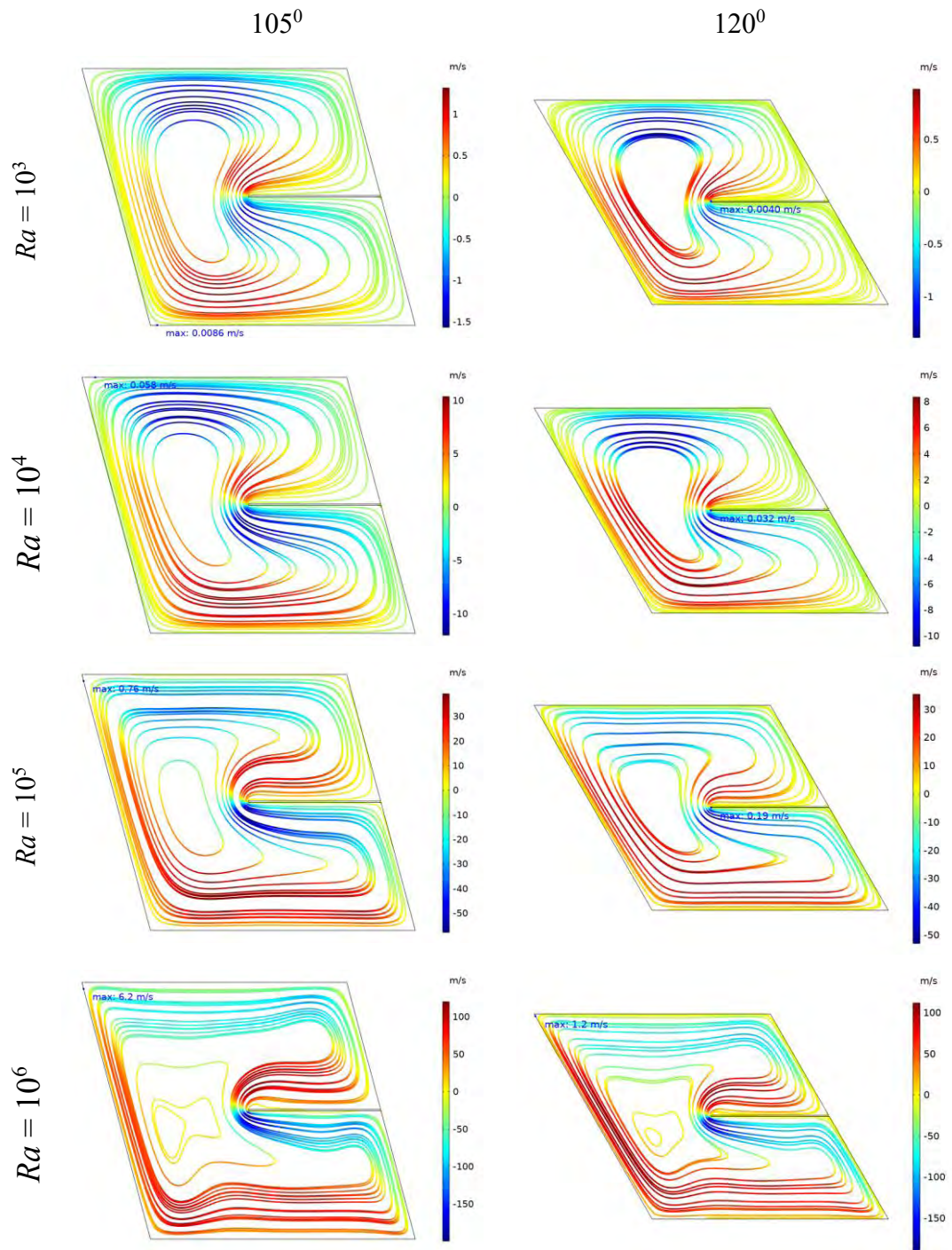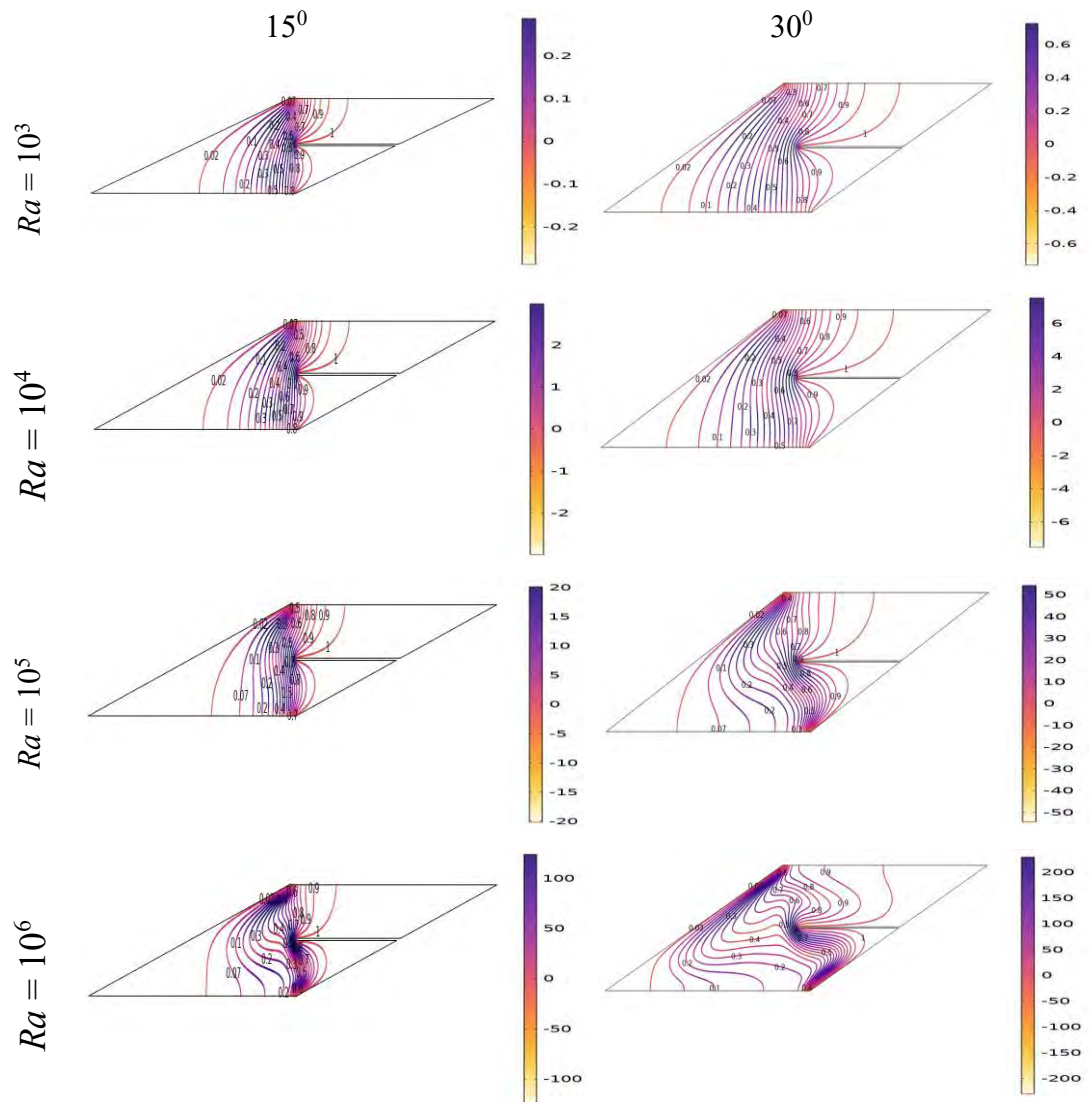
Figure 3.17(a): Isotherm variations for skew angles ($\alpha = 15^0$, *and* $\alpha = 30^0$) at $L = 0.50$.
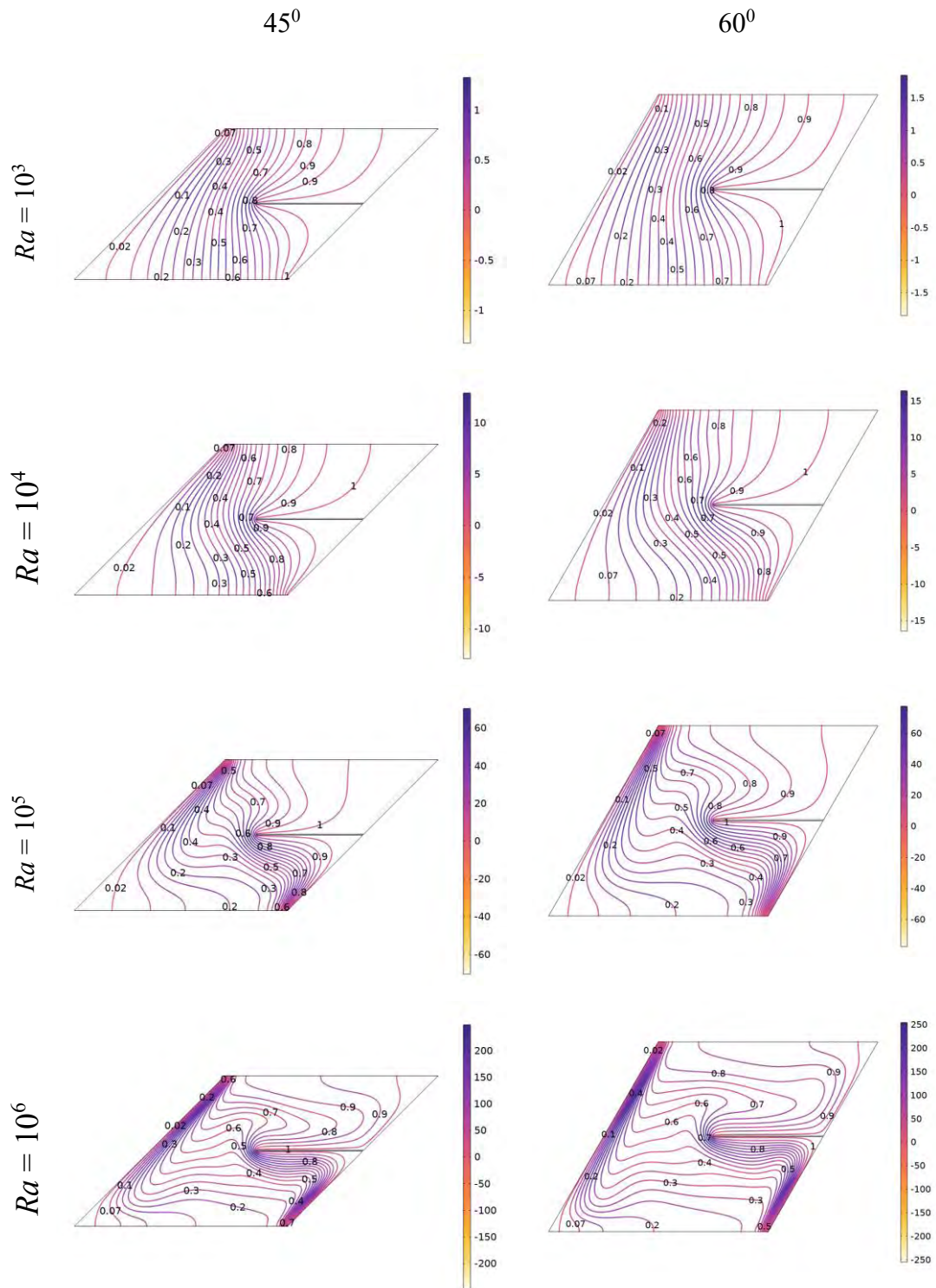
Figure 3.17(b): Isotherm variations for skew angles ($\alpha = 45^0$, *and* $\alpha = 60^0$) at $L = 0.50$.

75^0 90^0
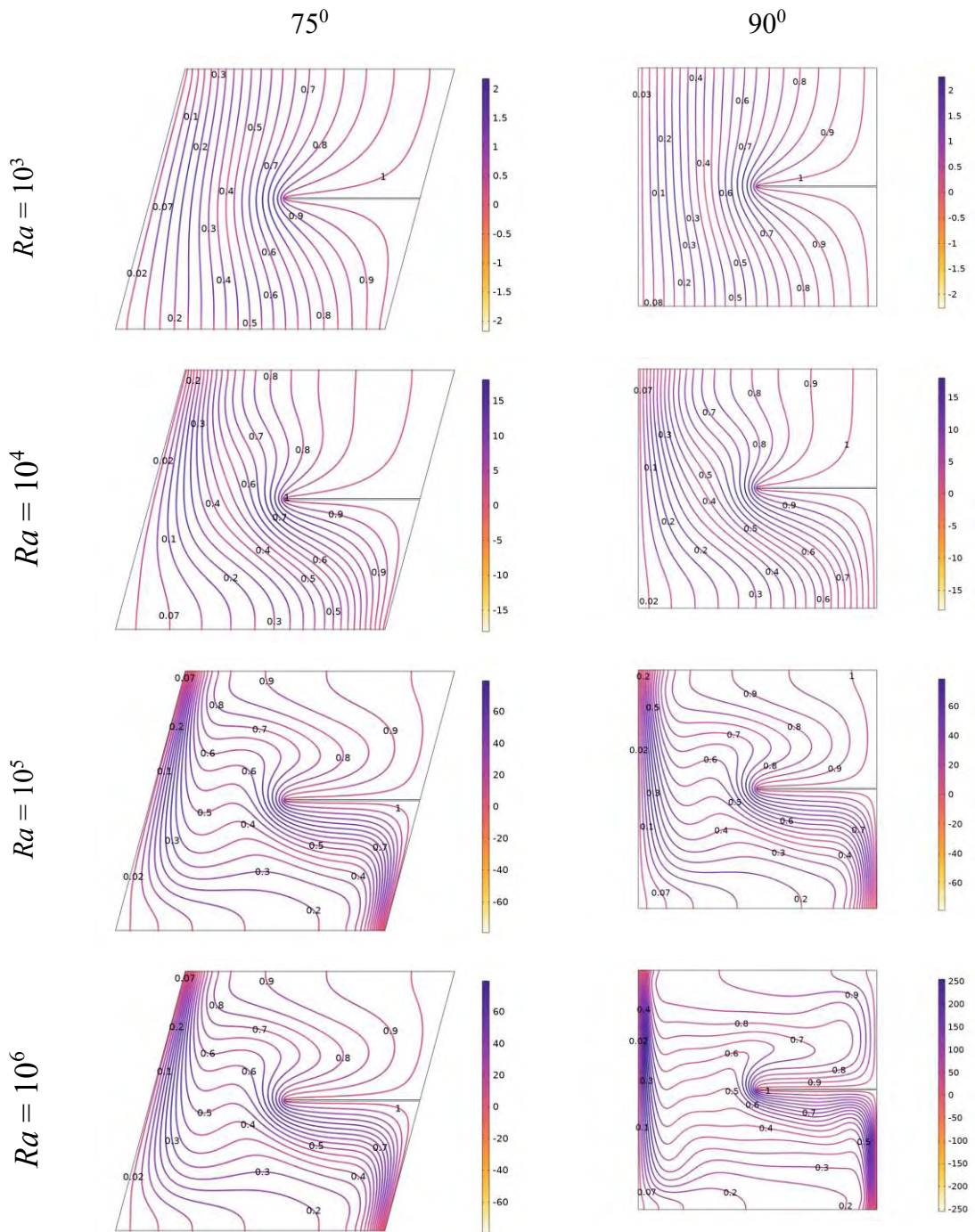
Figure 3.17(c): Isotherm variations for skew angles ($\alpha = 75^0$, *and* $\alpha = 90^0$)
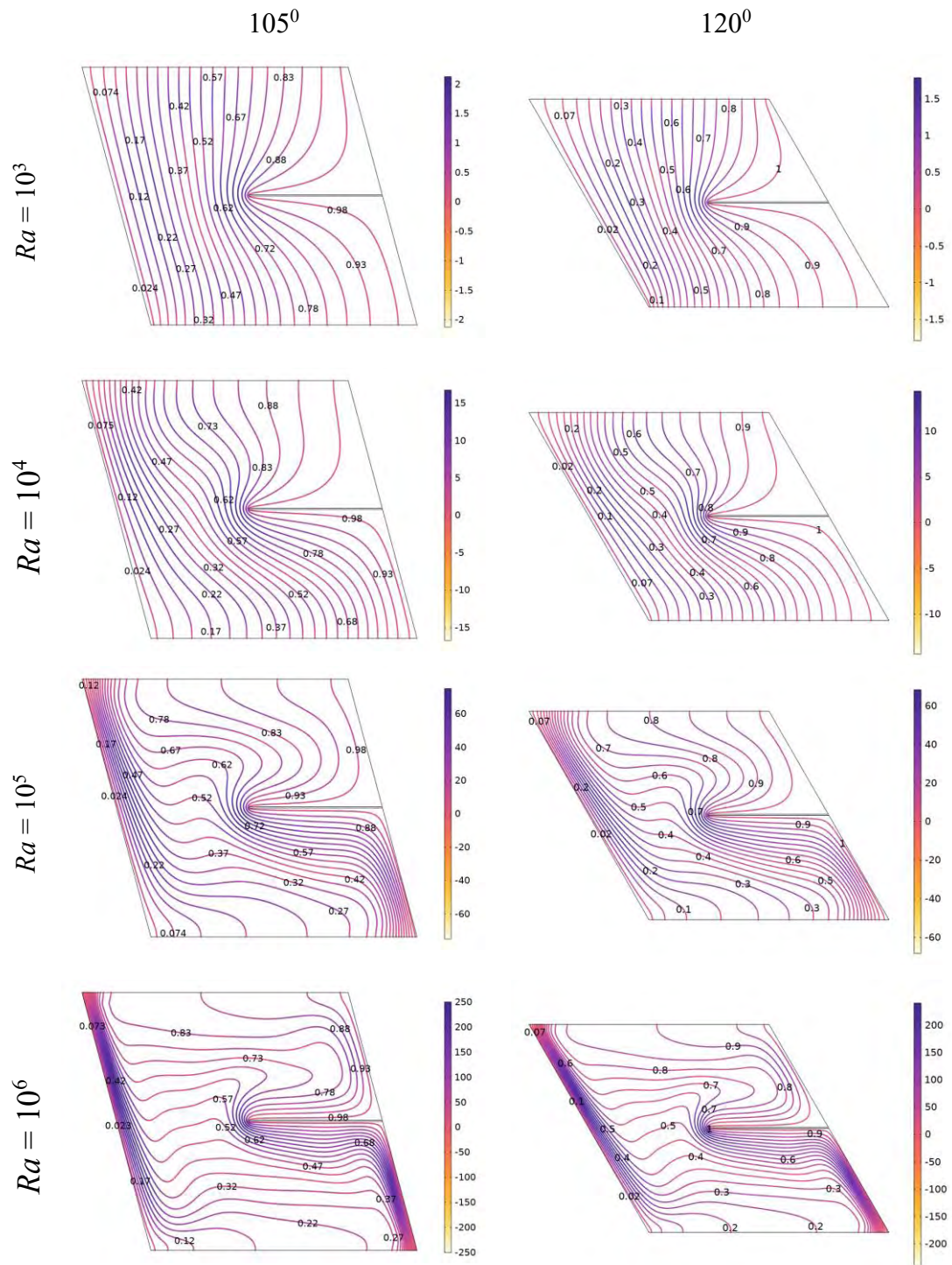
at $L = 0.50$.

Figure 3.17(d): Isotherm variations for skew angles ($\alpha = 105^0$, and $\alpha = 120^0$) at $L = 0.50$.

135^0 150^0
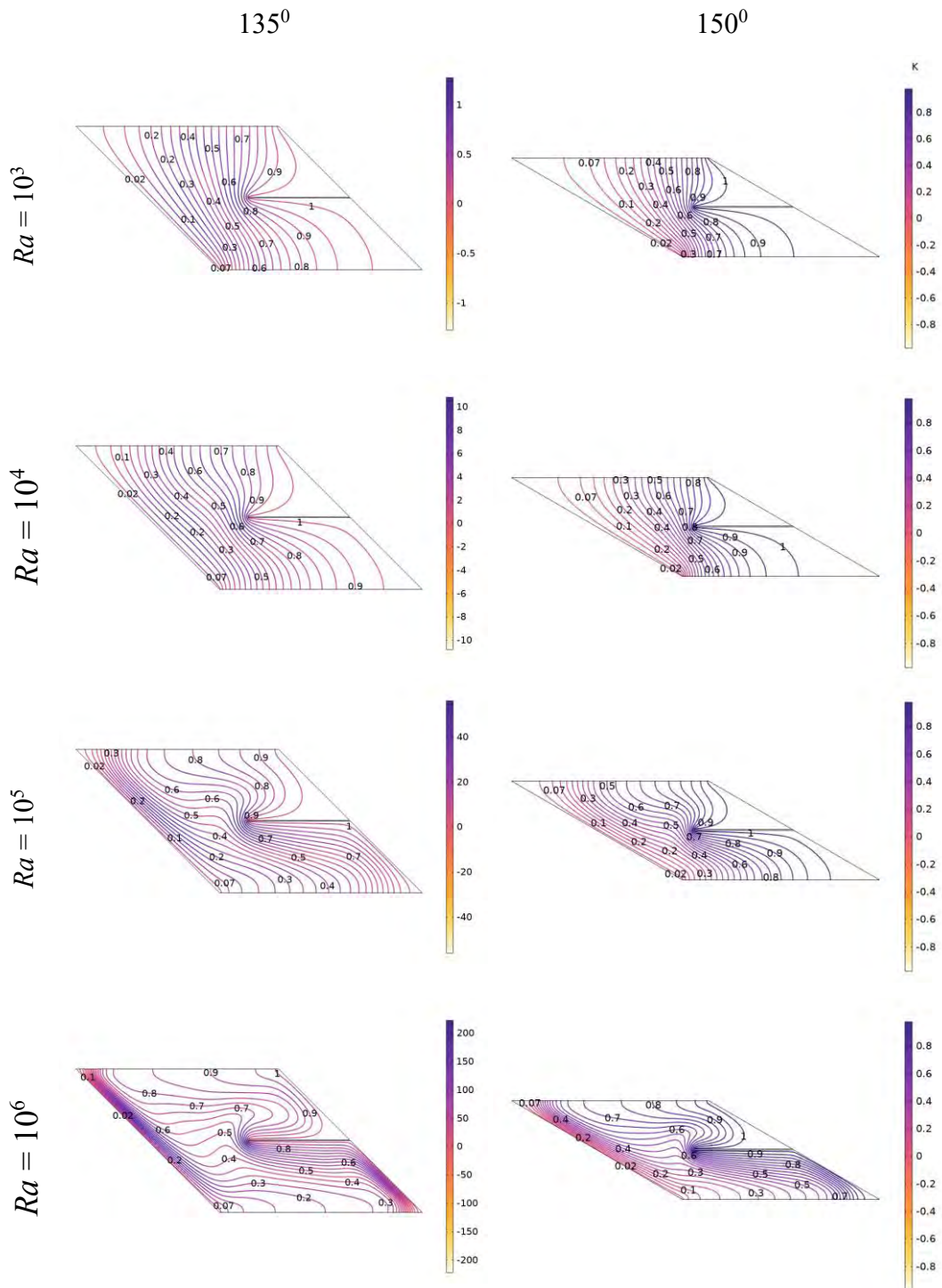
Figure 3.17(e): Isotherm variations for skew angles ($\alpha = 135^0$, *and* $\alpha = 150^0$)

at $L = 0.50$

165^{0}
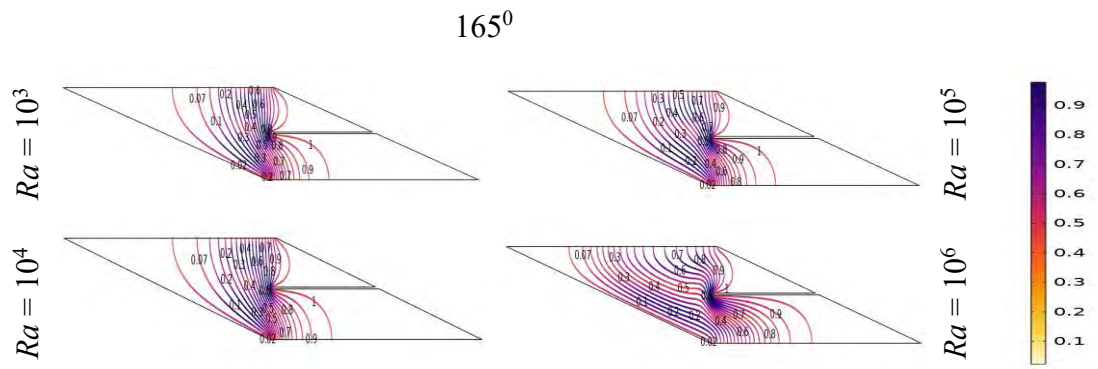
Figure 3.17(f): Isotherm variations for skew angle ($\alpha = 165^{0}$) at $L = 0.50$

Velocity profiles for *L* = 0.50 at *Pr* = 1.41

Figure 3.18(a)-(b) show Effect of Rayleigh number $(10^3 \leq Ra \leq 10^6)$ on velocity profile along the horizontal centerline for different skew angles $(15^0 \leq \alpha \leq 165^0)$ with *L* = 0.50 and baffle thickness D = 0.005 at a given location of baffle within the cavity. It seems that at $Ra = 10^3$ and $Ra = 10^4$, the dimensionless velocity rises only insignificantly, as seen in Figure 3.18(a)-(b). we can see from the figure 3.18, the dimensionless velocity changes consequently in the first half of the arc length for the higher values of the Rayleigh number. But in the second half its movement insignificant.
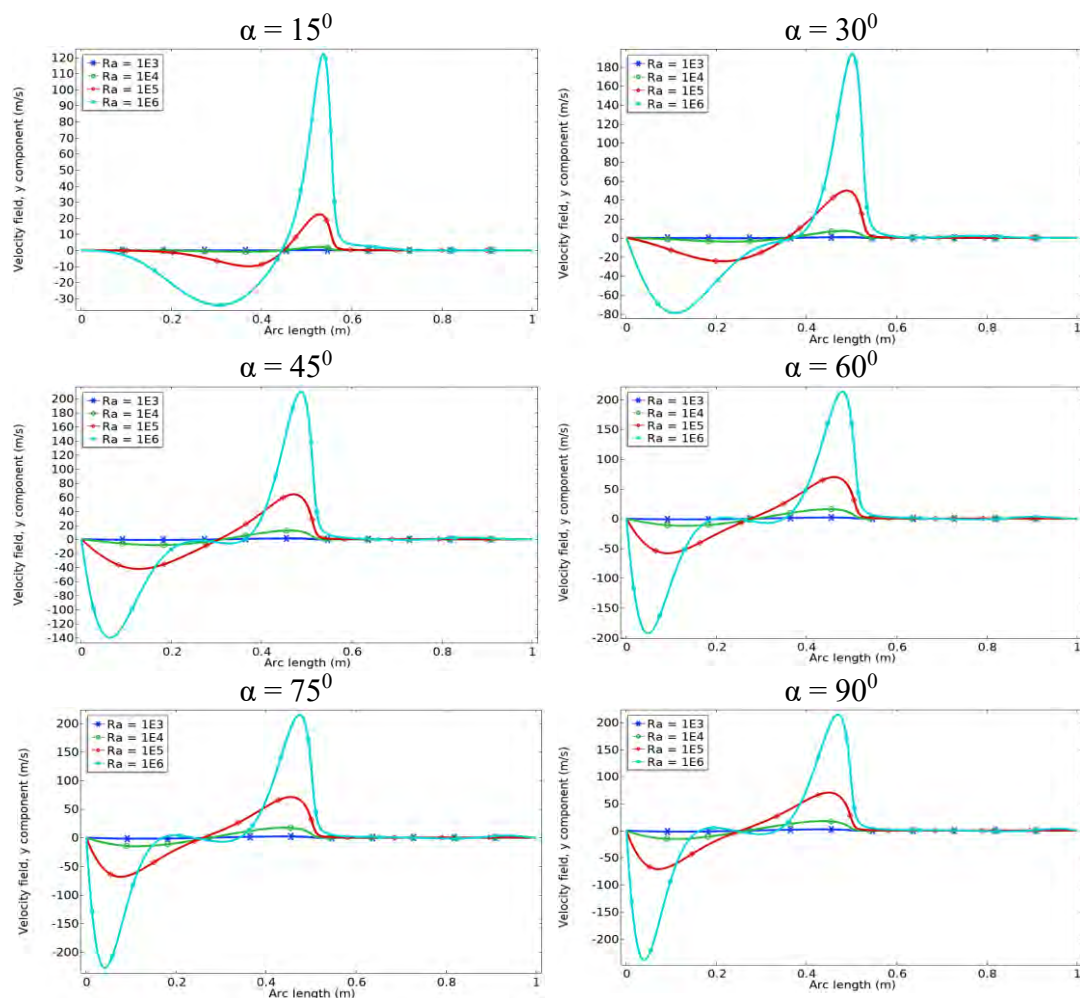
Figure 3.18 (a): Effect of Rayleigh number on **velocity profile** along the horizontal centerline for different skew angles $(15^0 \leq \alpha \leq 90^0)$ with *L* = 0.50.

α = 105⁰

α = 120⁰

α = 135⁰

α = 150⁰

α = 165⁰
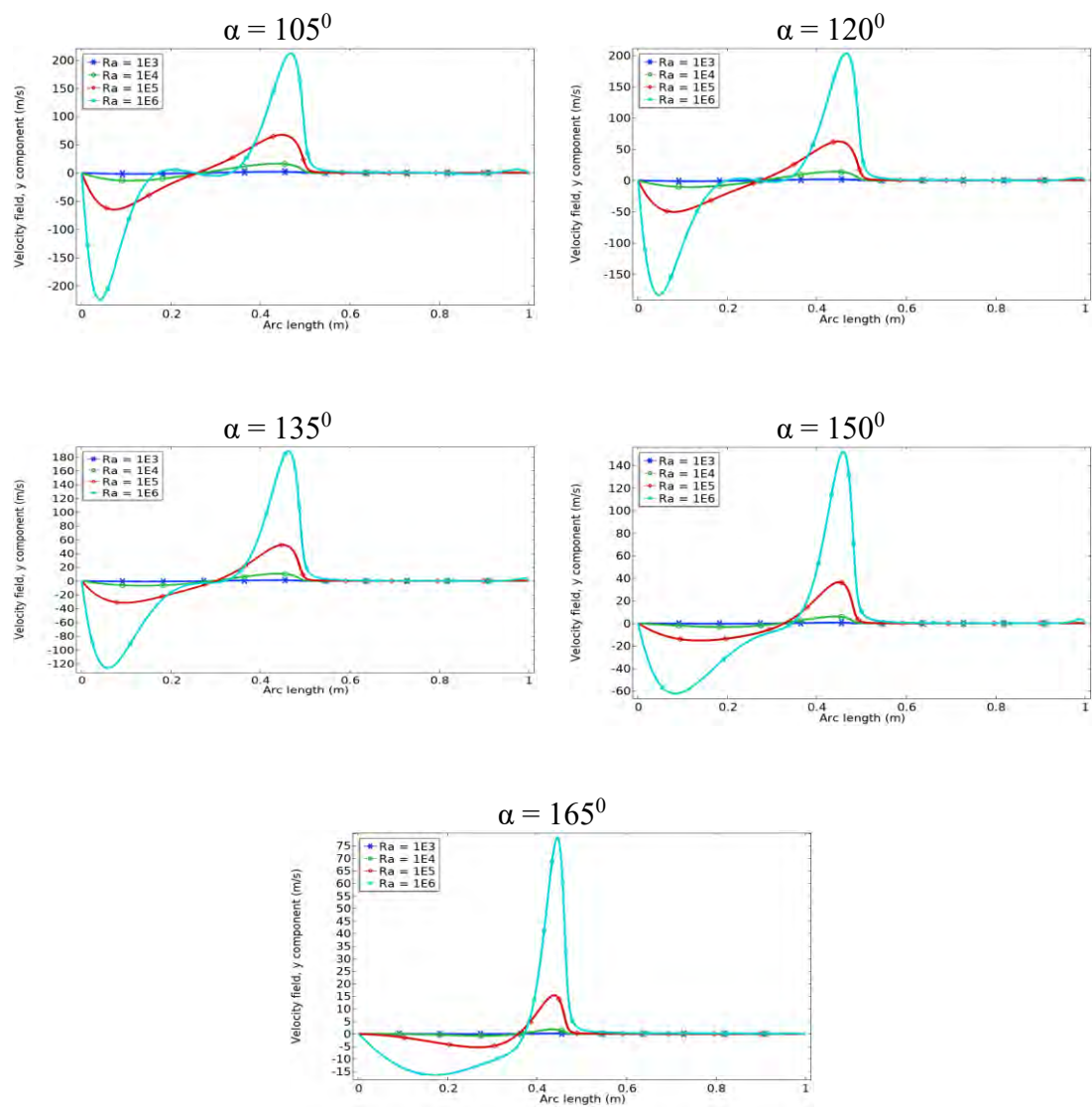
Figure 3.18 (b): Effect of Rayleigh number on **velocity profile** along the horizontal centerline for different skew angles $(105^0 \leq \alpha \leq 165^0)$ with $L = 0.50$.

Temperature profiles for *L* = 0.50 at *Pr* = 1.41

Figure 3.19(a)-(b) demonstrate the impact of temperature line distributions along the horizontal central axis for different Rayleigh numbers and skew angles. The baffle thickness D = 0.005, the skew angles, and the Rayleigh number $(10^3 \leq Ra \leq 10^6)$ values with sinusoidal amplitude $(\lambda = 0.50)$ are calculated for the temperature profiles. Similarly, we can say like velocity profiles; the dimensionless temperature profiles increase only insignificantly when $Ra = 10^3$ and $Ra = 10^4$. When the Rayleigh number increases, the temperature lines within the cavity become more significant, which implies that the curvature of the temperature lines becomes more prominent because of the increased significance of the temperature lines within the cavity.

Figure 3.19 (a): Effect of Rayleigh number on **temperature profile** along the horizontal centreline for different skew angles $(15^0 \leq \alpha \leq 90^0)$ with $L = 0.50$.

α = 105⁰

α = 120⁰

α = 135⁰

α = 150⁰

α = 165⁰
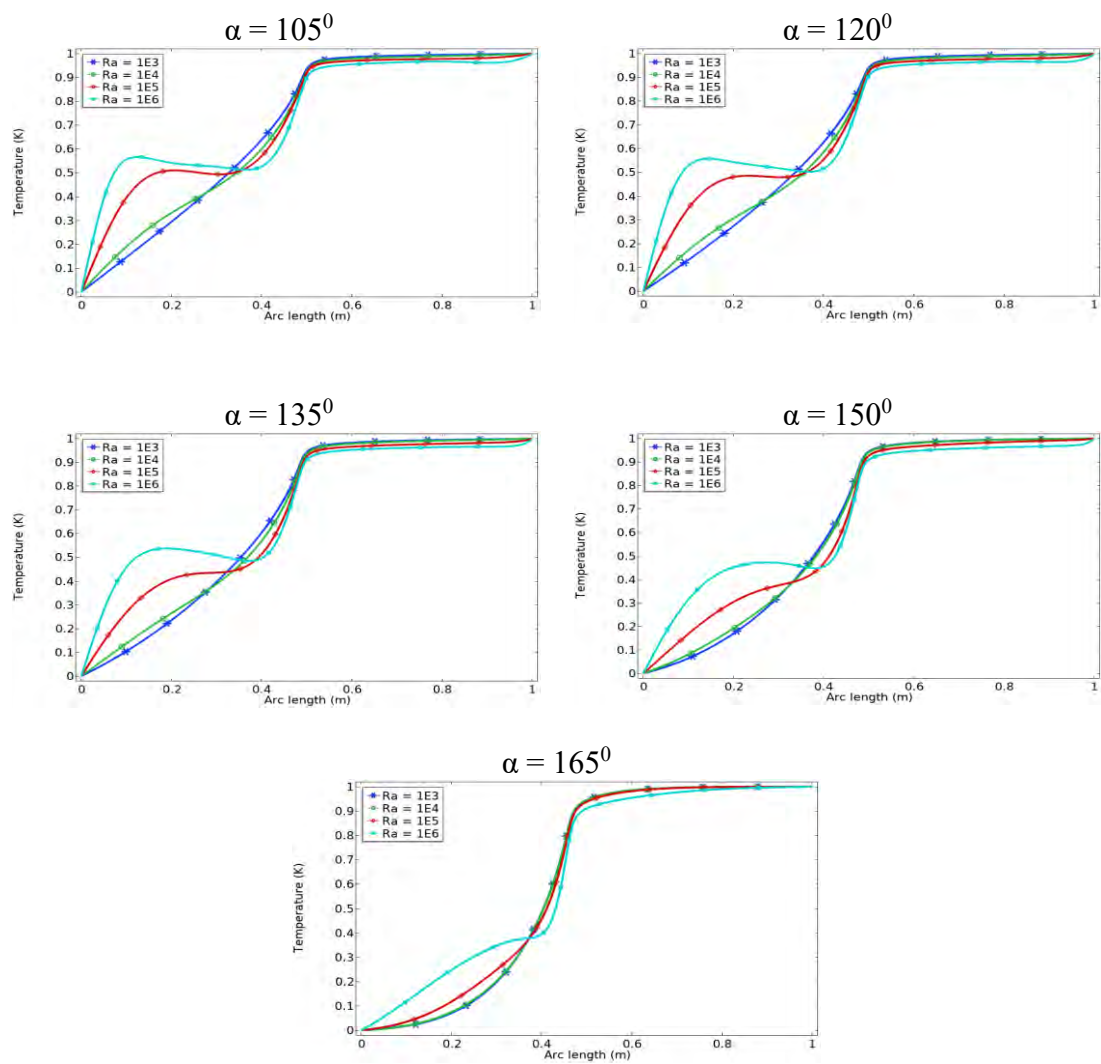
Figure 3.19 (b): Effect of Rayleigh number on **temperature profile** along the horizontal centerline for different skew angles $(105^0 \leq \alpha \leq 165^0)$ with $L = 0.50$.

Local Nusselt number for *L* = 0.50 at *Pr* = 1.41

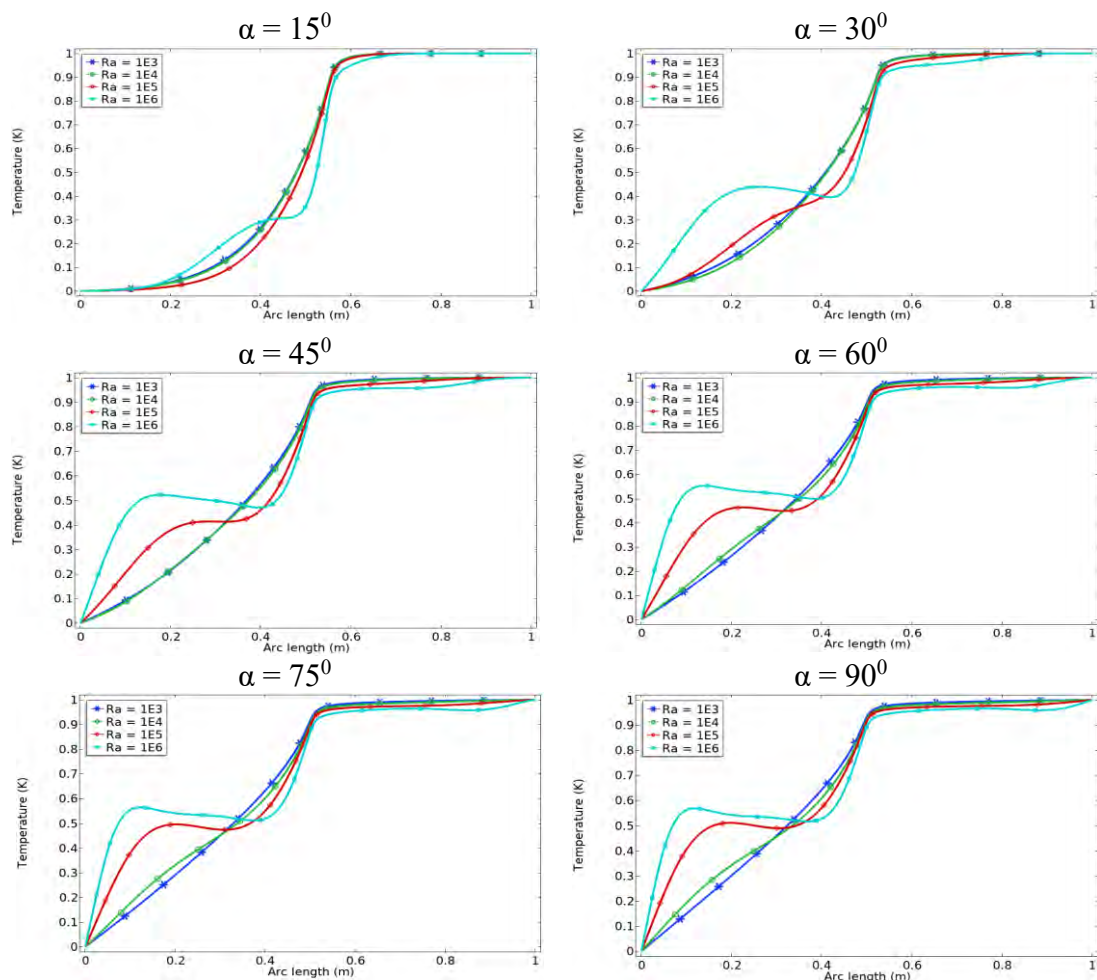Figure 3.20(a)-(b) Effect of Rayleigh number on local Nusselt number along the heated inclined right wall for different skew angles $(15^0 \leq \alpha \leq 165^0)$ with *L* = 0.50, which includes baffle exteriors. Also observed was that as the skew angle reaches $\alpha = 90^0$, the top side of the Baffle becomes crucial for all Rayleigh numbers. after that, when the skew angle exceeds $\alpha = 90^0$, the top side of the Baffle becomes more momentous. It also demonstrates that when the Rayleigh number increases, the curvature lines of the Local Nusselt number become more noticeable and curvier. However, we also found that in these graphs at the skew angles $(\alpha = 15^0, \text{and } 165^0)$, the Local Nusselt number is not changed noticeably.
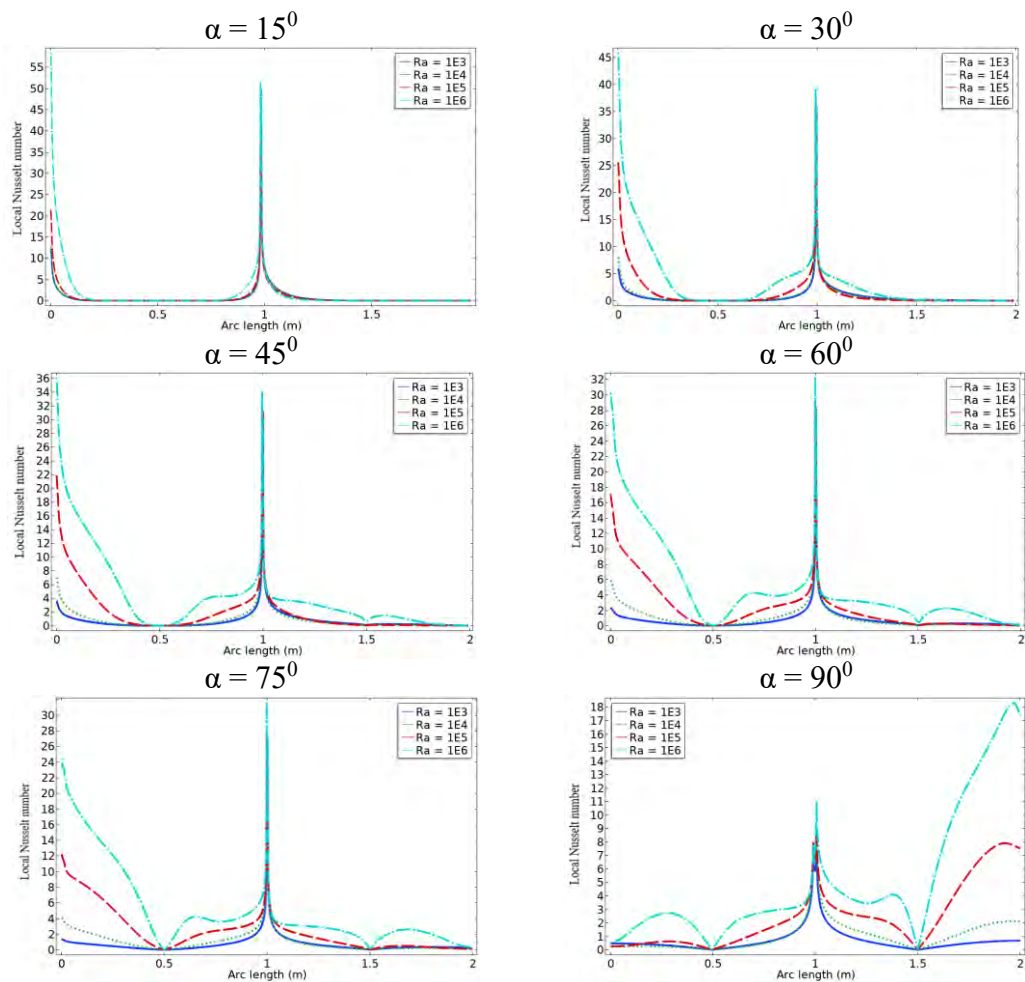
Figure 3.20(a): Effect of Rayleigh number on **local Nusselt number** along the heated inclined right wall for different skew angles $(15^0 \leq \alpha \leq 90^0)$ with *L* = 0.50.
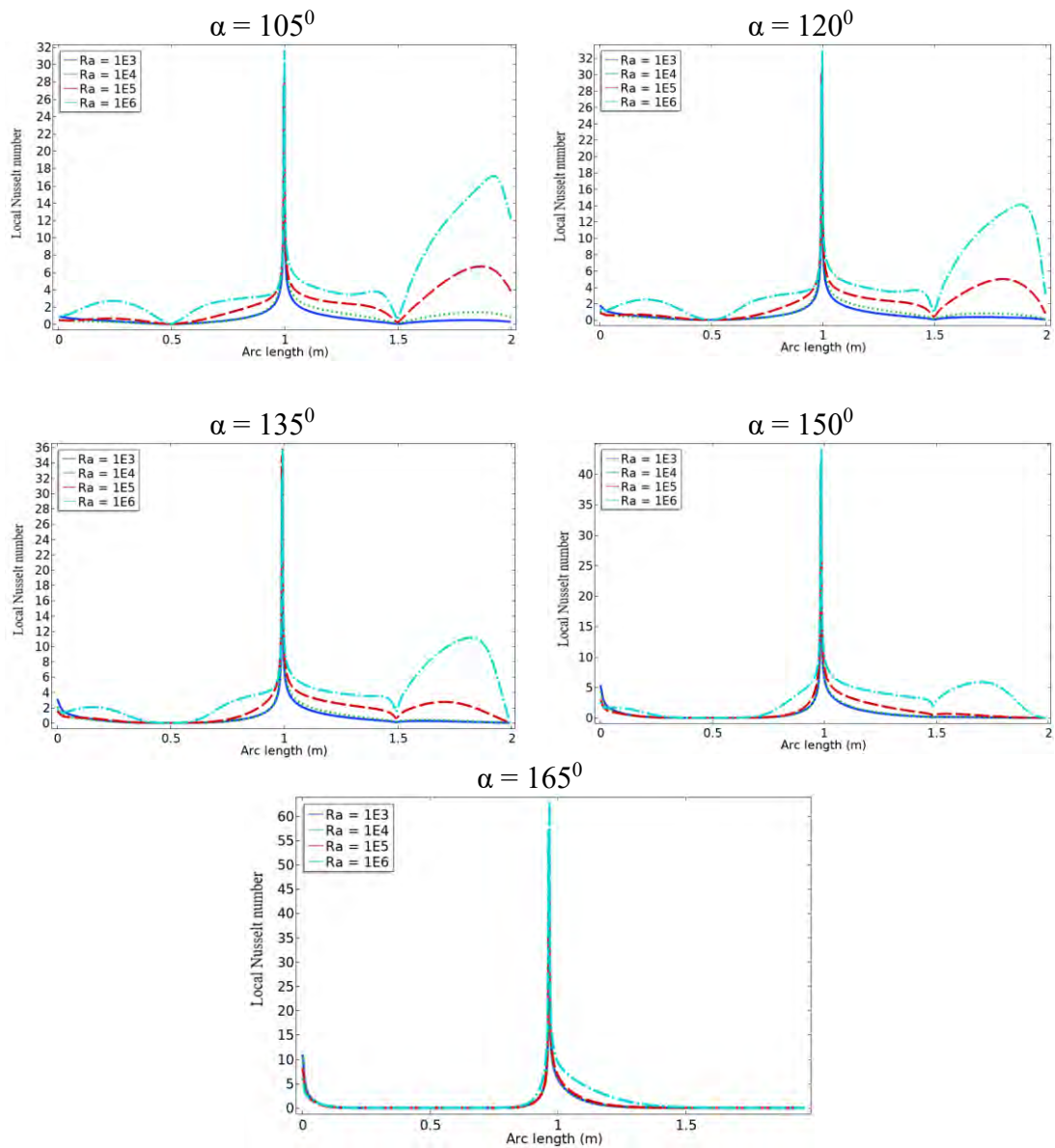
Figure 3.20 (b): Effect of Rayleigh number on **local Nusselt number** along the heated inclined right wall for different skew angles $(105^0 \leq \alpha \leq 165^0)$ with $L = 0.50$.

Average fluid temperature for *L* = 0.50 at *Pr* = 1.41

At a constant baffle size (L) and position, the average fluid temperature was measured across various Rayleigh numbers (Ra) and skew angles ($15^0 < \alpha \leq 165^0$). The quantitative data in Table 3.5 shows the numerical results. Figure 3.21 shows that increase the skew angle for various Rayleigh numbers causes the average fluid temperature to increase slowly to $\alpha = 45^0$. After then, According to Table 3.5 and Figure 3.21, the average fluid temperature decreases very gradually when the skew angles increase to $\alpha = 90^0$. Furthermore, for all the Rayleigh numbers, the fluid's temperature rises by the remaining skew angles. However, when the Rayleigh number is between $Ra = 10^3$ and $Ra = 10^6$ for all skew angles, the temperature increases to $\alpha = 150^0$. Table 3.5 shows that for $Ra = 10^6$ and $\alpha = 150^0$, the mean fluid temperature within the cavity is **2.7796661231853808**. That's remarkable.
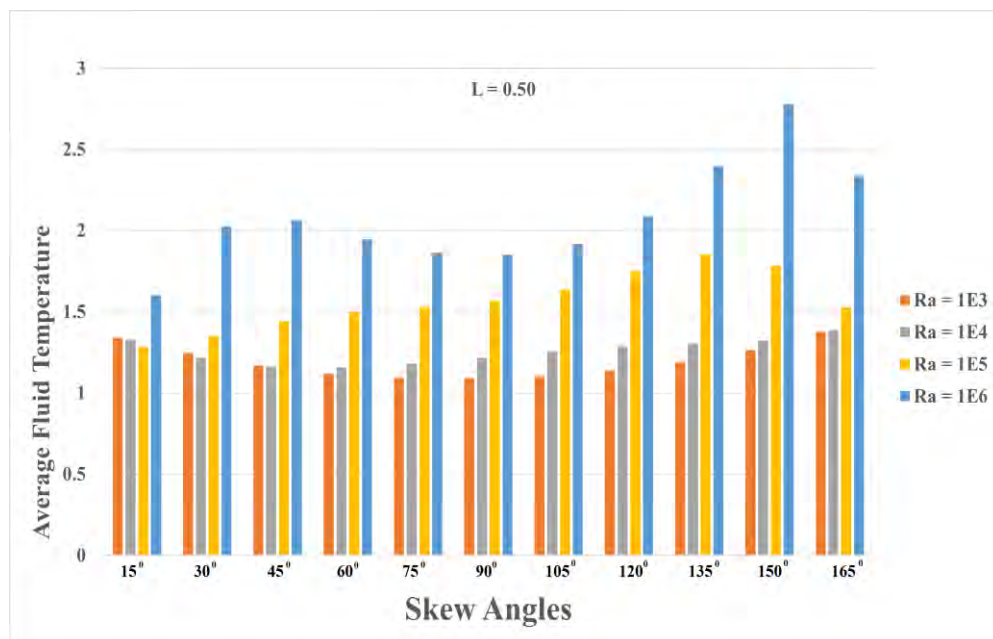
Figure 3.21: Effect of Rayleigh number on average fluid temperature for different skew angles $(15^0 \leq \alpha \leq 165^0)$ with *L* = 0.50.

Table 3.5: Average fluid temperature variations for various angle at L= 0.50.

Angles	Average fluid temperature			
	$Ra = 10^3$	$Ra = 10^4$	$Ra = 10^5$	$Ra = 10^6$
$\alpha = 15^0$	1.3408756700	1.3283495406	1.2814309556	1.6017035187
$\alpha = 30^0$	1.2466087555	1.2181630163	1.3506975091	2.0260972282
$\alpha = 45^0$	1.1697804137	1.1643746072	1.4421009848	2.0645714631
$\alpha = 60^0$	1.1192745117	1.1581082093	1.4976676268	1.9474060385
$\alpha = 75^0$	1.0936807014	1.1800764322	1.5302797859	1.8635495932
$\alpha = 90^0$	1.0902912780	1.2163077719	1.5690859630	1.8503019718
$\alpha = 105^0$	1.1051905388	1.2556759633	1.6383226877	1.9179360574
$\alpha = 120^0$	1.1380427453	1.2871677612	1.7496126881	2.0892083423
$\alpha = 135^0$	1.1900106855	1.3040285267	1.8561840284	2.3973113464
$\alpha = 150^0$	1.2653885280	1.3229230248	1.7837681490	**2.7796661231**
$\alpha = 165^0$	1.3756245251	1.3878225308	1.5275206248	2.3352839975

Average Nusselt number for *L* = 0.50 at *Pr* = 1.41

Impact of the average Nusselt number Nu_{avg} on the right inclined wall is seen in Figure 3.22-3.23, which includes a baffle surface to accommodate the effect of Rayleigh numbers (Ra) and different skew angles. In comparison, the remaining parameter's values are constant. For the fixed baffle size and position, the average Nusselt number augments proportionally to increase of the Rayleigh number. Consequently, the rate of heat transfer rises with increasing skew angle up to $\alpha = 90^0$. For the higher Rayleigh number over the length of the baffle, the buoyancy force increases, and heat transfer progresses. Due to the convergence of these curves, it is simple to observe that as the Rayleigh number grows, the effect of skew angles on the heated wall becomes more evident. The numerical value of a mean Nusselt number along a right inclined wall, including a baffle surface with various Ra, is investigated in Table 3.6. Moreover, Table 3.6 displays that the most crucial

value of the average Nusselt number for $L = 0.50$ is **4.946919651676246** along the heated region exposed at $Ra = 10^6$, and $\alpha = 90^0$.
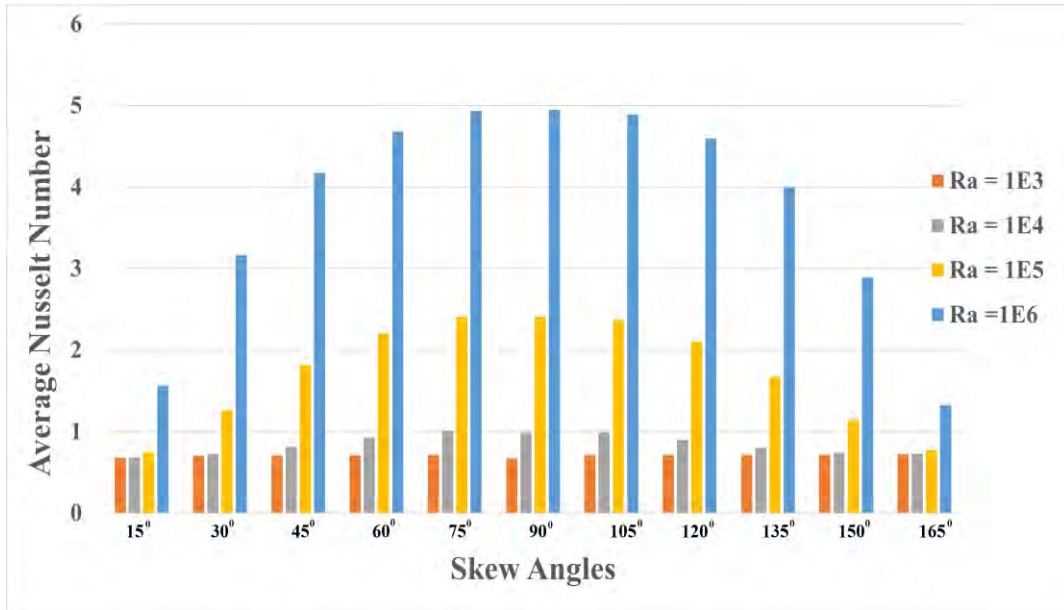
Figure 3.22: Impact of Nu_{avg} for various skew angles and Ra at $L = 0.50$.
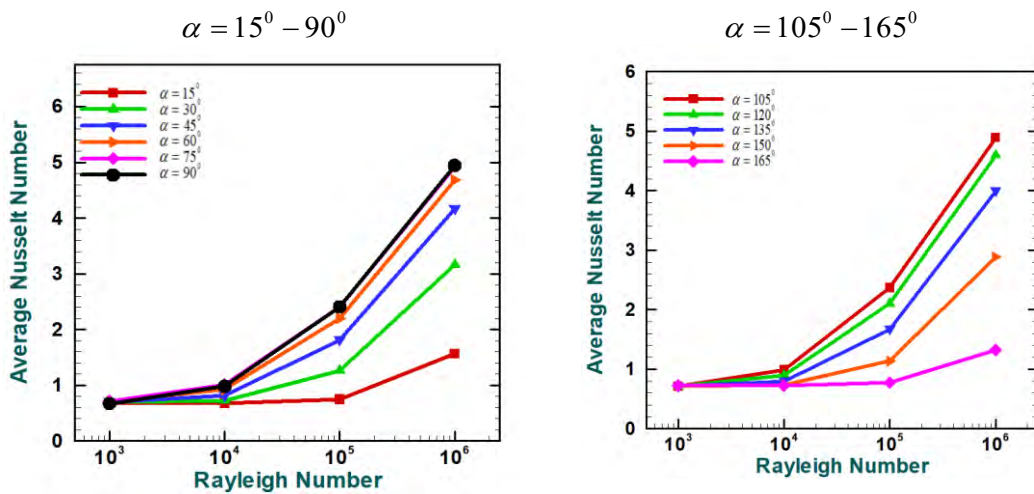
Figure 3.23: Impact of Nu_{avg} for various skew angle and Ra at $L = 0.50$.

Table 3.6: Average Nusselt number variations for various angle at $L = 0.50$.

Angles	Average Nusselt number			
	$Ra = 10^3$	$Ra = 10^4$	$Ra = 10^5$	$Ra = 10^6$
$\alpha = 15^0$	0.6790639444	0.6789698591	0.7470317659	1.5651626337
$\alpha = 30^0$	0.7033315536	0.7245220084	1.2631044489	3.1636523424
$\alpha = 45^0$	0.7072195048	0.8112130522	1.8140130665	4.1700532931
$\alpha = 60^0$	0.7100698586	0.9251558719	2.2003592516	4.6820249764
$\alpha = 75^0$	0.7129388230	1.0101215639	2.4067898323	4.9312143022
$\alpha = 90^0$	0.6716049764	0.9852357230	2.4078930287	**4.9469196516**
$\alpha = 105^0$	0.7114457597	0.9900600142	2.3686432448	4.8891336753
$\alpha = 120^0$	0.7123883969	0.9001751585	2.1039311678	4.5922981424
$\alpha = 135^0$	0.7117384764	0.8004694436	1.6722252979	3.9969765397
$\alpha = 150^0$	0.7143276019	0.7357080411	1.1388151723	2.8878226859
$\alpha = 165^0$	0.7249782791	0.7262669497	0.7734922767	1.3238379655

Effectiveness:

As displayed in Figure 3.24 for various baffle sizes, the impact of the baffle effectiveness inside the cavity with three distinct values is Rayleigh number (Ra), while the remaining parameters are kept constant. From Figure 3.24, the effectiveness of the baffle increasing with increasing the Rayleigh number at fixed baffle size and position and illustrates that the baffle position (B) has a negligible influence on baffle efficiency for all values of baffle length (L). Moreover, Table 3.7 reviews the statistical value of baffle effectiveness within the cavity for three distinct baffle surfaces, and Ra. From this Table 3.7, it can be noted that $E_f < 1$ for $B = 0.5$ at $Ra = 10^4$, although it is more than 1 at $Ra = 10^5$ and $Ra = 10^6$ for all the baffle lengths. Based on the numerical data, it seems that the baffle placement does not much affect their efficacy for baffle lengths $L = 0.20$ and 0.0. Moreover, from Table 3.4 the best baffle effectiveness is **1.133198480** audited at $B = 0.50$, $L = 0.50$ and $Ra = 10^6$.
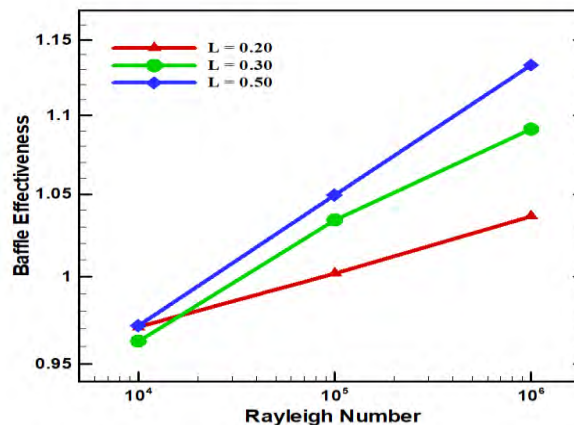
Figure 3.24: Baffle effectiveness

Table 3.7: Baffle effectiveness for various baffle lengths at several Ra.

Baffle effectiveness			
Baffle size	$Ra = 10^4$	$Ra = 10^5$	$Ra = 10^6$
$L = 0.20$	0.97082578	1.002069822	1.036471742
$L = 0.30$	0.96283171	1.034152063	1.091026113
$L = 0.50$	0.97164991	1.049468746	**1.133198480**

Figure 3.25 indicates the influence of the skew effectiveness within the enclosure for numerous skew angles with four various values of Rayleigh number (Ra) while the other parameters are held constant. Similarly, as seen in Figure 3.25, we have separated the effectiveness into two groups. Figure 3.25 shows that the effectiveness of skew angles decreases mildly with increasing skew angles for the Rayleigh numbers $Ra = 10^3$ and $Ra = 10^4$, respectively, and demonstrates that the Rayleigh number has a minor impact on the efficiency for all values of skew angles. On the other hand, increases in Rayleigh number also increase the effectiveness.

Furthermore, the statistical significance of skew effectiveness inside the cavity for four different Rayleigh numbers is discussed in Table 3.8. It can be shown in Table 3.8 that A_{ef} is less than 1 for $Ra = 10^4$ and $Ra = 10^5$ including the skew angle up to $\alpha = 75^0$, except for $\alpha = 15^0$, and A_{ef} is more than 1 for all other skew angles, with the exception of $\alpha = 75^0$. According to the numerical data, the skew angles have little effect on their effectiveness for skewness. However, because of the varying values of the skew angle, effectiveness varies dramatically as the Rayleigh number changes from 10^3 to 10^6, except for $\alpha = 105^0$, which includes all the variations in the skew angle. Furthermore, according to Table 3.8, the most influential effectiveness of skew angles is **1.536918079** audited at an angle $\alpha = 150^0$ and $Ra = 10^6$.

$$\alpha = 15^0 - 90^0 \qquad\qquad \alpha = 105^0 - 165^0$$

(a)   (b)
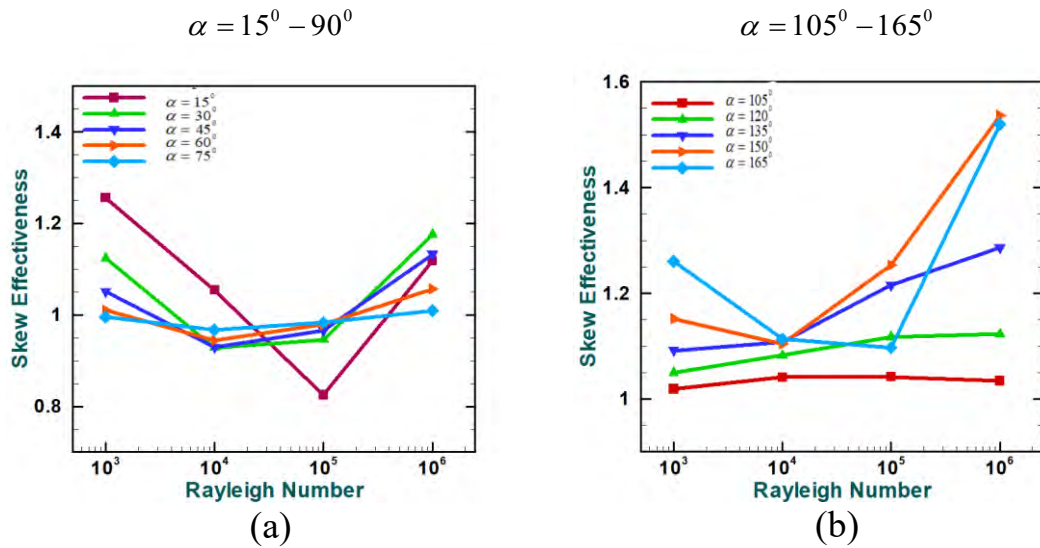
Figure 3.25: A_{ef} for different angle and Ra at $Pr = 1.41$.

Table 3.8: Skew effectiveness A_{ef} for various skew angles at several Rayleigh number.

Angles	Skew effectiveness			
	$Ra = 10^3$	$Ra = 10^4$	$Ra = 10^5$	$Ra = 10^6$
$\alpha = 15^0$	1.256022397	1.054367590	0.825132279	1.118135982
$\alpha = 30^0$	1.123991977	0.927885311	0.945453949	1.175268543
$\alpha = 45^0$	1.050702168	0.928805216	0.965684785	1.132844790
$\alpha = 60^0$	1.010503330	0.944025392	0.978775695	1.057086350
$\alpha = 75^0$	0.995612615	0.966995438	0.983657374	1.008954042
$\alpha = 105^0$	1.018820290	1.041252137	1.041651809	1.034378225
$\alpha = 120^0$	1.049426876	1.082432877	1.116984403	1.122576169
$\alpha = 135^0$	1.091771196	1.107861524	1.215568796	1.286600289
$\alpha = 150^0$	1.151930729	1.104064613	1.253204889	**1.536918079**
$\alpha = 165^0$	1.260685699	1.113161335	1.096814861	1.519846444

The numerical result was verified by comparing the local Nusselt number obtained by the code to previously published data for existing study. The finite element technique is used to solve governing equations. It is found that the results of the comparisons with the published works are in perfect accord. The effects of the skew angle and the length of the baffle on the skewed cavity have been investigated. Different concepts and findings have been examined in depth in the appropriate chapters of the thesis. The current chapter summarizes the ideas given and the findings acquired in previous work that has been previously reported. This is added to a section discussing the potential for additional research in related exploration domains.

4.1 SUMMARY OF THE MAJOR OUTCOMES

Three distinct baffle lengths are employed in this study: Case-1 ($L = 0.20$), Case-2 ($L = 0.30$), and Case-3 ($L = 0.50$), with the Prandtl number selected as $Pr = 1.41$ in each of the studies.

The following main conclusions could be drawn from the present study:

(i) When the Rayleigh number increases, both the flow strength and the heat transfer increase in all circumstances. Increase in the Rayleigh number causes changes in the velocity profiles, the local Nusselt number, the heat transfer rate, and an increase in the average Nusselt number. For the most considerable value of the Rayleigh number $Ra = 10^6$, the best results are obtained in Cases 1 and 3. There is a strong influence of the natural convection parameter Ra on the flow and temperature fields.

(ii) The influence of the baffle length on fluid flow and temperature field is pronounced in all cases having higher baffle length increases the heat transfer rate as well as the average fluid temperature whereas the average Nusselt number decreased. The best result is found for the baffle length of $L = 0.50$.

(iii) At the baffle length $L = 0.20$, the optimal heat transfer rate is attained for the highest $Ra = 10^6$.

(iv) The maximum velocity gradually increasing with increases in the Rayleigh number in the streamline for all the cases of the baffle lengths.

(v) The maximum velocity grows gradually with increasing skew angle up to $\alpha = 90^0$ for all instances of the baffle lengths in the streamline. After that, by increasing the skew angle to $\alpha = 165^0$, the maximum velocity steadily falls.

(vi) The baffle effectiveness is enriched by increasing Ra for different values of baffle length. It is also found that the baffle effectiveness grows with the expansion of the baffle length. The maximum baffle effectiveness was **1.133198480** at the baffle length $L = 0.50$ and $Ra = 10^6$.

(vii) By raising Ra for various values of the skew angle, the skew effectiveness may dramatically improve. Further, we observed that the effectiveness of the skew angle changes irregularly with the change of the skew angle. When the Rayleigh number $Ra = 10^6$ and the skew angle $\alpha = 150^0$, the maximum skew effectiveness was **1.536918079.**

4.2 FURTHER WORKS

The following can be put forward for the further works as follow-ups of the present research as.

❖ Investigation can be performed by using magnetic fluid instead of electrically conducting fluid within the porous medium and changing the boundary conditions of the cavity's walls.

❖ The study can be extended for turbulent flow using different fluids, different thermal boundary conditions such as constant heat flux or radiation and unsteady flow.

❖ Only two-dimensional fluid flow and heat transfer has been analyzed in this thesis. So, this deliberation may be extended to three-dimensional analyses to investigate the effects of parameters on flow fields and heat transfer in cavities.

❖ This thesis only considers a single baffle; however, it may be developed to include parallel or series baffles.

❖ The investigation may be prolonged by varying the form of the cavity.

❖ The research may be refined to include nanofluids.

REFERENCES

[1] Hagen, K.D. "Heat Transfer with Applications," Prentice-Hall, Englewood Cliff, 1999, 688.

[2] Çengel and Yunus, "Heat Transfer: A practical approach," (2nd ed.), Boston: McGraw-Hill, 2003, ISBN 978-0-07-245893-0.

[3] S. V. Patankar "Numerical Heat Transfer and Fluid Flows" 1st ed., Hemisphere Publishing Corporation, United States of America, 1980.

[4] Batchelor, G. Keith, "An Introduction to Fluid Dynamics," Cambridge University Press 1967, ISBN 0-521-09817-3.

[5] J. N. Reddy, "An Introduction to the Finite Element Method," McGraw-Hill, New York, 1993.

[6] J. H. Ferziger and M. Perić, "Computational Methods for Fluid Dynamics," 3rd ed. Springer, 2002.

[7] G. De V. Davis, "Natural convection of air in a square cavity: A benchmark numerical solution," Int. J. Num. Meth. Fluid, 1983, 3(3), 249-264.

[8] S. H. Tasnim, Mchael, R. Collins, "Numerical analysis of heat transfer in a square cavity with a baffle on the hot wall," Int. Comm. Heat Mass Trans., 2004, 639-650.

[9] H. Ambarita, K. Kishinami, M. Daimaruya, T. Saitoh, H. Takahashi, J. Suzuki, "Laminar Natural convection heat transfer in an air-filled square cavity with two insulated baffles attached to its horizontal walls," Therm. Sci. Eng., 2006, 14(3).

[10] S. Jani, Mahmoodi, M. Amini, "Magnetohydrodynamic free convection in a square cavity heated from below and cooled from other walls," Int. J. Mech. Mech. Eng., 2013, 7(4).

[11] A. Nag, A. Sarkar, V.M.K. Sastri, "Effect of thick horizontal partial partition attached to one of the active walls of a differentially heated square cavity," Num. Heat Trans. Part A, 1994, 611-625.

[12] Barakos, E. Mitsoulis, D. Assimacopoulos, "Natural convection flow in a square cavity revisited: Laminar and turbulent models with wall functions," Int. J. Num. Meth. Fluid, 1994, 18, 695-719.

[13] P. Mayeli and G. J. Sheard, "Natural convection and entropy generation in square and skew cavities due to large temperature differences: A Gay-Lussac type vorticity stream-function approach," Int. J. Num. Meth. Fluid, 2021, 93(7), 2396-2420.

[14] M. A. Sheremet, I. Pop, "Natural convection in a square porous cavity with sinusoidal temperature distributions on both side walls filled with a nanofluid: Buongiorno's mathematical model," Trans. Por. Med. (Springer), 2014, 8(8), 411-429.

[15] B. Ren, Chung-Gang Li, M. Tsubokura, "Laminar natural convection in a square cavity with 3D random roughness elements considering the compressibility of the fluid," Int. J. Heat Mass Trans., 2021, 173(1):121248.

[16] M. Amini, S. Jani, M. Mahmoodi, J. E. Jam, "Numerical investigation of natural convection heat transfer in a symmetrically cooled square cavity with a thin fin on its bottom wall," Therm. Sci., 2014, 18(4), 1119-1132.

[17] A. Elatar, M. A. Teamah, M. A. Hassab, "Numerical study of laminar natural convection inside square enclosure with single horizontal fin," Int. J. Therm. Sci., 2016, 99, 44-51.

[18] A. H. I. Ali, S. Dia, M. Y. Kheyal, C. Mbow, A. C. Beye, "Numerical study of natural convection in a porous square enclosure with sinusoidally varying temperature profile on the bottom wall," J. Fluid Dyn., 2017, 7(3), 263-275.

[19] M. F. A. Asad, M. A. Hossain, M. M. A. Sarker, "Numerical investigation of MHD mixed convection heat transfer having vertical fin in a lid-driven square cavity," AIP Conference Proceedings 2121(1):030023, 2019.

[20] R. K. Nayak, S. Bhattacharyya, I. Pop, "Heat transfer and entropy generation in mixed convection of a nanofluid within an inclined skewed cavity," Int. J. Heat Mass Trans., 2016 (102), 596-609

[21] S. Thohura, M. M. Molla, M. M. A. Sarker, "Numerical Simulation of non-Newtonian power-low fluid flow in a lid-driven skewed cavity," Int. J. Appl. Comp. Math, 2019, 5 (14).

[22] E. Erturk, B. Dursun, "Numerical solutions of 2-D steady incompressible flow in a driven skewed cavity," J. Appl. Math. Mech., 2007 (87), 377-392.

[23] R. K. Nayak, S. Bhattacharyya, I. Pop, "Numerical study on mixed convection and entropy generation of Cu-water nanofluid in a differentially heated skewed enclosure," Int. J. Heat Mass Trans., 2015 (85), 620-634.

[24] S. Thohura, M. M. Molla, M. M. A. Sarker, M. C. Paul, "Study of mixed convection flow of power-law fluids in a skewed lid-driven cavity," Heat Trans., 2021, 50(5), 6328-6357.

[25] A. Misirlioglu, A. C. Baytas, I. Pop, "Natural convection inside an inclined wavy enclosure filled with a porous medium," Springer, 2006, 64(2), 229-246.

[26] A. I. Alsabery, M. A. Sheremet, M. Ghalambaz, A. J. Chamkha, I. Hashim, "Fluid Structure interaction in natural convection heat transfer in an oblique cavity with a flexible oscillating fin and partial heating," Appl. Therm. Eng., 2018 (145), 80-97.

[27] M. Si-Ameur, S. Benmenzer, "Natural convection induced by volumetric heating in an inclined porous cavity," Comp. Therm. Sci., 2017, 9(1):77-92.

[28] A. C. Baytas, "Entropy generation for natural convection in an inclined porous cavity," Int. J. Heat Mass Trans., 2000 (43), 2089-2099.

[29] M. S. Selamat, R. Roslan, I. Hashim, "Natural convection in an inclined porous cavity with spatial sidewall temperature variations," J. Appl. Math., 2012.

[30] S. S. karan, H. T. Cheong, M. Bhuveswari, "Natural convection in an inclined porous triangular enclosure with various thermal boundary conditions," Therm. Sci., 2019, 23(2A), 537-548.

[31] F. Wu, W. Zhoyu, X. Ma, "Natural convection in a porous rectangular enclosure with sinusoidal temperature distributions on both side walls using a thermal non-equilibrium model," Int. J. Heat Mass Trans., 2015 (85), 756-771.

[32] L. Wang, C. Huang, X. Yang, Z. Chai, and B. Shi, "Effects of temperature-dependent properties on natural convection of power-law nanofluids in rectangular cavities with sinusoidal temperature distribution," Int. J. Heat Mass Trans., 2019, 128(3), 688-699.

[33] A. Sabeur-Bendehina, L. Adjlout, O. Imine, "Effect of sinusoidal distribution of the temperature on laminar natural convection in wavy rectangular enclosure," J. Appl. Sci., 2006, 6(3):710-715.

[34] Y. Varol, H. F. Oztop, I. Pop, "Numarical analysis of natural convection for a porous rectangular enclosure with sinusoidally varying temperature profile on the bottom wall," Int. Comm. Heat Mass Trans., 2008, 35, 56-64.

[35] L. Hassinet and M. S. Ameur, "Numerical study on natural convection in a porous cavity partially heated and cooled by sinusoidal temperature at vertical walls," J. Por. Med., 2019, 22(1), 73-85.

[36] N. H. Saeid, "Natural convection in porous cavity with sinusoidal bottom wall temperature variation," Int. Comm. Heat Mass Trans., 2005, 32(3-4), 454-463.

[37] I. Zahmatkesh, "Natural convection and entropy generation in a porous enclosure with sinusoidal temperature variation on the side walls, Journal of fluid," Heat Mass Trans., 2014, 2368-6111, 23-29.

[38] W. Feng, G. Wang, W. Zhou, "Numerical study of natural convection in a porous cavity with sinusoidal thermal boundary condition," Chem. Eng. Tech., 2015, 39(4), 747-774.

[39] A. Chattopadhyay, S. K Pandit, S. S. Sarma, I. Pop, "Mixed convection in a double lid-driven sinusoidally heated porous cavity," Int. J. Heat Mass Trans, 2016, 361-378.

[40] H. T. Cheong, S. Sivasankaran, M. Bhuvaneswari, "Natural convection in a wavy porous cavity with sinusoidal heating and internal heat generation," Int. J. Num. Meth. Heat Fluid Flow, 2017, 27 (2), 287-309.

[41] M. F. A. Asad, M. N. Alam, C. Tunc, M. M. A. Sarker, "Heat transport exploration of free convection flow inside enclosure having vertical wavy walls," J. Appl. Comp. Mech., 2021, 7(2), 520-527.

[42] H. F. Oztop, E. Abu-Nada, Y. Varol, A. Chamkha, "Natural convection in a wavy enclosure with volumetric heat sources," Int. J. Therm. sci., 2011 (50), 502-514.

[43] S. Singh and R. Bhargava, "Numerical study of natural convection within a wavy enclosure using meshfree approach: effect of corner heating," Sci. world J. (Hindawi), 2014, 842401.

[44] M. F. A. Asad, M. J. H. Munshi, M. M. A. Sarker, "Effect of fin length and location on natural convection heat transfer in a wavy cavity," Int. J. Therm. Sci. Tech., 2020, 7(3).

[45] A. Alsabery, M. Sheremet, A. J. Chamkha, I. Hashim, "Impact of nonhomogeneous nanofluid model on transient mixed convection in a double lid-driven wavy cavity involving solid circular cylinder," Int. J. Mech. Sci., 2019, 150, 637-655.

[46] A. K. Hussein, M. Ghodbane, Z. Said and R. S. Ward, "The effect of the baffle length on the natural convection in an enclosure filled with different nanofluids," J. Therm. Analy. Calorim., 2020, 147, 791-813.

[47] C. Taylor, P. Hood, "A numerical solution of the Navier–Stokes equations using finite element technique" Comp. Fluids, 1973, 1, 73–100.

[48] I. E. Sarris, I. Lekakis, N. S. Vlachos, "Natural convection in a 2D enclosure with sinusoidal upper wall temperature," Num. Heat Trans. Appl., 2002, 42(5), 513-530.

[49] M. Sankar, B.V. Pushpa, B. M. R. Prasanna,Y. Do, "Influence of size and location of thin baffle on natural convection in a vertical annular enclosure," J. Appl. fluid Mech., 2016, 9(6), 2671-2684.

[50] M. F. A. Asad, M. M. A. Sarker, M. J. H. Munshi, "Numerical investigation of natural convection flow in a hexagonal enclosure having vertical fin," J. Scient. Res., 2019, 11(2), 173-183.

[51] G. Djaomazava, M. A. Randriazanamparany, F. D' Assise Rakotomanga, "Numerical study of natural convection in a vertical channel one of whose walls has sinusoidal protuberances," Int. J. Hyd. Eng., 2019, 8(1);1-6.

[52] E. Bilgen, and R. Ben Yedder, "Natural convection in enclosure with heating and cooling by sinusoidal temperature profiles on one side," Int. Comm. Heat Mass Trans., 2007, 50, 139-150.

[53] S. Khudhayer, Y. A. Jasmin, T. K. Ibrahim, "Natural convection in a porous horizontal cylindrical annulus under sinusoidal boundary condition," J. Mech. Eng. Res. Dev., 2020, 230-244.

[54] M. F. A. Asad, M. N. Alam, H. Ahmed, M. M. A. Sarker, M. Alsulami, K. A. Gepreel," Impact of closed space rectangular heat source on convective flow through triangular cavity," Res. Phys., 2021, 23, 104011.

[55] R. L. Frederick, S. G. Moraga, "Three-dimensional natural convection in finned cubical enclosures," Int. J. Heat Fluid Flow, 2007, 28, 289-298.

[56] T. Islam, M. F. A. Asad, N. Akter, "Numerical Study of Magnetohydrodynamic Natural Convection Heat Transfer and Fluid Flow of Nanofluid in a Skewed Cavity," J. Eng. Math. Stat., 2020, 14-36.